Multiobjective Optimization and Multivariable Control of Offshore Wind Turbine System

Tore Bakka

Multiobjective Optimization and Multivariable Control of Offshore Wind Turbine System

DOCTOR OF PHILOSOPHY AT THE FACULTY OF ENGINEERING AND SCIENCE, SPECIALIZATION IN MECHATRONICS

University of Agder

Faculty of Engineering and Science
2013

Doctoral Dissertation by the University of Agder 68
ISBN: 978-82-7117-739-3
ISSN: 1504-9272

Printed in the Printing Office, University of Agder
Kristiansand

Preface

This PhD dissertation contains research results obtained during my stay at the University of Agder, Department of Engineering during the period of September 2010 - September 2013. My principal supervisor has been Professor Hamid Reza Karimi and my co-supervisor has been Professor Geir Hovland, they are both with the Department of Engineering at the University of Agder. From September to December in 2012 I was a visiting researcher at the University of Wisconsin-Madison (UWM), USA. My host professor during my abroad stay at (UWM) was Professor Neil A. Duffie.

Acknowledgments

These last three years as a PhD student have gone by so fast, but I guess that is a good thing. It means that I have not been bored, but rather been having a good time. I can safely say that the University of Agder is a nice place to be, both the university premises and all my coworkers are impeccable. To be allowed to dig down in some of your favorite subjects for three years, while traveling the world attending conferences, is indeed a privilege. There are some specific people I would like to thank for making this possible.

First of all, I would like to thank my principal supervisor, Professor Hamid Reza Karimi. Without his great supervision and guidance throughout these three years, I can not imagine I would be able to complete my PhD work. Even though he has a busy schedule, he always found time to help and guide me on my way. I remember one time I had some issues with an LMI problem. Hamid was flying somewhere and he scribbled down some LMI calculations on the back of his boarding card, took a picture with his phone and sent it to me. That's a dedicated supervisor.

During these last years I have also learned to know the other PhD students in the mechatronics group. These guys are Morten, Jesper, Magnus, Knut, Øyvind and Yulin. They are a nice bunch of people who have provided a very nice social and academic environment.

This project is carried out in conjunction with Norwegian Center for Offshore Wind Energy (NORCOWE). NORCOWE is an interdisciplinary resource center for exploitation of offshore wind energy as a natural sustainable energy source. On a regular basis there have been meetings to discuss the project and once a year there

has been a summer school, where a variety of different offshore wind related topics have been dealt with. I am very grateful for having been a part of this center, it has been fruitful in so many ways and it has added a second dimension to my PhD work.

A special thanks goes to my girlfriend Helen, who has stood by me and corrected more than one typo during the last three years.

My largest motivation to pursue a career within science comes from my grandfather. From an early age he taught me about math and physics and got me interested in science. To this day, at an age of 83, he still sits down with my old high school math books to do some math problems just for the fun of it. I hope I will do the same.

Tore Bakka
Grimstad, Norway
June 2013

Abstract

Renewable energy is a hot topic all over the world. Nowadays, there are several sustainable renewable power solutions out there; hydro, wind, solar, wave and biomass to name a few. Most countries have a tendency to want to become greener. According to the European Wind Energy Association (EWEA), the world wide capacity increased with 44.601 [MW] in 2012. From this number, 27 % accounts for new installed wind power, which is the second biggest contributor after solar (37 %).
In the past, all new wind parks were installed onshore. During the last decade more and more wind parks were installed offshore, in shallow water (less than 30 [m]). Now, some of the issues related to onshore turbines can be avoided, such as the visual impact, noise and shadow flicker. If one is to speculate about what the future may hold, it is evident that the next step for companies is to install floating wind parks in deeper water (more than 30 [m]). Offshore conditions far from the shore provide with higher and more stable wind conditions. In such deep water, it is no longer economically viable to install bottom-fixed turbines. A solution is to use floating turbine. A floating turbine gives new and interesting challenges to the control community.

This dissertation mainly deals with pitch control of a floating wind turbine. The modeling is also to some extend dealt with, e.g. it is the main topic of paper A. Paper A deals with the bond graph methodology as a graphical approach to model wind turbines. This is an alternative to the more classical Newtonian approach. The purpose is not to validate a specific wind turbine system, but rather explore how the bond graph can contribute with a model and give a better understanding

of how the overall system works. The emphasis has not been on the hydro- or aero- dynamics, but rather on the electro-mechanical system. Papers B, C and D are more dedicated to the control of the turbine. The models used for the control purpose are obtained from the wind turbine simulation software FAST (Fatigue, Aerodynamic, Structures and Turbulence). In paper B, several linear models of the turbine are obtained, one model for each $10th$ azimuth angle. All these models are made continuous based on an affine parameter-varying structure. Using upper bounded inequalities, the parameter dependency is removed from the linear matrix inequality (LMI) representation. Pole placement constraint is also added to the set of LMIs before it is solved for a dynamic H_∞ output-feedback controller.
Papers C and D are dealing with static H_∞ output-feedback control with constrained information. Constrained information means that not all the available information is used by the controller. There can be different reasons for this, e.g. some of the information is simply not needed, some of the sensors are especially prone to failure, switching between controllers which do not need the same information, etc. Paper C uses a model of the turbine based on a single operating point. Paper D is a direct continuation of paper C. This paper uses a model based on several operating points and a linear parameter-varying (LPV) model is derived. The affine model is parameter-dependent on the wind speed, which is estimated using an extended Kalman filter.

All simulations are carried out using Matlab/Simulink and all LMI calculations are performed using YALMIP interfaced with Matlab.

Publications

The following four papers are appended and will be referred to by their Latin character. The papers are printed in their originally published state except for changes in format and minor errata.

A. T. Bakka and H. R. Karimi, "Bond graph modeling and simulation of wind turbine systems", *Journal of Mechanical Science and Technology*, vol. 24 (6), 2013.

B. T. Bakka and H. R. Karimi, "Robust H_∞ Dynamic Output Feedback Control Synthesis with Pole Placement Constraints for Offshore Wind Turbine Systems", *Mathematical Problems in Engineering vol. 2012*, Article ID 616507, 18 pages, doi:10.1155/2012/616507, 2012.

C. T. Bakka and H. R. Karimi, "H_∞ Static Output Feedback Control Design with Constrained Information for Offshore Wind Turbine System", *Journal of The Franklin Institute*, vol. 350 (8), pages 2244-2260, 2013.

D. T. Bakka, H. R. Karimi and S. Christiansen, "Linear Parameter-Varying Modeling and Control of an Offshore Wind Turbine with Constrained Information", *Submitted to: IET Control Theory & Applications*, 2013.

The following papers are not included in the dissertation but constitute an important part of the background.

I. H. R. Karimi and T. Bakka, "Stochastic Stability Analysis and Output Feedback Control of Wind Turbine Systems with Wireless Sensor Networks", *Proceedings of the* 24^{th} *International Congress on Condition Monitoring and Diagnostic Engineering Management*, page 1086-1095, 2011.

II. T. Bakka and H. R. Karimi, "Wind Turbine Modeling Using The Bond Graph", *IEEE International Symposium on Computer-Aided Control System Design (CACSD)*, page 1208-1213, 2011.

III. T. Bakka, H. R. Karimi and N. A. Duffie, "Gain Scheduling for Output H_∞ Control of Offshore Wind Turbine", *Proceedings of the* 22^{nd} *International Offshore and Polar Engineering Conference*, page 496-501, 2012.

IV. T. Bakka and H. R. Karimi, "Multi-objective Control Design with Pole Placement Constraints for Wind Turbine Systems", *Advances on Analysis and Control of Vibrations - Theory and Applications*, INTECH ISBN 978-953-51-0699-9, page 179-194, 2012.

V. T. Bakka and H. R. Karimi, "A Linear Parameter-Varying Approach to H_∞ Control of an Offshore Wind Turbine", *Proceedings of the* 23^{nd} *International Offshore and Polar Engineering Conference*, page 434-439, 2013.

Contents

List of Figures

List of Tables

Chapter 1

Introduction

The wind turbine has been in use for several centuries. The first wind machines were only used for mechanical labor, such as grinding corn or pumping water. The first who benefited from the wind turbine in an electrical way, was James Blyth in Scotland in 1887. He used it to charge his batteries, in order to have light in his cabin. The modern wind power industry did not start until the late 1970s, and from this point the research within wind power has accelerated.

Nowadays, wind energy is one of the most promising sources for renewable energy. According to The World Wind Energy Association the worldwide capacity at the end of 2012, has reached 282,275 [MW]. Since 2001, the annual growth in capacity has been about 21%. The top world leading countries are China, USA, Germany, Spain and India. Together they represent 73% of the total global capacity. Although the majority of the installed capacity is on land, many offshore parks have been built in recent years. Most of these parks have turbines which are either fixed to the soil or they stand on monopoles or other structures. Some of the major offshore wind farms in Europe are located in the UK and Denmark, to name a few; Greater Gabbard (UK), Whalney (UK), Sheringham Shoal (UK), Horns Rev (DK) and Rødsand (DK). The turbines in these farms are installed in shallow waters, typical depths ranging from 10-30 [m]. For many countries such as Spain, US, Japan, Korea and Norway it would be beneficial to also be able to install wind turbines in deeper waters, in depths up to several hundred meters. The existing well established bottom fixed turbines are not suited for such deep water. During the last couple of

years floating solutions have started to emerge. Hywind is one example of a floating wind turbine solution. The demonstration turbine was installed back in 2009 and is still in operation. The floating turbine is located in the North Sea, right off the Norwegian west coast. The system uses a monopile spar buoy tower where a large portion of the tower is extended below the surface, see Fig. 1.1. In order to stabilize the turbine, heavy ballast is installed at the bottom of the tower, bringing the center of gravity down. Three mooring lines attached to the seabed keep the turbine in place in addition to adding stiffness to the system.

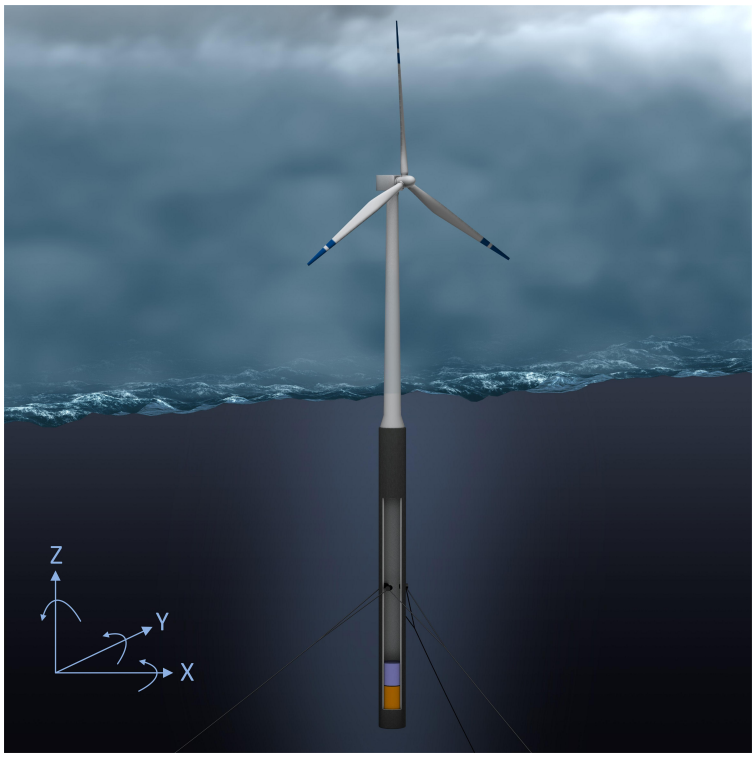

Figure 1.1: Hywind demonstration turbine

In the coming years the offshore wind industry is likely to see a development similar the oil and gas industry, that is, moving installations further from the shore. In the 1970s and 1980s the oil and gas industry saw taller and taller platforms, some stand as high as incredible 400-500 meters above the seabed. Today, no oil company in the world would even consider building such tall platforms. A floating solution is the obvious choice. Offshore conditions offer stronger and more stable wind conditions, which in relation to power production is beneficial. Due to this fact, it is

possible to have fewer and bigger turbines in offshore wind farms than in an onshore wind farm. And, they would be out of harm's way for most people. At the same time, it is evident that the challenge to understand the dynamic behavior of floating turbines are quite different than for bottom-fixed turbines. For this, demonstration turbines need to be deployed and observed, such as Hywind. Also advanced simulation softwares need to be developed and used by industry and institutions. During the last decade, several wind turbine softwares have emerged. In this dissertation FAST has been used. FAST has been developed by the National Renewable Energy Laboratory (NREL) in Denver, US. They also provide a variety of simulation models.

1.1 Wind Turbine Basics

The available power passing through an area A is defined as:

$$P = \frac{1}{2}\rho A v^3, \tag{1.1}$$

where ρ is the air density and v is the wind speed. Obviously, it is not possible to extract all the energy available in the area A with a wind turbine. For this to happen, the wind would have to completely stop after hitting the turbine blades. In (Eggleston and Stoddard, 1987) it is shown that the total useful power extracted by a wind turbine can be formulated as:

$$P_a = C_P(\lambda,\beta)\,P = \frac{1}{2}\rho\pi R^2 C_P(\lambda,\beta)\,v^3, \tag{1.2}$$

where R is the blade radius, $C_P(\lambda,\beta)$ is the power coefficient and depends on λ and blade pitch angle β. λ is defined as the tip-speed-ratio and is defined as: $\lambda = \omega_r R/v$, where ω_r is the rotational velocity of the rotor. C_P indicates the relationship between how much power is available in the wind and how much can be converted to electrical power. It can be proven that the theoretical upper limit for C_P is $16/17 \approx 0.59$, and is known as the Betz limit. The Betz limit is well above what is practically possible. Todays turbines can reach values of about 0.5. The behavior of a typical C_P is illustrated in Fig. 1.2, where several power coefficient values are plotted depending

on the tip-speed-ratio (λ) and the blade pitch angle (β).

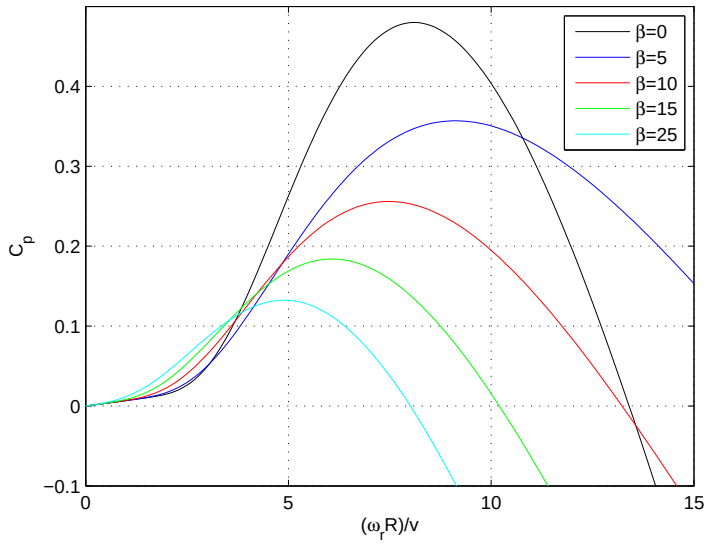

Figure 1.2: Typical C_P curve

Typical wind turbines are built up by five major components; tower, nacelle, rotor, generator and drive train. The nacelle is on top of the tower and houses the drive train and the generator. The drive train is divided into two parts, the low-speed-shaft and the high-speed-shaft. The rotor is attached to the low-speed-shaft and is driven by the wind. The velocity of the low-speed-shaft is geared up typically about hundred times. The low-speed-shaft drives the induction generator and electrical power is produced. Although lately, drive trains without gearboxes are being developed. These are called direct drive solutions, where the wind directly drives a permanent magnet synchronous generator.

In the early days of wind power production, wind turbines operated on fixed speed, stall regulated control. These types of turbines are also known as the Danish-concept. They have to operate at a fixed rotational speed in order for it to be connected to the grid. The frequency of the produced power needs to match the frequency of the grid, for it to be connected. The blades are rigidly fixed to the nacelle and are designed to become aerodynamically stalled at high wind speeds. That is, as the wind speed increases beyond the turbine's rated value, the lift-drag-ratio becomes smaller. It is desirable to have a high lift force and a low drag force. With

this operation method the power can only be maximized at one wind speed. This limits the power output as the wind speed varies. Another disadvantage is the high thrust force on the tower.

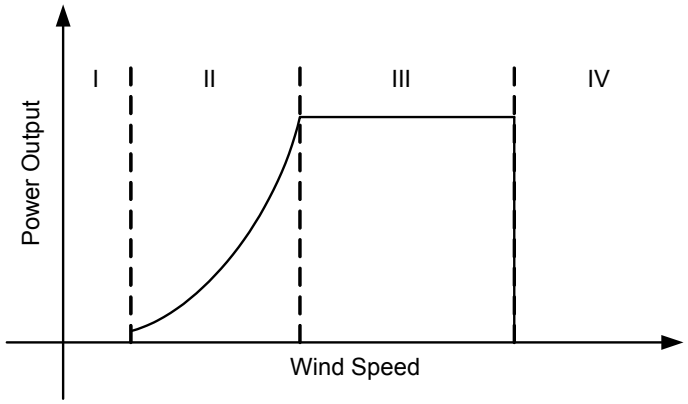

Figure 1.3: Region of operation for a typical wind turbine

A typical modern wind turbine operates as illustrated in Fig. 1.3. These turbines operate with variable-speed and variable-pitch. That is, in region II the generator speed is allowed to vary while the pitch angle is kept constant at some optimal value. The control aim is to maximize the generated power, by controlling the generator torque. By keeping the tip-speed-ratio constant, this can be achieved. When changing the generator torque, one also allows the generator speed to vary. The consequence is that additional power electronics are needed in order to make sure the turbine stays connected to the grid. In region III the control aim is to keep the generator torque constant, by means of pitching the blades. The first and last region in Fig. 1.3 is when the wind speed is too low and too high for energy production, respectively.

The different degrees of freedoms (DOFs) for the floating turbine with reference to the global coordinate system are illustrated in Fig. 1.1. There are six DOFs in total for the tower, three translational and three rotational. They are presented in Table 1.1.

It is tempting to just take a well designed onshore controller and install it on an offshore turbine. In principle one can do this, but there is no guarantee that the closed-loop system will be stable. The major difference between an onshore and an offshore turbine is the natural frequencies. The natural frequencies will decrease

	Translational	Rotational
x-axis	Surge	Pitch
y-axis	Sway	Roll
z-axis	Heave	Yaw

Table 1.1: Tower DOFs for floating turbine

significantly once the turbine is mounted on a floating foundation. In an onshore turbine the lowest tower natural frequency is typically 0.5 [Hz], which is the tower fore-aft bending mode. Once this turbine is put offshore, some additional vibration modes appear. These are much more low frequent, and the lowest natural frequencies are in the area 0.01 - 0.04 [Hz]. When the turbine is designed, the designers already know the wind and wave frequencies in the area, and design the turbine structure accordingly. This is to make sure that the surrounding environment will not excite any of the structure's vibration modes. For bottom-fixed turbines, the soil also plays a major role in relation to the natural frequencies in the structure, as discussed in (AlHamaydeh and Hussain, 2011). A controller for the onshore turbine, typically has a natural frequency of 0.1[Hz], i.e. lower than the tower fore-aft bending mode. If this controller was implemented on the offshore turbine, then the controller would be faster than the tower vibration modes. This can become a stability issue once the wind speed is above rated. One can quite easily visualize why this becomes a problem. It has already been discussed that in the above rated wind speed conditions the controlling variable is the blade pitch angle. When the wind speed increases, the blades will pitch out of the wind in order to not gain higher generator speed. This means that the aerodynamic forces acting on the tower will decrease and it will start to move forward. It is noted that, it is during this motion, that the stability issue occurs and it is directly related to the pitching frequency of the blades. Let us consider two scenarios: 1) the onshore controller is being used, 2) the offshore controller is being used. In the first scenario, the blades are being pitched out of the wind at a higher frequency than the tower is moving forward. The consequence is that the tower will lose most of its aerodynamic damping, known as negative aerodynamic damping. The result is that the tower and eventually the generator will start to oscillate and eventually become unstable. In the second scenario the blades are being pitched out of the wind with a lower frequency than the tower

is moving forward. Therefore, the tower will not lose as much of the aerodynamic damping, and the overall system will maintain its stability.

1.2 Motivation

This project is carried out in conjunction with the Norwegian Center for Offshore Wind Energy (NORCOWE). NORCOWE is an interdisciplinary resource center for exploitation of offshore wind energy as a natural sustainable energy source. The vision of NORCOWE is to combine Norwegian offshore technology and leading Danish and international communities on wind energy in order to provide innovative and cost efficient solutions and technology for large water depths and harsh offshore environments. It is a goal that NORCOWE will help build strong clusters on offshore wind energy in Norway by developing new knowledge and by providing skilled persons for the industry.

In order to maintain and increase the interest from industry, wind turbine modeling and control needs to continue moving forward. Improved models, better controllers and economically feasible solutions will always be a driving force in this industry. This dissertation tries to stay in front of the wind turbine research and contribute with new control strategies for offshore wind turbines.

1.3 Objectives

As discussed in Section 1.1, the control of a floating wind turbine is not a straight forward task. The control objectives in the different regions of operation (Fig. 1.3) have been discussed. The control focus in this dissertation is limited to region III. The focused is on developing new control strategies for a variable speed and variable pitch offshore floating wind turbine. The main emphasis is on multiobjective optimization and multivariable control schemes, which can be adjusted to varying operating conditions and can correct unmodelled dynamics. The floating turbine can be influenced by the coupled dynamics between the tower and the blades, known as negative damping. This needs to be handled in order to maintain the turbine stability. Regarding performance, the controller needs to dampen loads and oscillations

on mechanical parts in the turbine and maintain rated values for speed and power. This indicates that several control objectives should be achieved at the same time, or if not possible, a trade-off between objectives should be achieved. Hence, the use of advanced control techniques should be used in order to get a reliable performance of the control system. Therefore, this dissertation is intended to contribute with new control strategies that incorporate these issues in their formulation and guarantee system stability, robustness and reliability.

1.4 Literature Review

This section will review the state-of-the-art within wind turbine modeling and control of floating wind turbines.

1.4.1 Wind Turbine Modeling

A wind turbine system can be divided into several interconnected subsystems, see Fig. 1.4. The complexity of the subsystems are often related to the control strategy. A model for control purpose should not be overly complicated, but it should still describe the most important dynamics. Which dynamics that are important or not, will differ depending on the control objective.

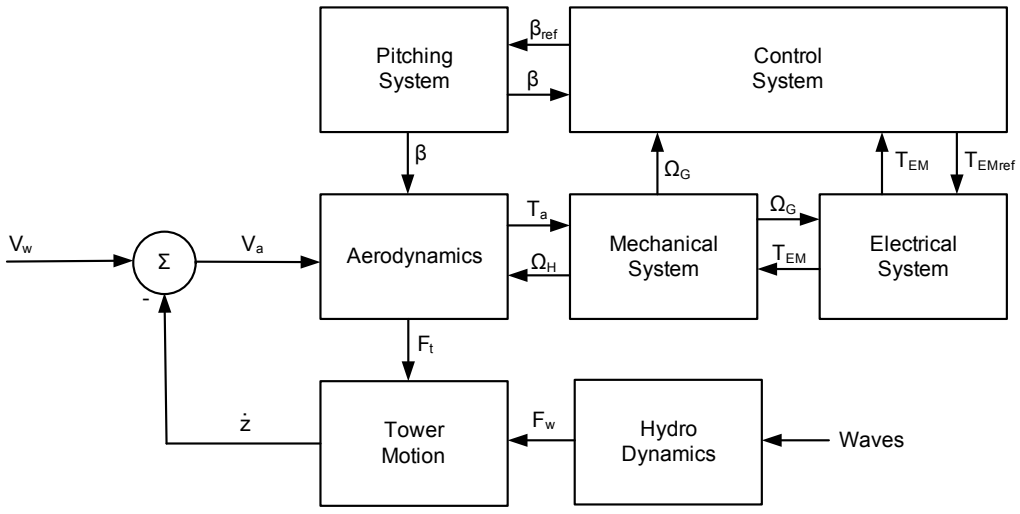

Figure 1.4: Interconnected subsystems

Structure:
The pitching system, tower, mechanical system and the electrical system can essentially be modeled as rigid bodies connected with springs and dampers. The mechanical system is often modeled as two inertias connected with a spring, damper and a gear. These models are in principle quite simple, but serves its purpose in providing a model usable for control design. In order to properly simulate the coupled dynamics in a wind turbine and the dynamic response to wind and wave loading, a more sophisticated approach is needed. During the last decade, several dedicated wind turbine simulation softwares have emerged. These new types of softwares are based on more advanced modeling approaches, such as: multibody dynamics, modal representation or finite element modeling. These approaches makes them more suitable for testing new turbine concepts and new control strategies. Examples of such softwares are FAST (Jonkman, 2010b), HAWC2 (Larsen and Hansen, 2007) and SIMO/RIFLEX. The latter is originally developed for modeling and simulation of offshore structures, but extended by (Fylling et al., 2009) to also include wind turbines. For a more complete overview of existing software for floating wind turbine design tools see (Cordle and Jonkman, 2011). In these softwares it is possible to perform simulations and analysis of the nonlinear equations of motion in time. During simulation, wind turbine aerodynamics, servo dynamics and structural responses to wind-inflow conditions are determined in time. Outputs of simulations include time-series data on the aerodynamic loads as well as loads and deflections of the structural parts of the wind turbine. They also have the capability to extract linearized representations of the nonlinear wind turbine model. In this way it is possible to perform controller design on linear representations of the wind turbine system.

Aerodynamics:
The aerodynamic of the wind turbine describes how much of the incoming wind can be converted to electrical energy and the forces developed on the turbine. There are two major methods to do this; the actuator disc model (Burton et al., 2001) and the blade element theory (Freris, 1990). The first approach regards the turbine as an actuator disk. Based on the area, wind speed and the pressure drop across of the

disk, it is possible to calculate potential energy capture. The second approach includes the geometry of the blades and studies the forces acting on the blades by the incoming wind. In order to get a complete picture of the aerodynamic load experienced by the wind turbine a combination of the two approaches are used, known as blade-element/momentum (BEM) theory. Most of the new available software uses BEM theory for the calculation of the aerodynamic loads.

Hydrodynamics:
Hydrodynamics are essentially a product of the aerodynamics. There is a long term statistical correlation between wind speed, wave height and wave period. That is, high wind speeds are usually followed by increased wave heights, which ultimately lead to larger loads on the floating turbine. The forces acting on the platform can be expressed by:

$$F^{Platform}(t) = -A\ddot{q} - B\dot{q} + F^{Hydro}(t) + F^{Line}(t), \tag{1.3}$$

where A is the added mass matrix, B is the added damping matrix, $F^{Hydro}(t)$ represent the hydrodynamic loads and $F^{Line}(t)$ represent the loads from the mooring lines. The hydrodynamic loads can be explained as a sum of three effects; hydrostatics, diffraction and radiation (Faltinsen, 1990; Newman, 1997). Hydrostatics include the buoyancy effect of the structure and the mooring lines. The diffraction forces occur when the wave field near the floating structure is affected, even if the floating structure is stationary. An unsteady fluid pressure around the structure is the cause of this force. Radiation forces occur when the structure is in motion and there are no incident waves present, i.e. the structure is generating waves which change the fluid pressure around the structure. This is handled by added mass and damping which is dependent on frequency of oscillation, speed forward, etc.

1.4.2 Floating Wind Turbine Control Systems

During the last decades a variety of model based techniques have been developed. These techniques offer a way to formulate the control problem in specific procedures, and make it possible to impose special demands and constraints to the closed

loop system. In classical control this is not possible. Also, classical control is restricted to Single-Input-Single-Output (SISO) systems. To get a wind turbine system to work properly, several sensor signals are used to calculate the appropriate generator torque and the three blade pitch angles. Indeed this makes the wind turbine a Multiple-Input-Multiple-Output (MIMO) system, and modern model based control is therefore preferred. The following section will describe a selection of the existing floating wind turbine control solutions.

In (Jonkman, 2008) and (Larsen and Hanson, 2007) the issue with negative aerodynamic damping at above rated wind speed is handled simply by slowing down the blade pitch controller. This fixes the instability problem in the platform pitch direction, but it also causes unacceptable rotational speed and electrical power variations. The PID controller is calculated based on a simple model of the turbine and by placing the poles of the closed loop system in a preferred area. In (Skaare et al., 2007) and (Skaare et al., 2011) information about the platform's motions are measured and used as an extra input signal to the conventional control system. In this way it is possible to subtract the additional rotor speed oscillations caused by the platform movement from the measured rotor speed. Details related to this control system are confidential. In (Christiansen et al., 2012) a minimum thrust approach is proposed. The thrust is reduced by minimizing the C_T coefficient by means of an LQR controller approach and state estimation. Structural control by utilizing tuned mass damper (TMD) was introduced by (Rotea et al., 2010). The idea is to add the TMD in the nacelle which will influence the pitch motion of the tower and reduce the tower loads. In (Henriksen, 2007) model predictive controller (MPC) was implemented mainly to an onshore wind turbine, but it was also extended to a simple model of a floating wind turbine.

1.5 Organization of the Dissertation

An introduction to how a typical floating wind turbine works and operates, as well as a literature review of wind turbine modeling and control have been given. Chapter 2 describes the modeling and control methods used throughout this dissertation.

Concluding remarks, suggestions for future work and contributions are discussed in Chapter 3. The contributing papers are found appended.

Chapter 2

Research Methodology

This chapter deals with the different modeling and control methods used throughout the dissertation. The formulations are given such that all LMI variables are written with boldface font. $diag\{...\}$ represents a block diagonal matrix. I and 0 represent identity matrix and zero matrix and the superscript T stands for matrix transposition The operator $sym(A)$ denotes $A + A^T$ and $\otimes$ denotes the Kronecker product. The notation $P > 0$ means that P is real symmetric and positive definite; the symbol $*$ denotes the elements below the main diagonal of a symmetric block matrix.

2.1 Wind Turbine Modeling

This section will describe the different modeling approaches performed in the dissertation.

2.1.1 Bond Graph Model

Bond graph is a unified approach to model many types of physical systems, producing both linear and nonlinear mathematical models. Engineers must work and interact in many different disciplines. An understanding of the intersections of these different disciplines is a valuable asset for any engineer. Using the language of bond graph, one may construct models of electrical, magnetic, mechanical, hydraulic, pneumatic as well as thermal systems. The bond graph approach is a systematic way to model dynamic systems, and there are standard ways to translate them into

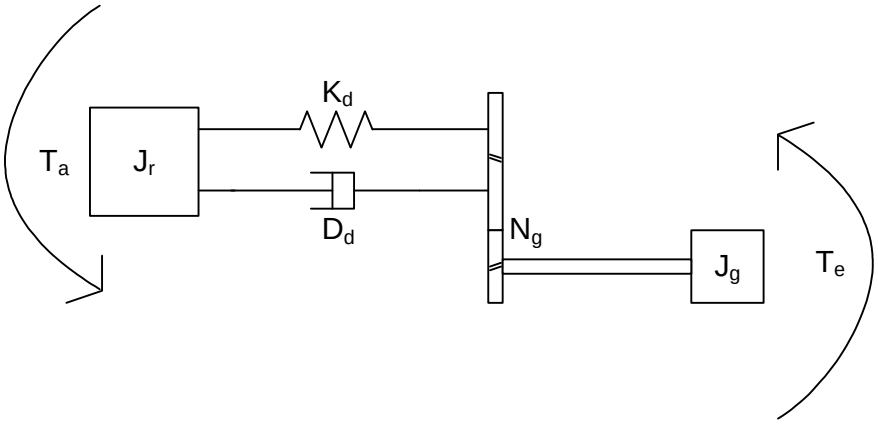

Figure 2.1: Sketch of drivetrain

differential equations or computer simulation schemes. In an educational point of view, bond graph provides a systematic understanding of how the different parts of the turbine works and behaves. An introduction to bond graph modeling is given in the introduction chapter of paper A.

The power is transferred between the different parts in the bond graph model with the use of power bonds. In bond graph notation, the definition of power is effort multiplied with flow. For example, in electric systems this would mean voltage multiplied with current, in mechanical systems it is force multiplied with velocity and in hydraulics it is pressure multiplied with flow.

As a bond graph example, a typical wind turbine drivetrain will now be modeled. The drivetrain can be modeled as two inertias connected with a spring, a damper and a gearbox, see Fig. 2.1. The derivation of the governing equations by utilizing Newtons 2^{nd} law for the drivetrain model is not too hard, since the complexity of the model is fairly low. The equations for the drivetrain model are found to be:

$$T_r = I_r\dot{\omega}_r + \dot{\phi}_\Delta D_d + \phi_\Delta K_d, \tag{2.1}$$

$$-T_g N_g = I_g N_g^2 \frac{\dot{\omega}_g}{N_g} - \dot{\phi}_\Delta D_d - \phi_\Delta K_d, \tag{2.2}$$

where

$$\phi_\Delta = \phi_r - \frac{\phi_g}{N_g}\ ,\ \dot{\phi}_\Delta = \omega_r - \frac{\omega_g}{N_g}. \tag{2.3}$$

The bond graph corresponding to Fig. 2.1 can be seen in Fig. 2.2.

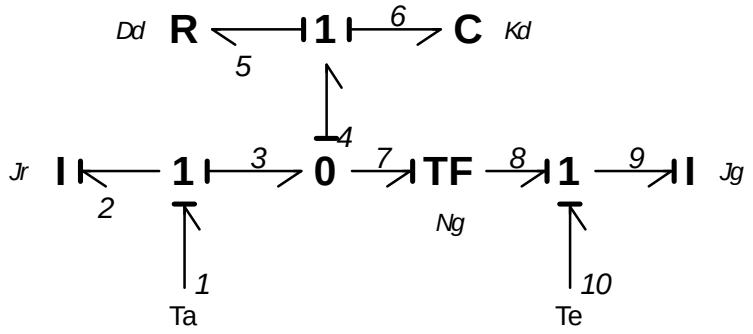

Figure 2.2: Bond graph of drivetrain

The bond graph model consists of three 1-junctions and one 0-junction. The 1-junction connected to the rotor inertia describes the rotor rotational speed. Since there are dynamics in between the rotor inertia and the generator inertia, they do not have the same speed. This is the reason for the 0-junction, because it is known that the transferred torque is the same (no loss included in the drivetrain). The 1-junction connected to the resistive- and the compliance element indicates the rotational speed difference between the two inertias. The connection also indicates that the compliance- and resistive element have the same rotational speed (flow), but different torque (effort). The last 1-junction is connected to the generator inertia and describes the generator rotational speed. The governing equations can be extracted in a specific way, the procedure can also be translated into a computer program. As long as the bond graph is drawn, then the governing equations are relatively easy to obtain either on your own or by a computer program. From the bond graph representation it is seen that there are three dynamic elements, two inertias and one spring. This indicates that three dynamic equations must exist. The equations are formulated in the following way:

$$\dot{p}_2 = e_2 = e_1 - e_3 = T_a - \frac{q_5}{C_6} - R_5 f_5, \tag{2.4}$$

$$\dot{q}_5 = f_5 = f_3 - f_7 = \frac{p_2}{I_2} - \frac{p_9}{N_g I_9}, \tag{2.5}$$

$$\dot{p}_9 \;=\; e_9 \;=\; e_{10} + e_8 = -T_e + \frac{1}{N_g}\left(\frac{q_5}{C_6} + R_5 f_5\right). \tag{2.6}$$

With some manipulations this is exactly the same as described in (2.1)-(2.2)-(2.3). If, for some reasons, the complexity of the drivetrain model were to be increased. That is, more inertias and more springs and dampers. Then it is not straight forward to derive the equations in the classical way. With the bond graph approach it is not more difficult, it will just take a bit more time.

2.1.2 FAST Model

The model under consideration is obtained from FAST (Fatigue, Aerodynamics, Structures and Turbulence). The program is developed at the National Renewable Energy Laboratory (NREL) in Denver, USA. The code models the wind turbine as a combination of both rigid and flexible bodies. These bodies are then connected via several DOFs. The code provides a nonlinear model with up to 24 DOFs. The developers of the software have provided a wide range of wind turbine models. The turbine model used in this dissertation is called OC3-Hywind and is an upscaled model of the Hywind demo floating turbine in Norway. The main specifications are summarized in Table 2.1. More detailed information about the specifications can be found in (Jonkman et al., 2009). Fig. 1.1 shows the floating wind turbine and the global coordinate system. The platform DOFs are also indicated on the figure, they include; translational heave, sway and surge motion and rotational yaw, pitch and roll motions. Heave movement is defined along the z-axis, sway is along the y-axis, and surge is along the x-axis. Yaw motion is defined about z-axis, pitch is about the y-axis and roll is about the x-axis. This adds up to six DOFs. Four more DOFs are related to the tower; two for longitudinal direction and two for lateral direction. Yawing motion of the nacelle provides one DOF. Variable generator- and rotor speeds give another two DOFs, this also includes drivetrain flexibility. Nine DOFs for the blades; three for blade flapwise tip motion for the first mode, three for tip displacement of each blade for the second flapwise mode and another three for the blade edgewise tip displacement for the first edgewise mode. The last two DOFs are for rotor- and tail furl. In total this adds up to 24 DOFs.

A linear model is needed in order to perform linear controller design. Also, the

Rated power	5 [MW]
Rated wind speed	11.6 [m/s]
Rated rotor speed	12.1 [RPM]
Rotor radius	63 [m]
Huh height	90 [m]

Table 2.1: OC3-Hywind basic specifications

model described above is so far too complicated. A linear model with fewer DOFs is needed. The most important dynamics should be represented in the linear model. drivetrain, generator and platform pitch are the selected DOFs. FAST does not include any pitch actuators, these will be added to the model at a later stage. The objective is to obtain a model describing the floating wind turbine system in region III (see Fig. 1.3). In this region the controlling variable is the blade pitch angle.

$$\begin{aligned} \dot{x} &= A_i x + B_i u, \\ y &= Cx, \qquad i = 1,2...,36. \end{aligned} \tag{2.7}$$

The matrices A_i and B_i in the state-space system are behaving in a periodic manner, the matrix values depend on the rotor azimuth angle. This periodic behavior is caused by a combination of several effects, such as aerodynamic loads, tower shadow, gravitational loads and deflection of the tower. The C matrix is not varying since there is no periodic behavior related to the measurements. In paper B the system in (2.7) is converted into an LPV model depending on azimuth angle, and further used for the controller design. A common way to simplify this system, is to take the average of all the 36 models and eventually use this for the controller design. This is what is done in paper C and D. Although, in paper D several linearization points are obtained. That is, one state-space system of the form in (2.7) is obtained at several wind speeds. This is eventually converted into an LPV system depending on wind speed. In this way, one ends up with a model which represents the floating turbine in a wider range of wind speeds.

FAST does not provide any pitch actuators. In papers C and D these are included in the wind turbine model after the linearization and after the average of the model

described in (2.7) is calculated. A typical blade pitch actuator can be modeled as a second order system (2.8).

$$\begin{aligned} \dot{x}_p &= A_p x_p + B_p u, \\ y &= C_p x_p, \end{aligned} \tag{2.8}$$

where

$$A_p = \begin{bmatrix} -2\omega_n\zeta & -\omega_n^2 \\ 1 & 0 \end{bmatrix}, B_p = \begin{bmatrix} 1 \\ 0 \end{bmatrix}, C_p = \begin{bmatrix} 0 & \omega_n^2 \end{bmatrix}.$$

The natural frequency is $\omega_n = 0.88$ and the damping ratio is $\zeta = 0.9$. There is a total of three pitch actuator models in the turbine model, one for each blade. The matrices in (2.9) represent the new state-space matrices, where the pitch actuators are included.

$$A_t = \begin{bmatrix} I_3 \otimes A_p & 0 \\ B \otimes C_p & A \end{bmatrix}, \; B_t = \begin{bmatrix} I_3 \otimes B_p \\ 0 \end{bmatrix}, \; C_t = \begin{bmatrix} 0 & C \end{bmatrix}. \tag{2.9}$$

These matrices are obtained by combining the three pitch actuator state-space models and the wind turbine state-space system. The blade pitch dynamics are now included in the model.

2.1.3 Linear Parameter-Varying Model

The wind turbine characteristics are constantly varying depending on the azimuth angle of the rotor and the wind inflow. In this dissertation two different LPV models are constructed. Paper B deals with the azimuth angle dependent model and paper D deals with the wind speed dependent model. LPV control techniques are a step in between linear control and nonlinear control. The control design is done based on linear techniques and when it is implemented, the benefits from nonlinear control are utilized. That is, it will perform and maintain stability in a larger region of operation.

Azimuth angle dependent model:
In paper B a model which is parameter-dependent on the rotor azimuth angle is presented. After inspecting the set of models in (2.7), it is concluded that they can be represented in a continuously manner by the use of *sine* and *cosine* functions. The two periodic matrices from state-space system (2.7) are now rewritten as:

$$\begin{aligned} A(z) &= A_n + \Delta A(z), \\ B(z) &= B_{2n} + \Delta B(z), \end{aligned} \tag{2.10}$$

where A_n and B_{2n} are the nominal plant matrices, $\Delta A(z)$ and $\Delta B(z)$ are contributing with the varying terms and z is the rotor azimuth angle. $\Delta A(z)$ and $\Delta B(z)$ are defined in the following way:

$$\begin{aligned} \Delta A(z) &= \sum_{i=1}^{2}\sum_{j=1}^{2} F_i \Delta_j(z) E_{jia}, \\ \Delta B(z) &= \sum_{i=1}^{2}\sum_{j=1}^{2} F_i \Delta_j(z) E_{jib}, \end{aligned} \tag{2.11}$$

where the matrices $\left(F_i,\, E_{jia},\, E_{jib}\right)$ have appropriate dimensions and values, $\Delta_1(z)$ and $\Delta_2(z)$ are $sin(\omega t)$ and $\cos(\omega t)$, respectively. In this way a continuous representation of the state-space system in (2.7) is obtained. The reason for formulating the LPV in such a way, is related to the controller design procedure.

Wind speed dependent model:
In paper D a model which is parameter-dependent on the wind speed is presented. Now the wind turbine system is linearized about several operating points. A set of nine operating points are obtained, ranging from 14 [m/s] to 22 [m/s]. The state-space systems are of the following standard form:

$$\begin{aligned} \dot{x} &= A_i x + B_i u, \\ y &= Cx, \qquad i = 1, 2 \ldots 9. \end{aligned} \tag{2.12}$$

The major difference between (2.7) and (2.12) is that the latter does not have any periodic behavior and it also represents the wind turbine system in a larger region of operation, in relation to wind speed. In (2.13) the varying matrices in (2.12) are represented in a continuous manner where σ is the wind speed.

$$\begin{aligned} A(\sigma) &= A_a + \sigma A_b, \\ B(\sigma) &= B_a + \sigma B_b, \end{aligned} \tag{2.13}$$

where the scalar parameter satisfies $\underline{\sigma} \leq \sigma(t) \leq \overline{\sigma}$ and $\underline{\rho} \leq \dot{\sigma}(t) \leq \overline{\rho}$. The matrices $(A_a,\, A_b,\, B_a,\, B_b)$ are found using least square method.
Pitch actuators are added to the system in the same way as in (2.9).

$$\begin{aligned} A_{aug}(\sigma) &= \begin{bmatrix} I_3 \otimes A_p & 0 \\ B_a \otimes C_p & A_a \end{bmatrix} + \sigma \begin{bmatrix} 0 & 0 \\ B_b \otimes C_p & A_b \end{bmatrix}, \\ B_{aug} &= \begin{bmatrix} I_3 \otimes B_p \\ 0 \end{bmatrix}, \\ C_{aug} &= \begin{bmatrix} 0 & C \end{bmatrix}. \end{aligned} \tag{2.14}$$

The new model is now wind speed dependent. It is rarely possible to obtain accurate measurements of the wind speed, this parameter will therefore be estimated. Wind speed estimation will be discussed in the next section.

2.1.4 Wind Speed Estimation

It is possible to estimate the effective wind speed based on measurements from the wind turbine. In this specific case the measurements are rotor speed, blade pitch angle and generator torque. The effective wind speed represents the wind field averaged over the rotor disc, i.e what is experienced by the blades. An extended Kalman filter is used based on a simple model of the drivetrain and a turbulence model, the output from the extended Kalman filter is the effective wind speed. For the actual development of the filter readers are referred to (Knudsen et al., 2011).
Both the drivetrain and the wind model are modeled as first order systems with no

losses.

$$
\begin{aligned}
J_{eq}\dot{\Omega}_{DT} &= T_a - T_g, && (2.15)\\
\dot{v}_t &= -\frac{\pi v_m}{2L} + n_1, && (2.16)\\
\dot{v}_m &= n_2, && (2.17)\\
\sigma &= v = v_m + v_t, && (2.18)
\end{aligned}
$$

where $J_{eq} = J_r + n_g^2 J_g$, $T_g = T_e n_g$, v_t is turbulence, v_m is the mean wind speed and L is the turbulence length scale parameter. The wind model is driven by Gaussian white noise, entering the model by n_1 and n_2. This model is nonlinear due to the nonlinear relationship between wind speed and aerodynamic torque. In order to estimate the states, the time update uses information about the model dynamics and the model uncertainties.

$$
\begin{aligned}
\hat{x}_k^- &= A_{ekf}\hat{x}_{k-1} + B_{ekf}u_{k-1}, && (2.19)\\
P_k^- &= A_{ekf}P_{k-1}A_{ekf}^T + Q, && (2.20)
\end{aligned}
$$

where matrices $\left(A_{ekf},\, B_{ekf},\, C_{ekf}\right)$ are state-space matrices of a linearized version of (2.15)-(2.16)-(2.17), Q is incremental process noise covariance and P_k is the state estimate error covariance. The measurement update uses information about the model outputs and measurement noise.

$$
\begin{aligned}
K_k &= P_k^- C_{ekf}^T \left(C_{ekf}P_k^- C_{ekf}^T + R\right), && (2.21)\\
\hat{x}_k &= \hat{x}_k^- + K_k\left(z_k - C_{ekf}\hat{x}_k^-\right), && (2.22)\\
P_k &= \left(I - K_k C_{ekf}\right)P_k^-, && (2.23)
\end{aligned}
$$

where R is measurement noise covariance, K_k is the Kalman gain and z_k is the measurements.

2.2 Control Synthesis

This section describes the system representation and the different control approaches which are used throughout the dissertation.

First of all, the model needs to be formulated on the generalized form (2.24). As seen from Section 2.1 the model description differs depending on the control synthesis.

$$\begin{aligned} \dot{x} &= Ax + Bu + B_w\omega, \\ z &= C_z x + D_z u, \\ y &= Cx + D_w\omega, \end{aligned} \tag{2.24}$$

where the additional terms B_w and D_w describe how the disturbance enter the system. C_z and D_z handle the signals of interest/performance measures, i.e. the controller objectives.

2.2.1 H_∞ Control

The closed-loop H_∞ norm of a transfer function from disturbance to signal of interest is defined in (2.25).

$$||T_{cl}||_\infty < \gamma. \tag{2.25}$$

In order to formulate the H_∞ norm in terms of a matrix inequality, some manipulations to its original expression are needed. The ∞-norm of a closed-loop system is the same as taking the 2-norm of the signal of interest z divided by the 2-norm of the systems exogenous input ω. First, lets define the Lyapunov stability criteria. A linear state-space system is asymptotically stable if all real parts of the eigenvalues of the A-matrix are negative. The Lyapunov criteria involve searching for the matrix $\mathbf{P}$. If it exists, then the system is stable. A quadratic Lyapunov function is defined in (2.26) and its derivative in (2.27).

$$V(t) = x^T\mathbf{P}x, \tag{2.26}$$

$$\dot{V}(t) = \dot{x}^T\mathbf{P}x + x^T\mathbf{P}\dot{x}. \tag{2.27}$$

The first crucial steps in obtaining the bounded real lemma (BRL) under zero initial condition are shown next. Firstly, remove the roots by squaring both sides of the inequality sign. Secondly, collect everything in one integral expression and lastly do the trick where the Lyapunov function is added and subtracted to the inequality. This can be done because it is known that: $\int_0^\infty \dot{V}(t)\mathrm{d}t - V(\infty) + V(0) = 0$ is true. In this way, only an integral expression is obtained.

$$
\begin{aligned}
& \sup_{\omega \neq 0} \frac{||z||_2}{||\omega||_2} < \gamma \;\Rightarrow\; \left[\int_0^\infty z^T z \,\mathrm{d}t\right]^{\frac{1}{2}} < \gamma \left[\int_0^\infty \omega^T \omega \,\mathrm{d}t\right]^{\frac{1}{2}} \\
\Rightarrow\; & \int_0^\infty \left(\frac{1}{\gamma} z^T z - \gamma \omega^T \omega\right) \mathrm{d}t \\
\leq\; & \int_0^\infty \left(\frac{1}{\gamma} z^T z - \gamma \omega^T \omega + \dot{V}(t)\right) \mathrm{d}t - \underbrace{V(\infty)}_{\textit{Always positive}} \underbrace{+V(0)}_{\textit{Always zero}} \\
\leq\; & \int_0^\infty \left(\frac{1}{\gamma} z^T z - \gamma \omega^T \omega + \dot{V}(t)\right) \mathrm{d}t. \qquad (2.28)
\end{aligned}
$$

Now, insert both the expressions for the signal of interest z from (2.24) and the derivative of the Lyapunov function $\dot{V}(t)$ (2.27) into (2.28). With some algebraic and matrix manipulations, the following matrix inequality is obtained. Also known as the BRL.

$$
\begin{aligned}
\begin{pmatrix} A^T\mathbf{P} + \mathbf{P}A & \mathbf{P}B_w & C_z^T \\ * & -\gamma I & 0 \\ * & * & -\gamma I \end{pmatrix} &< 0, \\
\mathbf{P} &> 0. \qquad (2.29)
\end{aligned}
$$

State-Feedback:

Papers C and D are based on the state-feedback LMI formulation. However, an output-feedback formulation is obtained using a change of variables. This will be discussed in more details in Section 2.2.2. First, the state-feedback formulation will be reviewed.

In state-feedback all states in the system are assumed measurable and available for

feedback. If this is not possible, there are procedures to observe or estimate these unavailable states, see for example (Grewal and Andrews, 2001). A static output-feedback controller can be formulated in the following way:

$$u = Kx, \tag{2.30}$$

where u is the calculated control signal, K is the gain and x is the state variable. Before it is possible to calculate the controller gain, the closed-loop state-space system needs to be found:

$$\left(\begin{array}{c|c} A_{cl} & B_{cl} \\ \hline C_{cl} & D_w \end{array}\right) = \left(\begin{array}{c|c} A+BK & B_w \\ \hline C_z+D_zK & 0 \end{array}\right). \tag{2.31}$$

It is noted that in (2.31) D_w is zero. Now the system in (2.31) can be included in (2.29). It is not yet a linear matrix inequality because of the nonlinear multiplication which occurs when the feedback loop is closed. This can be handled by performing congruence transformation with $diag\{\mathbf{P}^{-1},\ I,\ I\}$ on the BRL and performing the substitution $\mathbf{X} = \mathbf{P}^{-1}$ and $\mathbf{Y} = K\mathbf{P}^{-1}$. The final LMI is as follows:

$$\begin{array}{rcl} \left(\begin{array}{ccc} sym\,(A\mathbf{X}+B\mathbf{Y}) & B_w & (C_z\mathbf{X}+D_z\mathbf{Y})^T \\ * & -\gamma I & 0 \\ * & * & -\gamma I \end{array}\right) & < & 0, \\ \mathbf{X} & > & 0. \end{array} \tag{2.32}$$

By minimizing γ, the LMI variables can be obtained and the controller gain can be calculated from the following expression:

$$K = \mathbf{Y}\mathbf{X}^{-1}. \tag{2.33}$$

Output-feedback:
In paper B a dynamic output-feedback controller is designed for the parameter-varying system described in (2.10). The controller has the following form:

$$\dot{\zeta} \;=\; A_k\zeta + B_k y,$$

$$u = C_k\zeta + D_k y, \tag{2.34}$$

where ζ is the states, y is the outputs from the state-space system, u is the calculated control signal and the matrices $(A_k,\ B_k,\ C_k,\ D_k)$ are the controller state-space matrices.

Since the state-space system is parameter-varying, the closed-loop system is divided into two parts, see (2.35). One part which handles the constant state-space matrices and one part which handles the parameter-varying matrices. It must also be mentioned that in this formulation the disturbance is also added to the signals of interest, denoted as D_{zw}.

$$\begin{aligned}
\left(\begin{array}{c|c} A_{cl} & B_{cl} \\ \hline C_{cl} & D_{cl} \end{array}\right) &= \left(\begin{array}{c|c} A_{cl1} & B_{cl1} \\ \hline C_{cl1} & D_{cl1} \end{array}\right) + \left(\begin{array}{c|c} A_{cl2}(z) & B_{cl2}(z) \\ \hline 0 & 0 \end{array}\right) \\
&= \left(\begin{array}{cc|c} A_n + B_{2n}D_kC & B_{2n}C_k & B_w + B_{2n}D_kD_w \\ B_kC & A_k & B_kD_w \\ \hline C_z + D_zD_kC & D_zC_k & D_{zw} + D_zD_kD_w \end{array}\right) \\
&+ \left(\begin{array}{cc|c} \Delta A(z) + \Delta B(z)D_kC & \Delta B(z)C_k & \Delta B(z)D_kD_w \\ 0 & 0 & 0 \\ \hline 0 & 0 & 0 \end{array}\right).
\end{aligned} \tag{2.35}$$

Because of the parameter-varying state-space matrices an additional term to the standard BRL is also necessary. This additional term is the second part of the summation in constraint (2.36). In order for the controller to guarantee stability and performance, the H_∞ norm of the closed-loop transfer function must not exceed γ. This is true if and only if there exists a symmetric matrix $\mathbf{X}$ such that

$$\begin{aligned}
&\begin{pmatrix} A_{cl1}^T\mathbf{X} + \mathbf{X}A_{cl1} & \mathbf{X}B_{cl1} & C_{cl1}^T \\ * & -\gamma I & D_{cl1}^T \\ * & * & -\gamma I \end{pmatrix} \\
&+ \begin{pmatrix} A_{cl2}^T(z)\mathbf{X} + \mathbf{X}A_{cl2}(z) & \mathbf{X}B_{cl2}(z) & 0 \\ * & 0 & 0 \\ * & * & 0 \end{pmatrix} < 0, \\
&\mathbf{X} > 0.
\end{aligned} \tag{2.36}$$

Again, the matrix inequality in (2.36) is not yet linear because of the nonlinear terms which occur when the feedback loop is closed. A change of variables is the remedy in the output-feedback case as well. Although, a set of slightly more sophisticated variables are needed. A second challenge is the parameter-varying terms. A proper LMI can not have parameters which are varying. These two issues will now be handled.

First the new matrices $\mathbf{P}$ and $\mathbf{P}^{-1}$ are defined and partitioned in the following way (Scherer et al., 1997):

$$\mathbf{P} = \begin{bmatrix} \mathbf{X} & N \\ N^T & \# \end{bmatrix}, \qquad \mathbf{P}^{-1} = \begin{bmatrix} \mathbf{Y} & M \\ M^T & \# \end{bmatrix}, \tag{2.37}$$

where $\mathbf{X}$ and $\mathbf{Y}$ are symmetric matrices of dimension $\Re^{n \times n}$. N and M will be calculated on the basis of $\mathbf{X}$ and $\mathbf{Y}$. The matrices noted as # are not necessary to be known. In addition, two additional matrices are defined:

$$\Pi_1 = \begin{bmatrix} \mathbf{Y} & I \\ M^T & 0 \end{bmatrix}, \qquad \Pi_2 = \begin{bmatrix} I & \mathbf{X} \\ 0 & N^T \end{bmatrix} \tag{2.38}$$

as can be inferred from the identity $\mathbf{P}\mathbf{P}^{-1} = I$ satisfying

$$\mathbf{P}\Pi_1 = \Pi_2. \tag{2.39}$$

Now, the following change of controller variables are defined

$$\begin{aligned} \hat{\mathbf{A}} &= NA_kM^T + NB_kC_2\mathbf{X} + \mathbf{Y}B_{2n}C_kM^T \\ &\quad + \mathbf{Y}\left(A_n + B_{2n}D_kC_2\right)\mathbf{X}, && (2.40) \\ \hat{\mathbf{B}} &= NB_k + \mathbf{Y}B_{2n}D_k, && (2.41) \\ \hat{\mathbf{C}} &= C_kM^T + D_kC_2\mathbf{X}, && (2.42) \\ \hat{\mathbf{D}} &= D_k. && (2.43) \end{aligned}$$

To take away the nonlinearities in (2.36), a congruence transformation with $diag\,(\Pi_1, I, I)$ on the matrix inequality (2.36) is performed. The result is the matrix inequality in (2.44). This expression is now linear, but the issue with the parameter-varying matrices is still present.

$$\begin{aligned}\Sigma_1 \;&+\; sym(G_1\Delta_1(z)H_1) + sym(G_2\Delta_1(z)H_1)\\ &+\; sym(G_1\Delta_1(z)H_2) + sym(G_2\Delta_1(z)H_2)\\ &+\; sym(G_3\Delta_2(z)H_3) + sym(G_4\Delta_2(z)H_3)\\ &+\; sym(G_3\Delta_2(z)H_4) + sym(G_4\Delta_2(z)H_4) < 0, \end{aligned} \tag{2.44}$$

where the matrix Σ_1 and the vectors G_i and H_i are defined in the following way:

$$\Sigma_1 = \begin{pmatrix} sym\left(A\mathbf{X} + B_{2n}\hat{\mathbf{C}}\right) & \hat{\mathbf{A}}^T + A + B_{2n}\hat{\mathbf{D}}C & B_w + B_{2n}\hat{\mathbf{D}}D_{zw} & \mathbf{X}C_z^T + \hat{\mathbf{C}}^T D_{zw}^T \\ * & sym\left(\mathbf{Y}A + \hat{\mathbf{B}}C_2\right) & \mathbf{Y}B_w + \hat{\mathbf{B}}D_{zw} & C_z^T + C^T\hat{\mathbf{D}}^T + D_z^T \\ * & * & -\gamma I & D_{zw}^T + D_{zw}^T\hat{\mathbf{D}}D_z^T \\ * & * & * & -\gamma I \end{pmatrix},$$

$$\begin{aligned} G_1 &= [F_1 \;\; 0_{1\times 8}]^T, \;\; G_2 = [0_{1\times 6} \;\; \mathbf{Y}F_1 \;\; 0_{1\times 2}]^T,\\ G_3 &= [F_2 \;\; 0_{1\times 8}]^T, \;\; G_4 = [0_{1\times 6} \;\; \mathbf{Y}F_2 \;\; 0_{1\times 2}]^T,\\ H_1 &= \left[E_{11a}\mathbf{X} + E_{11b}\hat{\mathbf{C}} \;\; E_{11a} + E_{11b}\hat{\mathbf{D}}C_2 \;\; E_{11b}\hat{\mathbf{D}}D_{21} \;\; 0\right],\\ H_2 &= \left[E_{12a}\mathbf{X} + E_{12b}\hat{\mathbf{C}} \;\; E_{12a} + E_{12b}\hat{\mathbf{D}}C_2 \;\; E_{12b}\hat{\mathbf{D}}D_{21} \;\; 0\right],\\ H_3 &= \left[E_{21a}\mathbf{X} + E_{21b}\hat{\mathbf{C}} \;\; E_{21a} + E_{21b}\hat{\mathbf{D}}C_2 \;\; E_{21b}\hat{\mathbf{D}}D_{21} \;\; 0\right],\\ H_4 &= \left[E_{22a}\mathbf{X} + E_{22b}\hat{\mathbf{C}} \;\; E_{22a} + E_{22b}\hat{\mathbf{D}}C_2 \;\; E_{22b}\hat{\mathbf{D}}D_{21} \;\; 0\right]. \end{aligned}$$

To remove the parameter-varying part of the matrix inequality the following lemma is used:

Lemma 1 (Khargonekar et al., 1990)*:* Given $\Sigma = \Sigma^T$, G, Δ and H of appropriate dimensions with $\Delta^T\Delta \leq I$, then the matrix inequality

$$\Sigma + sym(G\Delta H) < 0$$

holds for all Σ if and only if there exists a scalar $\varepsilon > 0$ such that

$$\Sigma + \varepsilon GG^T + \varepsilon^{-1} H^T H < 0.$$

By utilizing Lemma 1 it is possible to remove the parameter-varying parts $\Delta_i(z)$ in the matrix inequality (2.44). A new matrix inequality which contains the constants ε_1 and ε_2 are obtained.

$$\begin{aligned} \Sigma_1 &+ 2\varepsilon_1 G_1 G_1^T + 2\varepsilon_1^{-1} H_1^T H_1 + 2\varepsilon_1 G_2 G_2^T + 2\varepsilon_1^{-1} H_2^T H_2 \\ &+ 2\varepsilon_2 G_3 G_3^T + 2\varepsilon_2^{-1} H_3^T H_3 + 2\varepsilon_2 G_2 G_4^T + 2\varepsilon_2^{-1} H_4^T H_4 < 0. \end{aligned} \tag{2.45}$$

By using the Schur complement, the inequality in (2.45) is converted into the inequality in (2.46). The set of LMIs needed to solve the H_∞ problem are as follows:

$$\begin{pmatrix} \Sigma_1 & \Sigma_2 \\ * & \Sigma_3 \end{pmatrix} < 0, \tag{2.46}$$

$$\begin{pmatrix} X & I \\ I & Y \end{pmatrix} > 0, \tag{2.47}$$

where

$$\begin{aligned} \Sigma_2 &= \begin{bmatrix} \varepsilon_1 G_1 & H_1^T & \varepsilon_1 G_2 & H_2^T & \varepsilon_2 G_3 & H_3^T & \varepsilon_2 G_4 & H_4^T \end{bmatrix}, \\ \Sigma_3 &= diag\{ -\tfrac{1}{2}\varepsilon_1 I_{2\times 2}, -\tfrac{1}{2}\varepsilon_1 I_{2\times 2}, -\tfrac{1}{2}\varepsilon_1 I_{2\times 2}, -\tfrac{1}{2}\varepsilon_1 I_{2\times 2}, \\ &\quad -\tfrac{1}{2}\varepsilon_2 I_{2\times 2}, -\tfrac{1}{2}\varepsilon_2 I_{2\times 2}, -\tfrac{1}{2}\varepsilon_2 I_{2\times 2}, -\tfrac{1}{2}\varepsilon_2 I_{2\times 2} \ \}. \end{aligned} \tag{2.48}$$

Pole placement:
An LMI region is any convex subset D of the complex plane that can be characterized as an LMI in z and $\bar{z}$ (Chilali and Gahinet, 1996) as follows:

$$D = \{z \in C : \bar{L} + \bar{M} z + \bar{M}^T \bar{z} < 0\}, \tag{2.49}$$

for some fixed real matrices $\bar{M}$ and $\bar{L} = \bar{L}^T$, where $\bar{z}$ is a complex number. This class of regions encompasses half planes, strips, conic sectors, disks, ellipses, and

any intersection of the above. From (Chilali and Gahinet, 1996), it is found that, all eigenvalues of the matrix A is in the LMI region $\{z \in C : [\bar{l}_{ij} + \bar{m}_{ij} z + \bar{m}_{ji} \bar{z}]_{i,j} < 0\}$ if and only if there exists a symmetric matrix X such that

$$\left[\bar{l}_{ij}\mathbf{X} + \bar{m}_{ij} A^T \mathbf{X} + \bar{m}_{ji} \mathbf{X} A\right]_{i,j} < 0, \qquad \mathbf{X} > 0. \tag{2.50}$$

The same issue appears for the pole placement constraint as for the output-feedback constraint. The change of variables and removing the parameter-varying terms needs to be done. This is performed in (2.51). The LMI is obtained in a manner similar to the one that was used for the H_∞ constraint.

$$\begin{pmatrix} \Sigma_4 & \Sigma_5 \\ * & \Sigma_3 \end{pmatrix} < 0, \tag{2.51}$$

where

$$\Sigma_5 = \begin{bmatrix} \varepsilon_1 P_1 & N_1^T & \varepsilon_1 P_2 & N_2^T & \varepsilon_2 P_3 & N_3^T & \varepsilon_2 P_4 & N_4^T \end{bmatrix},$$

$$\begin{aligned} \Sigma_4 = \Bigg(\bar{L} \otimes \begin{pmatrix} \mathbf{X} & I \\ I & \mathbf{Y} \end{pmatrix} + \bar{M} \otimes \begin{pmatrix} A\mathbf{X} + B_{2n}\hat{\mathbf{C}} & A + B_{2n}\hat{\mathbf{D}}C_z \\ \hat{\mathbf{A}} & \mathbf{Y}A + \hat{\mathbf{B}}C_z \end{pmatrix} \\ + \bar{M}^T \otimes \begin{pmatrix} A\mathbf{X} + B_{2n}\hat{\mathbf{C}} & A + B_{2n}\hat{\mathbf{D}}C_z \\ \hat{\mathbf{A}} & \mathbf{Y}A + \hat{\mathbf{B}}C_z \end{pmatrix}^T \Bigg), \end{aligned}$$

$$\begin{aligned} G_1 &= [F_1 \ 0_{1\times 6}]^T, \ G_2 = [0_{1\times 6} \ \mathbf{Y}F_1]^T, \ G_3 = [F_2 \ 0_{1\times 6}]^T, \\ G_4 &= [0_{1\times 6} \ \mathbf{Y}F_2]^T, \ H_{1-2} = \left[E_{11a}\mathbf{X} + E_{11b}\hat{\mathbf{C}} \ E_{11a} + E_{11b}\hat{\mathbf{D}}C_2\right], \\ H_{2-2} &= \left[E_{12a}\mathbf{X} + E_{12b}\hat{\mathbf{C}} \ E_{12a} + E_{12b}\hat{\mathbf{D}}C_2\right], \\ H_{3-2} &= \left[E_{21a}\mathbf{X} + E_{21b}\hat{\mathbf{C}} \ E_{21a} + E_{21b}\hat{\mathbf{D}}C_2\right], \\ H_{4-2} &= \left[E_{22a}\mathbf{X} + E_{22b}\hat{\mathbf{C}} \ E_{22a} + E_{22b}\hat{\mathbf{D}}C_2\right], \ N_1 = I_{2\times 2} \otimes H_{1-2}, \\ N_2 &= I_{2\times 2} \otimes H_{2-2}, \ N_3 = I_{2\times 2} \otimes H_{3-2}, \ N_4 = I_{2\times 2} \otimes H_{4-2}, \\ H_1 &= M \otimes G_{1-2}, \ H_2 = M \otimes G_{2-2}, \ H_3 = M \otimes G_{3-2}, \ H_4 = M \otimes G_{4-2}. \end{aligned}$$

Remark 1. It is observed that the inequalities (2.46), (2.47) and (2.51) are linear in $\left(\mathbf{X},\ \mathbf{Y},\ \hat{\mathbf{A}},\ \hat{\mathbf{B}},\ \hat{\mathbf{C}},\ \hat{\mathbf{D}}\right)$ and thus the standard LMI techniques can be exploited to find the LMI solutions. It is also seen from the above results that there exists much freedom contained in the design of control law, such as the choices of appropriate ε_1 and ε_2. This design freedom can be exploited to achieve other desired closed-loop properties.

The desired region D is a disk (Fig. 2.3), with center located along the x-axis (distance q from the origin) and radius r. This determines the region

$$D = \begin{pmatrix} -r & q+z \\ q+\bar{z} & -r \end{pmatrix}. \tag{2.52}$$

From this expression the matrices $\bar{L}$ and $\bar{M}$ are found, which are the two matrices that determine the LMI region.

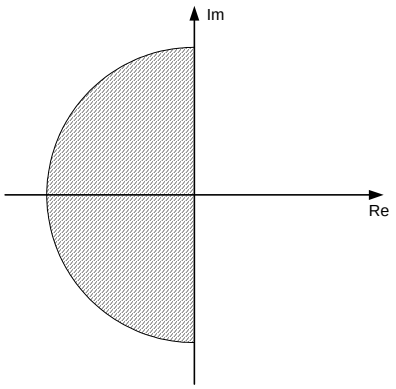

Figure 2.3: LMI region D

All constraints in (2.46), (2.47) and (2.51) are now subjected to the minimization of the objective function, which is the H_∞-norm. They need to be solved in terms of $\left(\mathbf{X},\ \mathbf{Y},\ \hat{\mathbf{A}},\ \hat{\mathbf{B}},\ \hat{\mathbf{C}},\ \hat{\mathbf{D}}\right)$.

Once all these matrices are obtained, the controller matrices are computed in the following way. First, obtain M and N from the factorization problem

$$MN^T = I - \mathbf{XY}. \tag{2.53}$$

This relationship can be solved by utilizing the singular value decomposition (SVD). It is known that s_d is a diagonal matrix and a new matrix $\bar{s}_d$ is defined, which is the square root of all the entries in s_d. In this way it is possible to find the matrices M and N as shown below.

$$\begin{aligned} svd(I-\mathbf{XY}) &= us_dv^T, && (2.54)\\ \bar{s}_d &= diag\{sqrt(s_d)\}, && (2.55)\\ M &= u\bar{s}_d, && (2.56)\\ N^T &= \bar{s}_dv^T. && (2.57) \end{aligned}$$

Second, the controller matrices are computed from the following relationship:

$$\begin{aligned} D_k &= \hat{\mathbf{D}}, && (2.58)\\ C_k &= \left(\hat{\mathbf{C}}-D_kC_2\mathbf{X}\right)\left(M^T\right)^{-1}, && (2.59)\\ B_k &= N^{-1}\left(\hat{\mathbf{B}}-\mathbf{Y}B_{2n}D_k\right), && (2.60)\\ A_k &= N^{-1}\left(\hat{\mathbf{A}}-NB_kC_2\mathbf{X}-\mathbf{Y}B_{2n}C_kM^T\right.\\ &- \left.\mathbf{Y}\left(A_n+B_{2n}D_kC_2\right)\mathbf{X}\right)\left(M^T\right)^{-1}. && (2.61) \end{aligned}$$

Once the controller matrices are obtained, the closed-loop system can be formed and simulations can be carried out.

2.2.2 Constrained Information

Constrained information means that not all the information available in the feedback loop is used by the controller. There can be several reasons for this, e.g. some of the information is simply not needed, some of the sensors are especially prone to failure, switching between controllers and they do not need the same information, etc. This can be achieved by forcing the LMI variables to possess a prescribed zero-nonzero structure. In papers C and D this issue is discussed. The controller is a static output-feedback H_∞ controller. As discussed in Section 2.2.1, state-feedback is relatively easy to handle. However, the output gain matrix is not computed as easily. In the output-feedback case, the gain matrix is not directly isolated from the

other LMI variables. In (Zečević and Šiljak, 2004, 2008, 2010) they propose an explicit solution for the gain matrix and in (Rubió-Massegú et al., 2012) they have found an even simpler solution. With the solution found in (Rubió-Massegú et al., 2012), it is possible to impose zero-nonzero constraints on the LMI variables.

Given a state-space system with matrices as in (2.9), the following representation of the H_∞ constraint can be used:

$$\begin{pmatrix} sym\left(A_t\mathbf{X}+B_t\mathbf{Y}\right)+\gamma^{-2}B_wB_w^T & \left(C_z\mathbf{X}+D_z\mathbf{Y}\right)^T \\ * & -I \end{pmatrix} < 0, \qquad \mathbf{X} > 0. \tag{2.62}$$

The formulation is exactly the same as the inequality in (2.32). This can be checked utilizing the Schur complement. For the state-feedback case, the gain matrix is calculated as $\tilde{K} = \mathbf{Y}\mathbf{X}^{-1}$. In the output-feedback case, the state gain matrix factors as the product $\tilde{K} = KC_t$. Now, when the output gain matrix is required, a solution to (2.62) needs to be found such that the product $\mathbf{Y}\mathbf{X}^{-1}$ factors as

$$\mathbf{Y}\mathbf{X}^{-1} = KC_t. \tag{2.63}$$

To solve this, (Rubió-Massegú et al., 2012) suggests the following change of variables

$$\mathbf{X} = Q\mathbf{X}_Q Q^T + R\mathbf{X}_R R^T, \tag{2.64}$$

$$\mathbf{Y} = \mathbf{Y}_R R^T, \tag{2.65}$$

where $\mathbf{X}_Q$ and $\mathbf{X}_R$ are symmetric matrices with dimensions $\Re^{(n-m)\times(n-m)}$ and $\Re^{m\times m}$, respectively, and $\mathbf{Y}_R$ has dimension $\Re^{p\times m}$. The matrix Q is the nullspace of C_t and R can be calculated as follows:

$$R = C_t^T\left(C_tC_t^T\right)^{-1} + QL, \tag{2.66}$$

where L is an arbitrary matrix with dimensions $\Re^{(n-m)\times m}$.
In papers C and D the main focus is to calculate a gain matrix with diagonal struc-

ture, it is completely up to the designer to decide on the zero-nonzero pattern in the matrix. In order to obtain a diagonal structure on the gain, simply force a diagonal structure on $\mathbf{X}_R$ and $\mathbf{Y}_R$, that is:

$$\mathbf{X}_R = diag\{\mathbf{X}_{R1}, \mathbf{X}_{R2}, \mathbf{X}_{R3}\}, \tag{2.67}$$

$$\mathbf{Y}_R = diag\{\mathbf{Y}_{R1}, \mathbf{Y}_{R2}, \mathbf{Y}_{R3}\}. \tag{2.68}$$

When these structure constraints are imposed on the LMI variables, $\mathbf{X}_Q$ is a full matrix.
In order to solve the LMI (2.62), first define $\nu = \gamma^{-2}$. Then maximize ν and solve the LMI in terms of $\mathbf{X}_Q, \mathbf{X}_R, \mathbf{Y}_R$. Once $\mathbf{X}$ and $\mathbf{Y}$ from (2.64-2.65) are calculated it is possible to find the gain matrix $K = \mathbf{Y}_R \mathbf{X}_R^{-1}$, satisfying $\mathbf{Y}\mathbf{X}^{-1} = KC_t$. Additional information and proofs about this can be found in the aforementioned references.

In paper D this methodology is extended to LPV systems. The control methodology is now performed based on an LPV representation of the floating wind turbine system, given in (2.14). The state-space system is parameter-dependent on the wind speed σ and the Lyapunov matrices need to depend on the same parameter. The new Lyapunov matrices (2.69) are now partitioned in the same affine way as the matrices $A(\sigma)$ and $B(\sigma)$ in (2.13).

$$\begin{aligned} \mathbf{X}_Q(\sigma) &= \mathbf{X}_{Q0} + \sigma \mathbf{X}_{Q1}, \\ \mathbf{X}_R(\sigma) &= \mathbf{X}_{R0} + \sigma \mathbf{X}_{R1}, \\ \mathbf{Y}_R(\sigma) &= \mathbf{Y}_{R0} + \sigma \mathbf{Y}_{R1}. \end{aligned} \tag{2.69}$$

In order to guarantee the controller stability and performance within the bounds of the scheduling parameter, some additional LMIs are required. The system is depending on one parameter and as indicated earlier this parameter has an upper and a lower bound, both on the parameter itself and on the derivative. One LMI is needed to check each vertex, i.e. this gives an addition of 2^i LMIs, where i is the number of vertices. As a consequence of the parameter dependency, at the upper left position in the H_∞ constraint (2.62), the expression is quadratic in σ. By imposing

the definiteness of the terms involving σ^2, that is

$$sym\left(A_{aug,b}Q\mathbf{X}_{Q1}\right)+sym\left(A_{aug,b}R\mathbf{X}_{R1}\right)\geq 0 \tag{2.70}$$

the quadratic function of σ is convex. Once again, by changing $\nu=\gamma^{-2}$ in the LMIs (2.62), the problem becomes convex and by maximizing ν it is possible to find the Lyapunov matrices in (2.69). In order to obtain the diagonal structure for the output-feedback gain the LMI variables $\mathbf{X}_R(\sigma)$ and $\mathbf{Y}_R(\sigma)$ also have to have a diagonal structure, i.e. $\mathbf{X}_{R0},\ \mathbf{X}_{R1},\ \mathbf{Y}_{R0}$ and $\mathbf{Y}_{R1}$ need to have diagonal structure.
The total set of LMIs needed to solve the LPV constrained static output-feedback problem are as follows:

$$\begin{pmatrix} sym\left(A_{aug}(\sigma_i)\mathbf{X}(\sigma_i)\right)+sym\left(B_{aug}(\sigma_i)\mathbf{Y}(\sigma_i)\right)+\nu B_{aug,w}B_{aug,w}^T\pm\rho_p\frac{\partial\mathbf{X}}{\partial\sigma} & \\ * & \left(C_z\mathbf{X}(\sigma_i)+D_z\mathbf{Y}(\sigma_i)\right)^T \\ & -I \end{pmatrix}<0,\ i=p=1,2 \tag{2.71}$$

$$sym\left(A_{aug,b}Q\mathbf{X}_{Q1}\right)+sym\left(A_{aug,b}R\mathbf{X}_{R1}\right)\geq 0, \tag{2.72}$$

$$\begin{pmatrix} \mathbf{X}_{Q0} & 0 \\ 0 & \mathbf{X}_{Q1} \end{pmatrix}>0, \tag{2.73}$$

$$\begin{pmatrix} \mathbf{X}_{R0} & 0 \\ 0 & \mathbf{X}_{R1} \end{pmatrix}>0, \tag{2.74}$$

$$\frac{\partial\mathbf{X}}{\partial\sigma}=Q\mathbf{X}_{Q1}Q^T+R\mathbf{X}_{R1}R^T. \tag{2.75}$$

From the optimization problem, the matrices $(\mathbf{X}_{Q0},\ \mathbf{X}_{Q1},\ \mathbf{X}_{R0},\ \mathbf{X}_{R1},\ \mathbf{Y}_{R0},\ \mathbf{Y}_{R1})$ are obtained. At each time step during the simulation, a new values for $A_{aug}(\sigma),\mathbf{X}_R(\sigma)$ and $\mathbf{Y}_R(\sigma)$ are calculated. The output-feedback controller $K(\sigma)$ is calculated from the expression $K(\sigma)=\mathbf{Y}_R(\sigma)\mathbf{X}_R^{-1}(\sigma)$. In this way the controller K will change depending on σ.

This chapter started with a presentation of the modeling approaches used throughout the dissertation. The presentation covers the bond graph model, a constant state-

space model and two LPV state-space models. The second topic in this chapter has been dedicated to the control approaches. It is described how the developed models are used for the control design purpose.

Chapter 3

Concluding Remarks

3.1 Conclusions

This dissertation has mainly dealt with multiobjective optimization and multivariable control of an offshore floating wind turbine. In paper A a basic model of the turbine is developed using bond graph methodology. The model consists of inertias, a gearbox, a spring and a damper. The topic of wind turbine modeling acts as a valid starting point for this project. Although the paper was published in 2013, it was actually written late in 2011. By gaining knowledge about the basic components of the turbine using bond graph modeling approach first, the next step was to start with the control. It was decided not to continue with bond graph modeling since the emphasis in this dissertation was not going to be on the modeling part. The author also believes that utilizing publicly available wind turbine simulations software, in this case FAST, would be more academically acceptable. This freed the author to be more dedicated to the control of the wind turbine. Papers B, C and D deal mainly with pitch control of a floating wind turbine. The models in each of the papers are all based on the nonlinear representation of the Hywind turbine. FAST's Hywind model consists of 24 degrees of freedom, but only a handful are selected for the linarized model. It is important that also the low-frequent degrees of freedom are represented in the linear model. In this way it is possible to have a linear model that represents the most important degrees of freedom, and the designed controller is able to stabilize the nonlinear turbine and maintain performance objectives.

All three control related papers deal with variations of H_∞ output-feedback control. And all control problems are represented using LMI formulation and solved using YALMIP interfaced with Matlab.

3.2 Contribution to Knowledge

Underneath follows a short statement about what the contributions are in the four appended papers and in which journals they are published.

Paper A: Bond Graph Modeling and Simulation of Wind Turbine Systems.
Paper A deals with the bond graph methodology as a graphical approach to model wind turbines systems. The purpose of the paper is not to validate a specific wind turbine system, but rather explore how the bond graph approach can contribute with a model and give a better understanding of how the overall system works. This paper served the author as a good starting point in getting familiar with the principles of wind turbine systems. *The paper was published in Journal of Mechanical Science and Technology, vol. 24 (6), 2013.*

Paper B: Robust H_∞ Dynamic Output-Feedback Control Synthesis with Pole Placement Constraints for Offshore Wind Turbine Systems.
Paper B deals with the problem of robust H_∞ dynamic output-feedback control design with pole placement constraints. A model of Hywind is linearized using FAST. The linear model of the floating wind turbine is represented based on an affine parameter-varying model structure, where the varying parameter is the rotor azimuth angle. The controller is designed based on a linear matrix inequality (LMI) formulation of the problem and the bounded parameter-varying parameters are removed using an upper bounded inequality technique. The closed-loop poles are placed in a selected area in the left half plane. The simulation result illustrates the effectiveness of the developed approach for the nonlinear OC3-Hywind model and is compared with FAST's baseline controller. *The paper was published in Mathematical Problems in Engineering, 2012.*

Paper C: H_∞ Static Output-Feedback Control Design with Constrained Information for Offshore Wind Turbine System.
Paper C deals with the problem of constrained information in the feedback loop. This is handled by a static output-feedback controller with a zero-nonzero pattern. The usefulness of this approach comes into play if a failure occurs. In this way the failure will only directly influence one of the control signals in the feedback loop. Simulation result shows that the controller behaves in a satisfactory manner and the overall system is stable, even if one of the sensors has stopped working. *The paper was published in Journal of the Franklin Institute, vol. 350 (8), pages 2244-2260, 2013.*

Paper D: Linear Parameter-Varying Modeling and Control of an Offshore Wind Turbine with Constrained Information.
Paper D deals with how it is possible to design a controller for a linear parameter-varying (LPV) system with constrained information in the feedback loop. The model of the floating wind turbine is represented based on an affine parameter-varying model structure. The model is varying with the wind speed, which is estimated using an extended Kalman filter (EKF). The constrained controller is obtained based on parameter-dependent Lyapunov functions and formulated in terms of linear matrix inequalities (LMIs). Simulation result shows that the closed-loop system behaves in a satisfactory manner and the overall system is stable, even if one of the sensors has stopped working. *This paper has been submitted to IET Control Theory & Applications, 2013.*

3.3 Future Work

A number of research directions can be proposed to improve the development of the modeling, control synthesis and system performance of the wind turbines.

One research direction is to continue with bond graph and try to make a bond graph-based controller for floating turbine and compare the dynamic response with for example FAST. At a point during the PhD period it was considered to make hardware-in-the-loop (HIL) simulations of a wind turbine model, but this was never

finished due to the project plan. By developing a bond graph model of a floating wind turbine and by substituting parts of the model by actual hardware, e.g. pitch actuator, one could perform HIL simulations. This would also be a good topic for implementation of an advanced controller into a micro-controller or a PLC (Programmable Logic Controller).

Another research direction is to focus more on the effects of wind and wave disturbances in the modeling and control parts. Incorporating knowledge about the specific behavior of these effects, e.g. wave frequencies, wind frequencies or amplitudes, could be utilized in the controller design and possibly get better performance. The exception is in paper D, where wind speed estimation is used to schedule the LPV controller.

Another topic that has not been directly emphasized in the dissertation is fatigue. There has been much focus on the damping of selected parts of the turbine, but not on the fatigue itself, although this is very much related. Fatigue calculations such as fatigue life or damage equivalent loads could be calculated either online or offline. It would be very interesting to have access to these (or other) values online, in this way one could have constant surveillance of the wellbeing of the turbine.

Finally, it could also be interesting to combine the modeling approaches from papers B and D. The LPV model in paper B is dependent on the azimuth angle and not wind speed. The LPV model from paper D is dependent on wind speed but not on the azimuth angle. By combining the two modeling approaches one could have a model which is more accurate at each specific wind speed.

REFERENCES

AlHamaydeh, M. and Hussain, S. (2011). Optimized frequency-based foundation design for wind turbine towers utilizing soil-structure interaction. *Journal of The Franklin Institute*, 348(7):1470–1487.

Burton, T., Sharpe, D., Jenkins, N., and Bossanyi, E. (2001). *Wind Energy Handbook*. John Wiley & Sons, Ltd., Chichester, UK.

Chilali, M. and Gahinet, P. (1996). H_∞ design with pole placement constraints: An LMI approach. *IEEE Transactions on Automatic Control*, 41(3):358–367.

Christiansen, S., Bak, T., and Knutsen, T. (2012). Minimum thrust load control for floating wind turbine. The Proceedings of IEEE Multi-Conference on Control Applications.

Cordle, A. and Jonkman, J. (2011). State of the art in floating wind turbine design tools. International Offshore and Polar Engineering Conference.

Eggleston, D. M. and Stoddard, F. S. (1987). *Wind Turbine Engineering Design*. Van Nostrand Reinhold Co.

Faltinsen, O. M. (1990). *Sea Loads on Ship and Offshore Structures*. Cambridge University Press.

Freris, L. (1990). *Wind Energy Conversion Systems*. Prentice Hall, Hertforshire, UK.

Fylling, I., Mo, K., Merz, K., and Luxcey, N. (2009). Floating wind turbine - Response analysis with rigid-body model. EWEA Conference.

Grewal, M. S. and Andrews, A. P. (2001). *Kalman Filtering: Theory and Practice Using Matlab*. John Wiley & Sons, Inc.

Henriksen, L. C. (2007). Model predictive control of a wind turbine. Master thesis, Technical University of Denmark.

Jonkman, J. (2008). Influence of control on the pitch damping of a floating wind turbine. ASME Wind Energy Symposium.

Jonkman, J. (2010a). Definition of the floating system for phase iv of oc3. Technical report nrel/tp-500-47535, National Renewable Energy Laboratory.

Jonkman, J. (2010b). NTWC design codes. Technical report, National Renewable Energy Center.

Jonkman, J., Butterfield, S., Musial, W., and Scott, G. (2009). Definition of a 5-MW reference wind turbine for offshore system development. Technical report NREL/TP-500-38060, National Renewable Energy Laboratory.

Khargonekar, P. P., Petersen, I. R., and Zhou, K. (1990). Robust stabilization of uncertain linear systems: Quadratic stabilizability and control theory. *IEEE Transactions on Automatic Control*, 35(3):356–361.

Knudsen, T., Bak, T., and Soltani, M. (2011). Prediction models for wind speed at turbine locations in a wind farm. *Wind Energy*, 14(7):877–894.

Larsen, T. J. and Hansen, A. M. (2007). How 2 HAWC2, The user's manual. Technical report, Risø.

Larsen, T. J. and Hanson, T. D. (2007). A method to avoid negative damped low frequent tower vibrations for a floating, pitch controlled wind turbine. *Journal of Physics: Conference Series*, 75.

Newman, J. N. (1997). *Marine Hydrodynamics*. The MIT Press.

Rotea, M., Lackner, M. A., and Saheba, R. (2010). Active structural control of offshore wind turbines. 48th AIAA Aerospace Sciences Meeting and Exhibit.

Rubió-Massegú, J., Rossell, J. M., Karimi, H. R., and Palacios-Quiñonero, F. (2012). Static output-feedback control under information structure constraints. *Automatica*, 49(1):313–316.

Scherer, C., Gahinet, P., and Chilali, M. (1997). Multi objective output feedback control via LMI optimization. *IEEE Transactions on Automatic Control*, 42(7):896–911.

Skaare, B., Hanson, T. D., Nielsen, F. G., Yttervik, R., Hansen, A. M., Thomsen, K., and Hansen, T. J. (2007). Integrated dynamic analysis of floating offshore wind turbines. Technical report, Risø.

Skaare, B., Hanson, T. D., Yttervik, R., and Nielsen, F. G. (2011). Dynamic response and control of the hywind demo floating wind turbine. EWEA Conference.

Zečević, A. I. and Šiljak, D. D. (2004). Design of robust static output feedback for large-scale systems. *IEEE Trans. on Automatic Control*, 49(11):2040–2044.

Zečević, A. I. and Šiljak, D. D. (2008). Control design with arbitrary information structure constraints. *Automatica*, 44(10):2642–2647.

Zečević, A. I. and Šiljak, D. D. (2010). *Control of complex systems: Structural constraints and uncertainty*. Springer.

Paper A

Bond Graph Modeling and Simulation of Wind Turbine Systems

T. Bakka and H. R. Karimi

This paper has been published as:

T. Bakka and H. R. Karimi, ”Bond Graph Modeling and Simulation of Wind Turbine Systems”, *Journal of Mechanical Science and Technology*, vol. 24 (6), 2013.

Bond graph modeling and simulation of wind turbine systems

T. Bakka and H. R. Karimi
Department of Engineering
Faculty of Engineering and Science, University of Agder
Jon Lilletunsvei 9, 4879 Grimstad, Norway.

Abstract — **This paper addresses the problem of bond graph methodology as a graphical approach for the modeling of wind turbine generating systems. The purpose of this paper is to show some of the benefits the bond graph approach has, in contributing a model for wind turbine systems. We will present a non-linear model of a wind turbine generating system, containing blade pitch, drive train, tower motion and generator. All which will be modeled by means of bond graph. We will especially focus on the drive train, and show the difference between modeling with a classical mechanical method and by using bond graph. The model consists of realistic parameters, but we are not trying to validate a specific wind turbine generating system. Simulations are carried out in the bond graph simulation software 20-sim (Kleijn, 2009).**

Keywords — Bond graph, modeling, wind turbine.

1 Introduction

The demand for energy world wide is increasing every day. And in these green times renewable energy is a hot topic all over the world. Wind energy is currently the most popular energy sector. The growth in wind power industry has been tremendous over the last decade. As of June 2012 the global wind capacity is 254,000 MW, according to the World Wind Energy Association World Wind Energy Association. Whenever we are talking about models of wind turbine systems, the turbine model becomes a critical part of the discussion. Over the years it has been some discussion about how to model the wind turbine accurately. In (Tamura et al., 2001; Zubia et al., 2001) they perform dynamic analysis on a one-mass-model, in (Petru and

Thiringer, 2002; Akhmatov and Knudsen, 1999) they examine a two-mass-model. In (Martins et al., 2007) they use actual measured data from a wind turbine and compare it with both a one-mass and a two-mass-model. They validate the model using a recorded case obtained in a fixed speed, stall regulated wind turbine. In (Muyeen et al., 2007) a six-, three- and a two-mass model are compared with each other. They argue that a six-mass model is needed for the precise transient analysis of the wind turbine system, and they develop a way to transform a six-mass model into a two-mass model. The goal of that paper is not to use the model in the control scheme, but in the use of transient stability analysis of grid connected system.

The pitching of the blades are usually executed by means of a hydraulic system, but for system modeling purposes it is often considered as a first or second order system. We are here dealing with variable speed generating system, therefore a wound machine or a double fed induction generator is needed. These can be modeled in different ways, ranging from complex electric equivalent circuits to a first order system.

Several advanced wind turbine simulation softwares have emerged during the last decade. HAWC2 (Larsen and Hansen, 2007), Cp-Lambda (Bottasso and Croce, 2009) and FAST (Jonkman and Buhl, 2005) are a few examples. They are developed at RISØ in Denmark, POLI-Wind in Italy and NREL in the US, respectively. In these codes the turbine and structure is considered as complex flexible mechanisms, and uses the finite-element-method (FEM) multibody approach. An aeroservo- elastic model is introduced, which consists of aerodynamic forces from the wind, the servo dynamics from the different actuators and the elasticity in the different joints and the structure. Both FAST and HAWC2 can simulate offshore and onshore cases while Cp-Lambda is limited to the onshore case.

As seen above there are many ways to model a wind turbine generating system, some are simple and some are very complex. In a simulation point of view it is desirable that the model is as simple as possible and can capture as much of the dynamics as appear in reality. This is an absolute demand, another important issue is to keep the central processing unit (CPU) labor to a minimum. For example if we are dealing with hardware in the loop (HIL) simulation, then it is necessary to download the model to a programmable logic controller (PLC). This argues in

favor of the importance in having a fast C-code. Things that can potentially have a negative effect on the execution of our C-code are for example; algebraic loops and differential causality on thedifferent elements in the system. These topics bring us to the use of the bond graph methodology. This is a unified approach to model all types of physical systems, producing both linear and nonlinear mathematical models. Engineers must work and interact in many different disciplines. An understanding of the intersections of these different disciplines is a valuable asset for any engineer. Using the language of bond graphs, one may construct models of electrical-, magnetic-, mechanical-, hydraulic-, pneumatic- as well as thermal systems. It is a systematic way to model these dynamic systems, and there are standard ways to translate them into differential equations or computer simulation schemes. After constructing the bond graph one can easily spot algebraic loops and whether you have integral causality on the dynamic elements by inspecting the bond graph. There are various ways to spot these things in typical simulation software such as MatLab (MATLAB, 2010), but it is beneficial to spot them before the implementation. It is a quite intuitive way in setting up the bonds and connecting the elements, this will be discussed in a later section. The outcome from the bond graph model is a set of first order differential equations, which afterwards can be used for systems response analysis or for example controller design. After constructing the bond graph one gets a better understanding of what actually happens in the system. In an educational point of view one can easily understand which element decides what in the system. For example in a simple mass-spring-damper system, one can easily see which component decides the speed and which component decides the force. With these arguments in mind we are motivated to explore the possibilities there are with the use of bond graph.

The wind turbine generating system can be divided into several subsystems, see Fig. A.1. The system setup is adopted from (Hammerum et al., 2007), where V_w is the wind speed, V_a is the wind speed for power production, $\dot{z}$ is the tower speed, F_t is the thrust force acting on the tower, β_{ref} is the pitch angle reference, β is the actual pitch angle, T_a is the aerodynamic torque, Ω_H is the hub speed, Ω_G is the generator speed, T_{EMref} is the generator torque reference and T_{EM} is the actual generator torque.

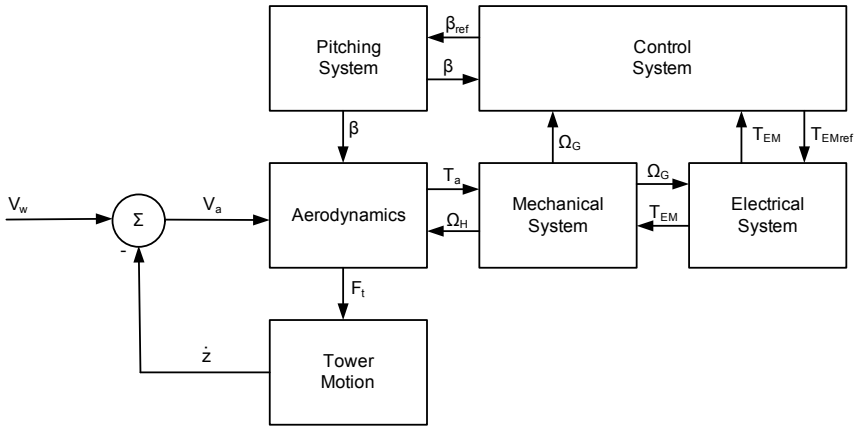

Figure A.1: Setup for wind turbine generating system

The expression for power produced by the wind is given by (Eggleston and Stoddard, 1987)

$$P_a = \frac{1}{2}\rho\pi R^2 v^3 C_p(\lambda,\beta). \tag{A.1}$$

The dimensionless tip-speed ratio (TSR) λ is defined as

$$\lambda = \frac{v_b}{v}, \tag{A.2}$$

where v_b is the tip speed of the blade and v is the wind speed. From (A.3) we can find the aerodynamic torque and the thrust force acting on the tower

$$T_a = \frac{1}{2}\rho\pi R^3 v^2 C_p(\lambda,\beta), \tag{A.3}$$

$$F_t = \frac{1}{2}\rho\pi R^2 v^2 C_T(\lambda,\beta), \tag{A.4}$$

where P_a is the aerodynamic power, ρ is the air density and R is the blade radius. C_p gives the relationship between how much power is available in the wind and how much can be converted to electrical power. Not all the available power can be converted, this is due to the fact that the wind cannot be completely drained of energy, otherwise the wind speed at the rotor front would reduce to zero and the rotation of the rotor would stop. It can be proven that the theoretical upper limit of C_p is $16/27 \approx 0.59$, this is known as the Betz limit. A general modern wind turbine has a maximum power coefficient of about 0.5. C_t is the thrust force coefficient,

both these coefficients are dependent on the TSR λ and the pitch angle β.

This paper is organized as follows. Section 2 gives a short overview on the bond graph methodology and its different elements. Section 3 describes the different parts of our system model; aerodynamics, pitch, drive train, tower motion and generator. In Section 4 the simulation results are presented and Section 5 gives the conclusion and states some suggestions regarding future work.

2 Introduction to Bond Graph

Bond graph is a graphical way of modeling physical systems. All these physical systems have in common the conservation laws for mass and energy. Bond graph, originated by Paynter (Paynter, 1961) in 1961, deals with the conservation of energy. This gives a unified approach to model physical systems. This section gives a short introduction to this modeling tool, the interested reader can find more information in (Karnopp et al., 2006; Borutzky, 2010). The bond graph approach has several advantages over conventional methods, i.e.: 1) providing a visual representation of the design; 2) controlling the consistency of the topological settings of the design; 3) providing the hierarchical modeling of designs; 4) extracting the system equations symbolically in a structured way.

Within physical systems, energy is transported from one item to another. This energy is either stored or converted to other forms. But the important thing is that it does not dissipate. If the energy is changing in one place, it also changes in an opposite way at another location. The definition of power is the change in energy (E) with respect to time:

$$P = \frac{d}{dt}(E). \tag{A.5}$$

The power is transferred between the different parts in the bond graph model with the use of power bonds, see Fig. A.2. In bond graph notation the definition of power is effort multiplied with flow. For example, in electric systems this would mean voltage multiplied with current, in mechanical systems it is force multiplied with velocity and in hydraulics it is pressure multiplied with flow.

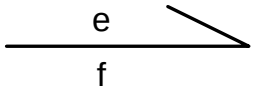

Figure A.2: Power bond with effort and flow

2.1 System Elements

In bond graph modeling there are a total amount of nine different elements. We will here introduce the causality assignments, but first we have to explore the cause and effect for each of the basic bond graph elements. Only elements with its preferred causality will be discussed. The importance of causality will be dealt with later in the paper.

Junctions:
There are two different types of junctions that connects the different parts in a bond graph model, the 0- junction and the 1-junction. The 0-junction is an effort equalizing connection, see Fig.. A.3 and its corresponding equation in (A.6). Since the efforts are the same, only one bond can decide what it is. The 1-junction is a flow equalizing connection, see Fig. A.4 and its corresponding equation in (A.7). Since the flows are the same, only one bond can decide what it is. Which bond decides the flow and which one decides the effort is indicated with the vertical causality stroke. If the vertical line is closest to the junction, then this element decides the effort, furthest away from the junction decides the flow.

Source element:
We can divide the source elements into two different kinds, effort- and flow-source. The effort source gives an effort into the system, then it is up to the system to decide the flow. This is what is meant with cause and effect, and its vice versa for the flow source. Fig. A.5 shows how the causality is indicated on the graphical elements. For the source elements these causality assignments are fixed.

Compliance Element:
The causality assignment for the C-element has two possibilities, but one is pre-

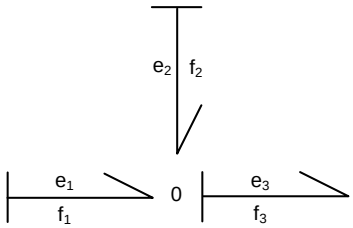

$$\begin{aligned} e_1 &= e_2 = e_3, \\ f_3 &= f_1 + f_2. \end{aligned} \tag{A.6}$$

Figure A.3: 0-junction

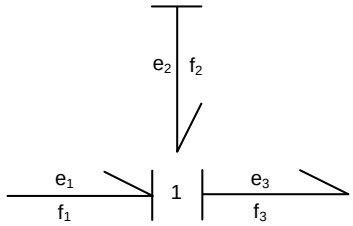

$$\begin{aligned} f_1 &= f_2 = f_3, \\ e_3 &= e_1 + e_2. \end{aligned} \tag{A.7}$$

Figure A.4: 1-junction

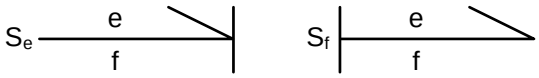

Figure A.5: Effort and flow source with their causality assignment

ferred in contrast to the other. This is discussed at the end of this section. The preferred case is seen in Fig. A.6 and its corresponding equation in (A.8). We see from both the equation and the figure that flow is given to the element/equation and it gives the effort in return.

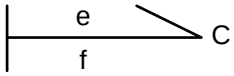

Figure A.6: Example of a compliance element with integral causality

$$\begin{aligned} e &= \frac{1}{C}\int f\,dt \\ &= \frac{q}{C}. \end{aligned} \tag{A.8}$$

The variable q is called *the generalized displacement*. For example, this can be rotational position of the rotor in a wind turbine.

Inertia Element:
There are two choices for the causality assignment for the I-element, also here one is preferred in contrast to the other. The preferred case is seen in Fig. A.7 and its

corresponding equation in (A.9).

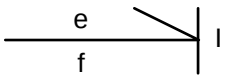

Figure A.7: Example of an inertia element with integral causality

$$\begin{aligned} f &= \frac{1}{I}\int e dt \\ &= \frac{p}{I}. \end{aligned} \tag{A.9}$$

The variable p is called *the generalized momentum*. For example, this can be rotor inertia times rotor velocity in a wind turbine.

Resistive Element:
It is a bit more freedom when it comes to the causality assignment for the R-element. Its equation do not include any dynamics, it is only an algebraic expression. The two causality choices are shown in Fig. A.8 and its corresponding equation in (A.10).

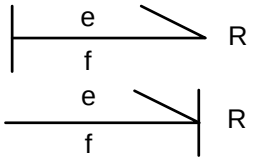

$$\begin{aligned} e &= Rf, \\ f &= \frac{1}{R}e. \end{aligned} \tag{A.10}$$

Figure A.8: Example of resistive element

Transformer:
The transformer element can work in two ways; either it transforms a flow into another flow or it transforms an effort into another effort. Fig. A.9 corresponds to (A.11)-(A.12), where m is the transformation ratio.

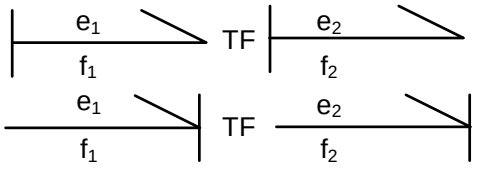

$$\begin{aligned} e_1 &= me_2, \\ f_2 &= mf_2. \end{aligned} \tag{A.11}$$

$$\begin{aligned} e_2 &= \frac{1}{m}e_1, \\ f_1 &= \frac{1}{m}f_2. \end{aligned} \tag{A.12}$$

Figure A.9: Example of the two transformers

For example, this can represent a mechanical gearing or an electric transformer.

Gyrator:
The gyrator can also work in two ways; either it transforms a flow into an effort or it transforms an effort into a flow. Fig. A.10 corresponds to (A.13)-(A.14), where r is the gyrator ratio.

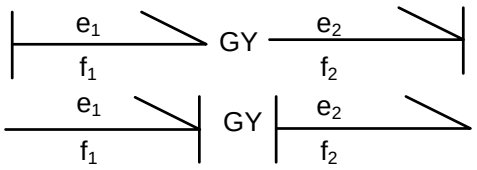

Figure A.10: Example of the two gyrators

$$\begin{aligned} e_1 &= rf_2, \\ e_2 &= rf_1. \end{aligned} \tag{A.13}$$

$$\begin{aligned} f_1 &= \frac{1}{r}e_2, \\ f_2 &= \frac{1}{r}e_1. \end{aligned} \tag{A.14}$$

This can for example be an electric motor, where you have voltage as input and a rotational speed as output.
The importance of integral causality is nicely explained in (Pedersen and Engja, 2003). First imagine a step in effort is imposed on a C-element, then the causality assignment will be opposite of what is shown in Fig. A.6. This means the flow output is proportional to the derivative of the input effort. From calculus we know that the derivative of the step function at the beginning is infinite, i.e. this do not give any physical meaning. We can imagine a simple electric circuit containing a voltage source coupled with a capacitor, if a step input were to be imposed on the voltage source, the capacitor would experience a very high current and it would blow up. From this we can conclude that nature integrates and only mathematicians differentiate! On the other hand, the ability to spot algebraic loops is one of the benefits with the use of bond graph as a modeling tool. These loops can be spotted simply by inspection of the bond graph representation, if the causality assignment on the R-elements are different from each other, then we have algebraic loops in the system. If they have the same causality, there are no algebraic loops. These loops occur for example if you have two resistors in series. In this circuit both resistors will try to decide what the current should be, i.e. they depend on each other. This will not necessarily cause problems to the simulation, but it might. Especially if the resistors are nonlinear, then the simulation could easily crash. The simulation

program will also be forced to spend time to solve this algebraic loop. If we can easily spot these loops early in the modeling process, then we can try to fix them by simply adding an element. For example, regarding our circuit with two resistors in series, we can add an inductive element to the circuit. Then it would be the inductive element which decides what the current should be and not the resistive elements. The resistive elements would simply have to take what current the inductive element lets through. We can give the inductive element a value such that the voltage drop over the element is very low, i.e. it does not play any major role in the circuit. Now when our model has no algebraic loops and all the dynamic elements have integral causality, the simulation should go smooth. If we have a large set of equations or a large block diagram it is not easy to spot these things right away, but with a bond graph representation of the model we can spot them simply by inspection.

We will end this section with a small example. We want to show how to set up a bond graph of a simple system, and also show the difference in relation to block diagrams. Fig. A.11 shows two equivalent circuits in two different domains, and they have exactly the same governing equations. The corresponding bond graph is shown in Fig. A.12 The easiest way to set up a bond graph when having a mechan-

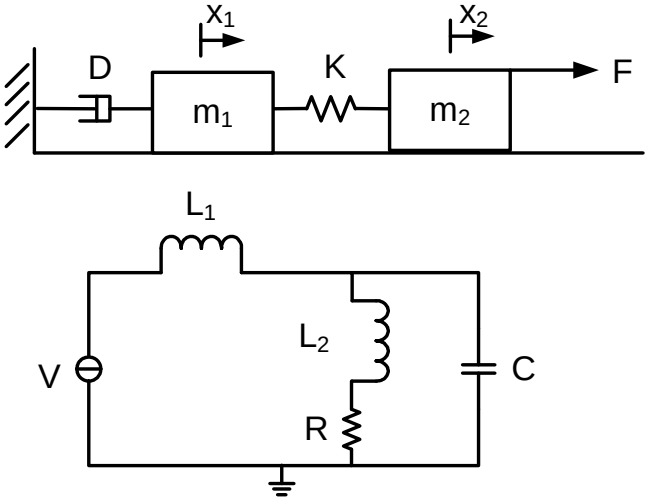

Figure A.11: Two equivalent circuits

ical system, is to start with setting up 1-junctions. One junction for each mass, this gives two 1-junctions in our example. We add a 0-junction in between, because we

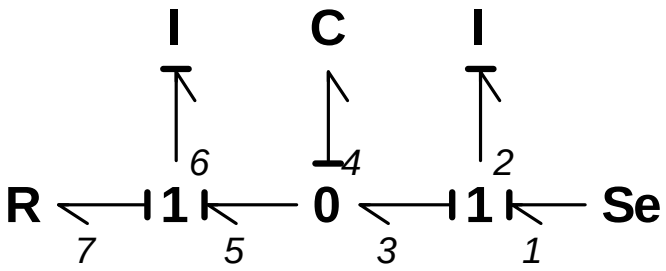

Figure A.12: Bond graph of the two equivalent circuits

know the speed is different but the force is the same. Force is transfered through the C-element (spring). The right side of the damper has the same speed as m_1, R-element and I-element is therefore connected to the left 1-junction.
Regarding the electric circuit, we know that the source and L_1 have the same current i_1. We know that L_2 and R have the same i_2, and we know that the parallel branches have the same voltage. In this way we end up with the exact same bond graph. We also note that the graph has integral causality. The two I-elements receive effort and give flow in return, the C-element receives flow and gives effort in return.
We will now find the governing equations. First we find $\dot{p}_i$, second we find $\dot{q}_i$. In mechanical terms this is $m\ddot{x}_i$ and $\dot{x}$, respectively. Subscript i corresponds to in which bond we are at.

$$\dot{p}_2 = e_2 = e_1 - e_3 = S_e - e_4 = S_e - \frac{q_4}{C_4}, \tag{A.15a}$$

$$\dot{p}_6 = e_6 = e_5 - e_7 = e_4 - R_7 f_7 = \frac{q_4}{C_4} - R_7 f_6 \tag{A.15b}$$

$$= \frac{q_4}{C_4} - R_7 \frac{p_6}{I_6},$$

$$\dot{q}_4 = f_4 = f_3 - f_5 = f_2 - f_6 = \frac{p_2}{I_2} - \frac{p_6}{I_6}. \tag{A.15c}$$

In mechanical domain terms, (A.15) correspond to (A.16).

$$m_2\ddot{x}_2 = F - Kx_0, \tag{A.16a}$$

$$m_1\ddot{x}_1 = kx_0 - Dx_1, \tag{A.16b}$$

$$x_0 = x_2 - x_1. \tag{A.16c}$$

These are exactly the same equations we will end up with if we do it in the classical Newtons 2*nd* law approach. The block diagram for these equations are shown in Fig. A.13. Block diagrams represent the structure of the mathematical model and displays which variables must be known in order to compute others. They do not reflect the physical structure. The reason is that feedback is represented in separate feedback loops.

By using bond graph as the modeling tool we get a good overview of the model's physical structure and we can do simulations in one step, instead of first deriving the equations and then drawing the block diagram.

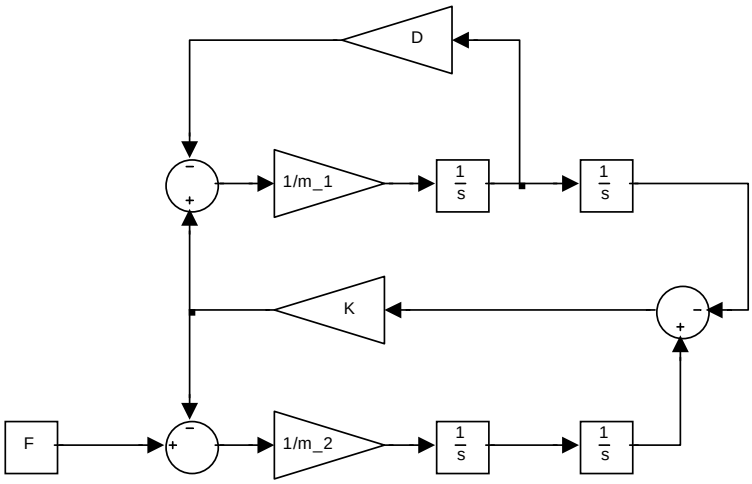

Figure A.13: Block diagram of mechanical example

3 Model Description

In the following section, the bond graph based modeling for the different subsystems shown in Fig. A.1, will be presented. It is shown that the bond graph method provides a hierarchical modeling for the entire wind turbine generating system as well as the system equations can be extracted symbolically in a structured way.

3.1 Aerodynamics

In the aerodynamics part we need to find a way to convert the wind into torque and thrust force, i.e. transform a flow into efforts. This is done by means of a modulated gyrator. We use the torque and thrust equations given in (A.3)-(A.4). The only difference between a MGY and a GY is that the gyrator ratio is not a constant parameter, but it is a varying parameter. In this case the transformation is dependent on two varying parameters, the pitch angle β and the rotor rotational speed ω_r. A

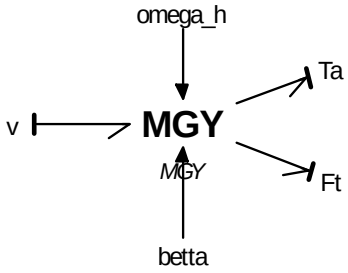

Figure A.14: Modulated gyrator transforming wind speed into aerodynamic torque and thrust force

generic equation is used to model C_p. This equation, based on the modeling turbine characteristics of (Heier, 1998), is shown in (A.17). The power coefficient used in the calculation of the torque is given in (A.17). A plot of the C_p curve is shown in Fig. A.15, the plot is made with different pitch- and λ- values. Similar formulas can be found regarding the thrust force coefficient C_T, in our calculations only a simple relation is used.

$$\lambda = \frac{\omega_r R}{v}, \tag{A.17a}$$

$$\lambda_i = \frac{1}{\frac{1}{\lambda+0.08\beta} - \frac{0.035}{\beta^2+1}} \tag{A.17b}$$

$$C_p = c_1 \left(\frac{c_2}{\lambda_i} - c_3\beta - c_4 \right) e^{-\frac{c_5}{\lambda_i}} + c_6\lambda, \tag{A.17c}$$

where $c_1 = 0.5176$, $c_2 = 116$, $c_3 = 0.4$, $c_4 =$, $c_5 = 21$, $c_6 = 0.0068$.

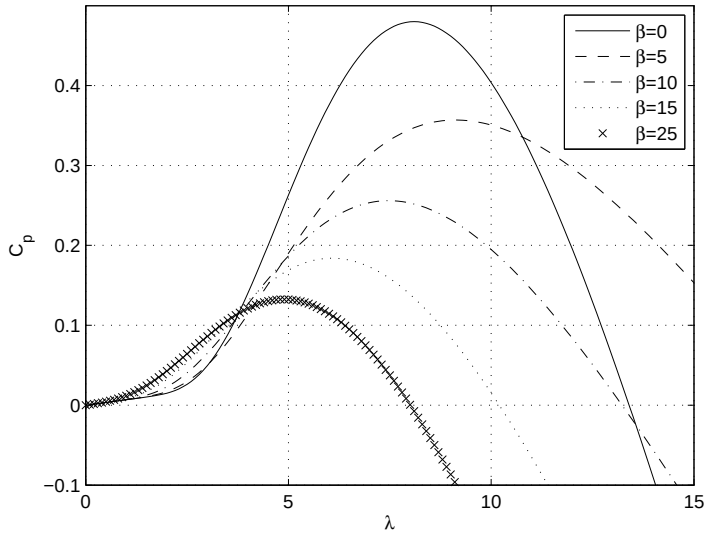

Figure A.15: C_p curve

3.2 Pitching System

The pitching mechanism can be modeled as a second order system;

$$\omega_n^2 \theta_{ref} \;=\; \ddot{\theta} + 2\zeta\dot{\theta} + \omega_n^2 \theta, \tag{A.18}$$

where θ_{ref} is the reference pitch angle, ω_n is the natural frequency and ζ is the damping ratio. By setting up the dynamic equation of the mass spring damper system in Fig. A.16, we can compare the elements in the equation with (A.18). In this way we can set up the bond graph in Fig. A.17 with appropriate coefficients.

$$F \;=\; \theta_{ref} \;\;,\;\; M \;=\; \frac{1}{\omega_n^2} \;\;,\;\; D \;=\; \frac{2\zeta}{\omega_n^2} \;\;,\;\; K \;=\; 1.$$

3.3 Drive Train

A sketch of a two-mass drive train model is seen in Fig. A.18. As discussed in the introduction there are many types of drive train models, ranging from for example one- to six mass models. For simplicity we will assume a two-mass-model is

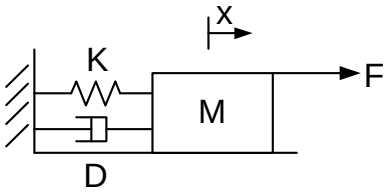

Figure A.16: Mass spring damper

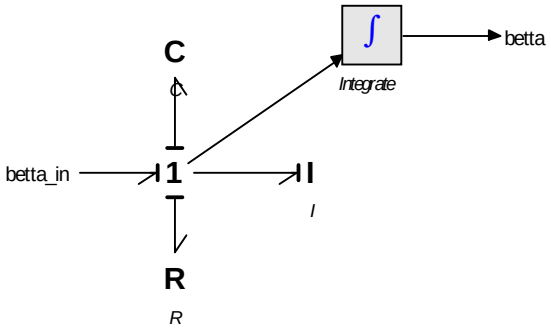

Figure A.17: Bond graph of pitching system

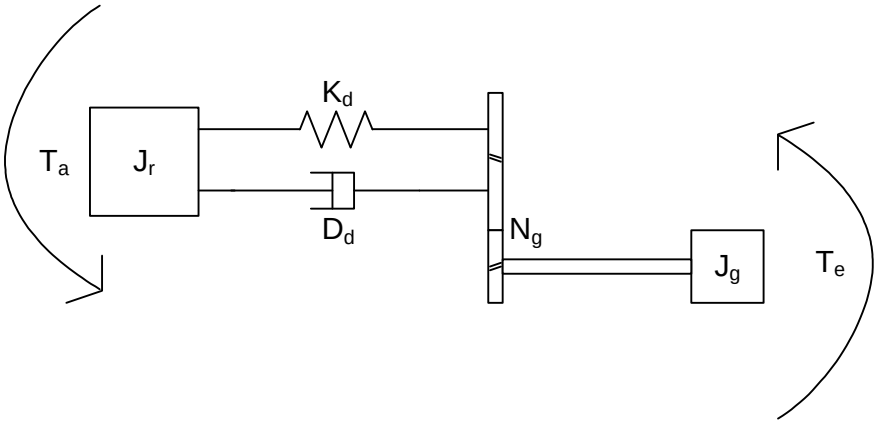

Figure A.18: Sketch of wind turbine

enough. To derive the governing equations from a two-mass model is not too hard. If we are talking about a six-mass model the work can be quite extensive, and the possibility of making a mistake in the process is high. This is one of the reasons bond graph is a safer choice. As the complexity of the mechanical system grows, our work as modelers stays about the same. If we have a six-mass model with many springs and dampers, this gives us many equations and to translate this into a block diagram can take quite some time. As for dealing with bond graph, the work is to set up the graphical representation. If we want to see the equations, these can be derived in a very specific way. Or, off course, we can choose to get them from the bond graph simulation program 20-sim. By utilizing Newton's second law on rotational form of the wind turbine sketch in Fig. A.18, we end up with the following differential equations:

$$T_r = I_r\dot{\omega}_r + \dot{\phi}_\Delta D_d + \phi_\Delta K_d, \tag{A.19a}$$

$$-T_g N_g = I_g N_g^2 \frac{\dot{\omega}_g}{N_g} - \dot{\phi}_\Delta D_d - \phi_\Delta K_d, \tag{A.19b}$$

where

$$\phi_\Delta = \phi_r - \frac{\phi_g}{N_g}\ ,\ \dot{\phi}_\Delta = \omega_r - \frac{\omega_g}{N_g}.$$

In a quite intuitive way we can translate the mechanical system in Fig. A.18 into a bond graph representation, as shown in Fig. A.19. This can again be simplified a bit in order to make a minimal bond graph representation, see Fig. A.20. The bond graph model consists of three 1-junctions and one 0-junction. The 1-junction connected to the rotor inertia describes the rotor rotational speed. Since there are dynamics in between the rotor inertia and the generator inertia, they do not have the same speed. This is the reason for the 0-junction, because we know the transferred torque is the same (no loss included in the drive train). The 1-junction connected to the resistive- and the compliance element indicates the rotational speed difference between the two inertias. This connection also indicates that the compliance- and resistive element have the same rotational speed (flow), but different torque (effort). The last 1-junction is connected to the generator inertia and describes the generator rotational speed. Once the bond graph representation is made, the procedure for

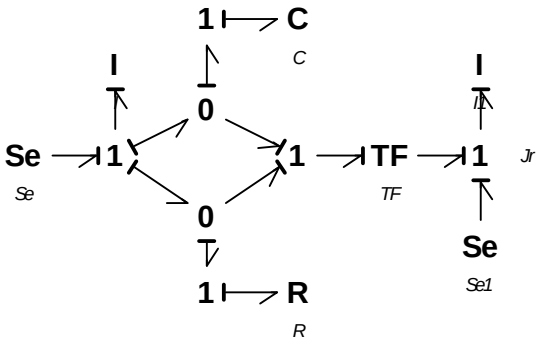

Figure A.19: Bond graph of drive train

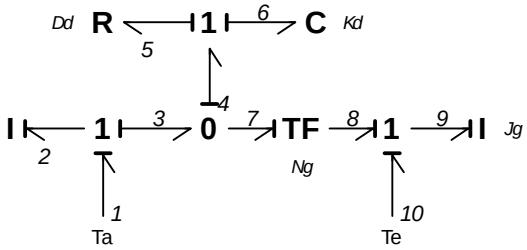

Figure A.20: Bond graph of drive train

extracting its governing equations is quite straight forward. One has to follow some certain rules, and at the end the equations will be the outcome. We can also choose

to get the equations from the simulation software. The equations can be derived as follows.

From the bond graph representation we see there are three dynamic elements, two inertias and one spring, i.e. three dynamic equations must exist. These first order differential equations are given in (A.20).

$$\begin{aligned}\dot{p}_2 = e_2 &= e_1 - e_3 \\ &= T_a - \frac{q_5}{C_6} - R_5 f_5, \end{aligned} \tag{A.20a}$$

$$\begin{aligned}\dot{q}_5 = f_5 &= f_3 - f_7 \\ &= \frac{p_2}{I_2} - \frac{p_9}{N_g I_9}, \end{aligned} \tag{A.20b}$$

$$\begin{aligned}\dot{p}_9 = e_9 &= e_8 + e_{10} \\ &= -T_e + \frac{1}{N_g}\left(\frac{q_5}{C_6} + R_5 f_5\right). \end{aligned} \tag{A.20c}$$

With some manipulations this is exactly the same as in (A.19).

3.4 Generator

There are many ways to model the generator dynamics. One of the recurring ways is with an equivalent circuit. In this system we assume that a first order transfer function will capture its dynamics. We do this in the same way as for the pitching system, but since it is first order we do not include the spring.

$$T_{ref} = \tau \dot{T}_e + T_e, \tag{A.21}$$

where T_{ref} is the reference torque and τ is the time constant. In this way we can set up the bond graph similar to Fig. A.17 with appropriate coefficients.

$$F = T_{ref} \ , \ M = \tau \ , \ D = 1.$$

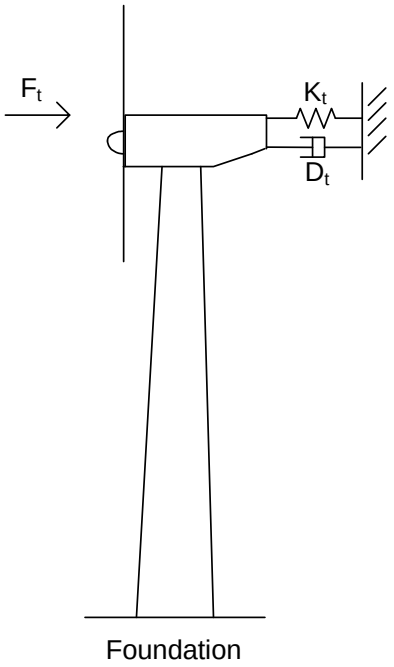

Figure A.21: Sketch of wind turbine structure

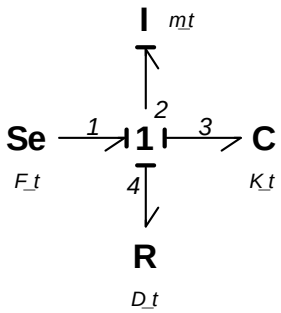

Figure A.22: Bond graph of tower motion

3.5 Tower

In Fig. A.21 we see the turbine sketch and where the thrust force is acting on the structure. It is assumed that the tower movement will not influence the mechanical system, it only affects its input, i.e. the wind speed. The bond graph model of the tower can be seen in Fig. A.22. Since the deflections of the tower are assumed to be small, we assume tower movement only in horizontal direction.

The dynamic equation from the bond graph model, shown in Fig. A.22, is given in (A.22).

$$\dot{p}_2 = S_e - R\frac{p_2}{I} - \frac{q_3}{C}, \tag{A.22a}$$

$$\dot{q}_3 = \frac{p_2}{I}. \tag{A.22b}$$

We can rewrite (A.22) in a non bond graph notation:

$$m_t\ddot{z} \;=\; F_t - D_t\dot{z} - K_t z, \tag{A.23}$$

where m_t is the tower mass, F_t is the thrust force acting on the tower, D_t is the tower damping and K_t is the tower stiffness.

4 Simulation Results

In this section we want to validate the bond graph design. The procedure is to first connected together all the subsystems from Section III. Second, the same model is implemented as block diagrams in Matlab/Simulink. This software is widely established throughout the academic community and the result from Matlab/Simulink will act as a reference output for validation purpose.
The bond graph representation of the system setup in Fig. A.1 is shown in Fig. A.23. The inputs to the systems are pitch angle, reference power and wind speed. The

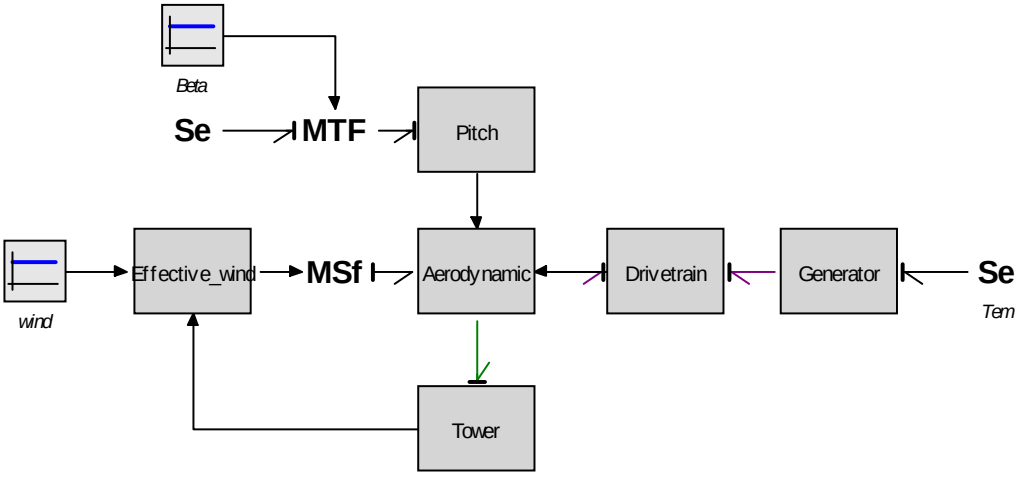

Figure A.23: Bond graph of wind turbine generating system

simulations are made with maximum pitch angle, maximum wind condition, maximum power and with initial conditions on the rotor and generator. All wind turbine parameters used in the simulations are found in (Henriksen, 2007). Once the simulations are carried out in the two softwares, time behavior of the most important dynamics are inspected. As seen in Figs. A.24-A.25, the behavior of the two systems are identical. This confirms the fact that we eventually end up with the same governing equations whether one uses the classical Newtons 2*nd* law or the bond graph approach.

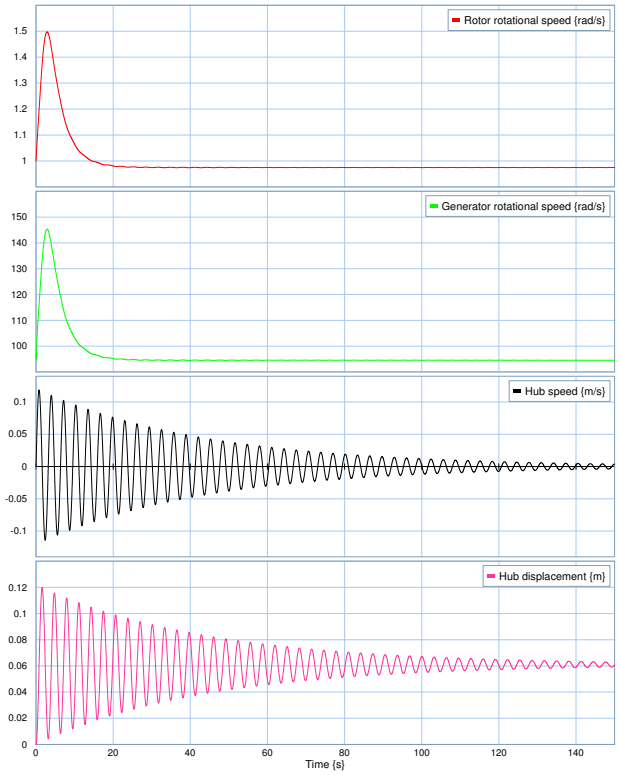

Figure A.24: Time behavior of the selected signals from 20-sim

5 Conclusion

The purpose of this paper is to make a nonlinear model of a wind turbine generating system by using the bond graph approach. We are not looking to validate a specific turbine system, but we want to show a simple and suitable way to model it. The nonlinear wind turbine consists of drive train, pitching system, tower and generator. To model dynamic systems in the classical way and the bond graph way is quite different, but the outcome is a model with exactly the same governing equations. We have tried to emphasize that the bond graph approach will give a better understanding of what actually happens in the system. This include; spotting algebraic loops right away and maintaining integral causality, to name a few. The approach is unified, which means one can model all types of physical systems with the same methodology. Today, most engineers must work and interact in many different disciplines. An understanding of the intersections of these different disciplines is a valuable asset for any engineer. Based on the results in this paper, interesting future research

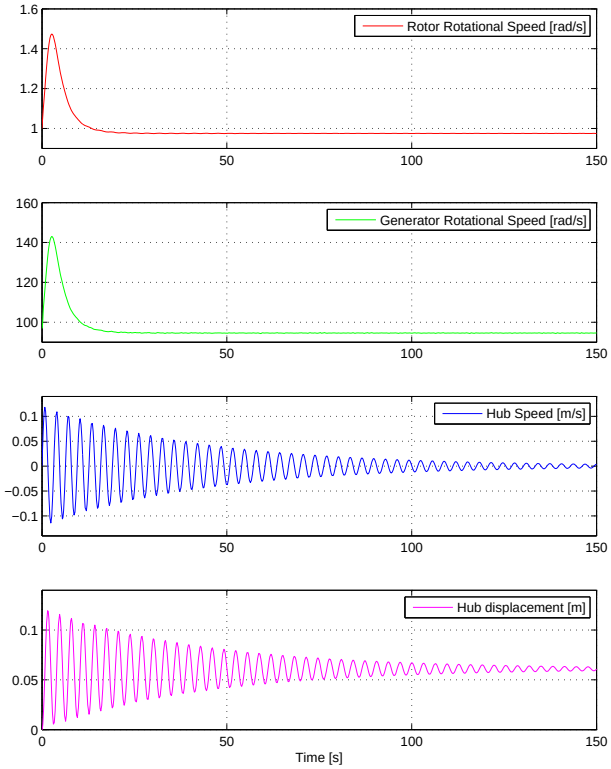

Figure A.25: Time behavior of the selected signals from Matlab/Simulink

include performing control design using bond graph and possibly constructing an offshore wind turbine model. Simulations can be carried out in the software 20-sim, or if one prefer, it is also possible to export the model to MatLab/Simulink via S-function.

6 Appendix

The wind turbine parameters used for this study in the model system are given in Table A.1.

Table A.1: Wind turbine generating system parameters

Pitch	
Natural frequency	$\omega_n = 0.88\ \left[\frac{rad}{s}\right]$
Damping ratio	$\zeta = 0.9\,[-]$
Maximum pitch angle	$\beta_{max} = 25\ [^\circ]$
Minimum pitch angle	$\beta_{min} = -5\ [^\circ]$
Drive Train	
Nominel power	$P_{nom} = 5e6\ [W]$
Rotor inertia	$I_r = 5.9154e7\ \left[Kg \cdot m^2\right]$
Generator inertia	$I_g = 500\ \left[Kg \cdot m^2\right]$
Drive train stiffness	$K_d = 8.7354e8\ \left[\frac{N}{rad}\right]$
Drive train damping	$D_d = 8.3478e7\ \left[\frac{N}{rad \cdot s}\right]$
Gear ratio	$N_g = 97\,[-]$
Generator	
Time constant	$\tau = 0.1\ [s]$
Nominal generator speed	$\omega_{gmax} = 122.91\ \left[\frac{rad}{s}\right]$
Minimum generator speed	$\omega_{gmin} = 70.16\ \left[\frac{rad}{s}\right]$
Structure/Tower	
Rotor radius	$R = 63\ [m]$
Hub height	$h = 90\ [m]$
Tower mass	$m_t = 4.2278e5\ [Kg]$
Tower stiffness	$K_t = 1.6547e6\ \left[\frac{N}{m}\right]$
Tower damping	$D_t = 2.0213e3\ \left[\frac{N}{m \cdot s}\right]$

Acknowledgment

This work has been (partially) funded by Norwegian Centre for Offshore Wind Energy (NORCOWE) under grant 193821/S60 from Research Council of Norway (RCN). NORCOWE is a consortium with partners from industry and science, hosted by Christian Michelsen Research.

REFERENCES

Akhmatov, V. and Knudsen, H. (1999). Modeling of windmill induction generators in dynamic simulation programs. International Conference on Electric Power Engineering.

Borutzky, W. (2010). *Bond Graph Methodology: Development and Analysis of Multidisciplinary Dynamic System Models*. Springer.

Bottasso, C. L. and Croce, A. (2009). Cp-lambda user manual. Technical report, Dipartimento di Ingnegneria Aerospaziale, Politecnico di Milano.

Eggleston, D. M. and Stoddard, F. S. (1987). *Wind Turbine Engineering Design*. Van Nostrand Reinhold Co.

Hammerum, K., Brath, P., and Poulsen, N. K. (2007). A fatigue approach to wind turbine control. *Journal of Physics: Conference Series*, 75(1).

Heier, S. (1998). *Grid Integration of Wind Energy Conversion Systems*. John Wiley and Sons Ltd.

Henriksen, L. C. (2007). Model predictive control of a wind turbine. Master thesis, Technical University of Denmark.

Jonkman, J. and Buhl, M. L. J. (2005). FAST users guide. Technical report NREL/EL-500-38230, National Renewable Energy Laboratory.

Karnopp, D. C., Margolis, D. L., and Rosenberg, R. C. (2006). *System Dynamics: Modeling and Simulation of Mechatronic Systems*. John Wiley and Sons Ltd.

Kleijn, C. (2009). 20-sim 4.1 reference manual. Technical report, Controllab Products B.V.

Larsen, T. J. and Hansen, A. M. (2007). How 2 HAWC2, The user's manual. Technical report, Risø.

Martins, M., Perdana, A., Ledesma, P., Agneholm, E., and Carlson, O. (2007). Validation of fixed speed wind turbine dynamic models with measured data. *Renewable Energy*, 32(8):1301–1316.

MATLAB (2010). Version 7.10.0 (r2010a). Technical report, The MathWorks Inc.

Muyeen, S. M., Ali, M. H., Takahashi, R., Murata, T., Tamura, J., Tomaki, Y., Sakahara, A., and Sasano, E. (2007). Comparative study on transient stability analysis of wind turbine generator system using different drive train models. *IET Renewable Power Generation*, 1(2):131–141.

Paynter, H. M. (1961). *Analysis and Design of Engineering Systems*. MIT Press.

Pedersen, E. and Engja, H. (2003). *Mathematical Modeling and Simulation of Physical Systems*. Lecture notes in course TMR4275 Modeling, Simulation and Analysis of Dynamic Systems at NTNU, Trondheim, Norway.

Petru, T. and Thiringer, T. (2002). Modeling of wind turbines for power system studies. *IEEE Transactions on Power Systems*, 17(4):1132–1139.

Tamura, J., Yamajaki, T., Ueno, M., Matsumura, Y., and Kimoto, S. (2001). Transient stability simulation of power system including wind generator by PSCAD/EMTDC. IEEE Porto Power Tech Conference.

Zubia, I., Ostolaza, X., Tapia, G., Tapia, A., and Saenz, J. R. (2001). Electrical fault simulation and dynamic response of a wind farm. International Conference on Power and Energy System.

Paper B

Robust H_∞ Dynamic Output Feedback Control Synthesis with Pole Placement Constraints for Offshore Wind Turbine Systems

T. Bakka and H. R. Karimi

This paper has been published as:

T. Bakka and H. R. Karimi, "Robust H_∞ Dynamic Output Feedback Control Synthesis with Pole Placement Constraints for Offshore Wind Turbine Systems", *Mathematical Problems in Engineering vol. 2012*, Article ID 616507, 18 pages, doi:10.1155/2012/616507, 2012.

Robust H_∞ Dynamic output-feedback Control Synthesis with Pole Placement Constraints for Offshore Wind Turbine Systems

T. Bakka and H. R. Karimi
Department of Engineering
Faculty of Engineering and Science, University of Agder
Jon Lilletunsvei 9, 4879 Grimstad, Norway.

***Abstract* — The problem of robust H_∞ dynamic output-feedback control design with pole placement constraints is studied for a linear parameter-varying model of a floating wind turbine. A nonlinear model is obtained and linearized using the FAST software developed for wind turbines. The main contributions of this paper are threefold. Firstly, a family of linear models are represented based on an affine parameter-varying model structure for a wind turbine system. Secondly, the bounded parameter-varying parameters are removed using upper bounded inequalities in the control design process. Thirdly, the control problem is formulated in terms of linear matrix inequalities (LMIs). The simulation results show a comparison between controller design based on a constant linear model and a controller design for the linear parameter-varying model. The results show the effectiveness of our proposed design technique.**

Keywords — Wind turbine, H_∞ control, LPV.

1 Introduction

Wind energy is nowadays one of the fastest growing renewable industries. As a consequence of the oil crises in the early 1970s and a general interest of renewable energy, the wind energy sector has had a tremendous growth over the last decades. With Europe leading the global market, the turbine capacity has had an annual growth rate of up to 30% (World Wind Energy Association).

Wind turbines are complex mechanical systems and they are highly nonlinear due to the conversion of wind speed to mechanical torque. This makes the wind turbine

a challenging task both to model and control. In literature, linear and nonlinear controllers have been extensively used for power regulation through the control of blade pitch angle (see for instance (Song and Dhinakaran, 2000; Melício et al., 2011; Kusiak et al., 2010; Kusiak and Zhang, 2012; Eide and Karimi, 2011; Karimi and Bakka, 2011; Karimi, 2011; Bianchi et al., 2007; Mullane et al., 2001; Valenciaga and Puleston, 2000; Steinbuch and Bosgra, 1988; Rocha et al., 2005) and the references therein). Recently, the problem of gain scheduling and output-feedback H_∞ control design for an offshore floating wind turbine was studied in (Bakka et al., 2012). Furthermore, a mixed H_2/H_∞ control design was proposed for an offshore floating wind turbine system was investigated in (Bakka and Karimi, 2012). However, the performance of these controllers are limited by the highly nonlinear characteristics of wind turbine. These controllers are designed on the basis of one operating condition, and therefore can only guarantee performance and stability at this point. By designing the controller on the basis of a Linear-Parameter-Varying (LPV) model, it is possible to overcome these limitations. So, in order to sustain the growth in the wind industry sector, design of advanced control methodologies is one research area where such improvement can be achieved. In recent years, several advanced wind turbine simulation softwares have emerged, such as HAWC2 (Larsen and Hansen, 2007), FAST (Jonkman and Buhl, 2005) and Cp-Lambda (Bottasso and Croce, 2009). In this paper we will use FAST interfaced with Matlab for all the simulations. The operation region of a wind turbine is often divided into four regions (Fig. B.1). In region I ($v < v_{cut-in}$) the wind speed is lower than the cut-in wind speed and no power can be produced. In region II ($v_{cut-in} \leq v < v_{rated}$) the pitch is usually kept constant while the generator torque is the controlling variable. In region III ($v_{rated} \leq v < v_{cut-out}$) the main concern is to keep the rated power and to limit loads on critical parts of the structure by pitching the blades. In region IV ($v > v_{cut-out}$) the wind speed is too high, and the turbine is shut down. In this paper we will focus on the above rated wind speed scenario, i.e. region III.

This paper makes three specific contributions. First, it suggests a family of linear models for a wind turbin system based on an affine parameter-varying model structure. Second, robust stabilization and disturbance attenuation of such parameter-varying models are investigated using H_∞ method such that the bounded parameter-

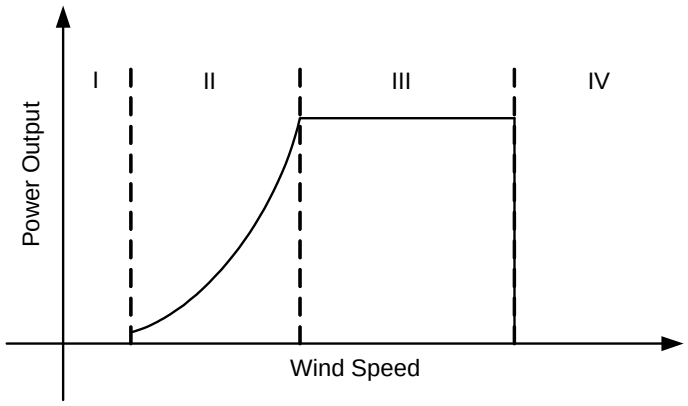

Figure B.1: Operating region of a typical wind turbine

varying parameters are removed using upper bounded inequalities in the control design procedure. Third, the control problem is formulated in terms of linear matrix inequalities (LMIs) and a dynamic output-feedback controller is computed. Finally, the simulation results show that the obtained controller can achieve the robust stability and disturbance attenuation, simultaneously.

This paper is organized as follows: Section II describes the model under consideration and how to include the parameter-varying terms in the closed loop system. Section III is devoted to the control design technique. Simulation results are presented in section IV. Finally, concluding remarks and suggestions to future works are discussed in Section V.

The notations used throughout the paper are fairly standard. I and 0 represent identity matrix and zero matrix; the superscript T stands for matrix transposition; $\Re^n$ denotes the n-dimensional Euclidean space; $\Re^{n\times m}$ is the set of all real m by n matrices. $\|.\|$ refers to the Euclidean vector norm or the induced matrix 2-norm. $diag\{\cdots\}$ represents a block diagonal matrix. The operator $sym(A)$ denotes $A+A^T$ and $\otimes$ denotes the kronecker product. The notation $P>0$ means that P is real symmetric and positive definite; the symbol $*$ denotes the elements below the main diagonal of a symmetric block matrix. Finally given a signal $x(t)$,$\|x(t)\|_2$ denotes the L_2 norm of $x(t)$; i.e., $\|x(t)\|_2^2 = \int_0^\infty x^T(t)x(t)\,dt$.

2 Wind Turbine Model

The wind turbine model is obtained from the wind turbine simulation software FAST (Jonkman and Buhl, 2005). The simulation model is an upscaled version of Statoil's Hywind 2.3 [MW] turbine, which is located off the Norwegian west coast. This upscaled version is also a floating turbine and has the capacity 5 [MW]. For specifications see (Jonkman et al., 2009).

FAST provides a fully nonlinear wind turbine model with up to 24 degrees of freedom (DOF). For the controller design we need a linear model, and we want the linear model to be as simple as possible. All the DOFs available can not be included, so we choose the ones we think will represent the most important dynamics. Linearization routines are available in the FAST package. The model is now linearized at each desired azimuth angle. We find this angle in the plane of rotor rotation. One linear model at each 10th angle is obtained, i.e. the total amount of 36 models are obtained. The models are of the following standard state space form.

$$\begin{aligned} \dot{x} &= A_i x + B_i u \\ y &= C_i x, \quad i = 1,2...36 \end{aligned} \tag{B.1}$$

where x is the state vector with dimensions $\Re^{n\times 1}$, u is the control signal with dimensions $\Re^{p\times 1}$, y is the model outputs with dimensions $\Re^{m\times 1}$ and A, B, C are the system matrices with dimensions $\Re^{n\times n}$, $\Re^{n\times p}$ and $\Re^{m\times n}$ respectively. The states in this linear model are tower fore-aft displacement (x_1), generator position (x_2), rotor position (x_3) and the last three states are the first derivative of x_{1-3}. The model input u, which will eventually be calculated by the controller, is the blade pitch angle. The model outputs in y are tower fore-aft displacement, generator speed and rotor speed.

A common way to simplify these models are to take the average of all the 36 models and use this as basis for the controller design. By doing this simplification, important information is easily lost. This is why in this paper we will try to do the controller design based on a model representation which tries to include as much as possible of the information in the 36 models. The matrices A and B are behaving in a periodic way, the matrix values depend on the rotor azimuth angle. Several

things are the cause of this periodic behavior, i.e. aerodynamic loads, tower shadow, gravitational loads and deflections of the tower due to thrust loading. The matrices associated with the output y are not varying. C is constant since it only handles the measurements. In (B.2) we define the varying matrices in an affine way, $A(z)$ and $B(z)$ vary in a continuous manner.

$$\begin{aligned} A(z) &= A_n + \Delta A(z), \\ B(z) &= B_{2n} + \Delta B(z), \end{aligned} \tag{B.2}$$

where A_n and B_{2n} are the nominal plant matrices, $\Delta A(z)$ and $\Delta B(z)$ contributes with the varying terms and z represent the rotor azimuth angle. We are looking to represent the parameter-varying terms in this way: $\Delta A(z) = F\Delta(z)E$, and a similar expression for $\Delta B(z)$. After analyzing the 36 models we find appropriate matrices F and E, but we also find out that more than one scheduling parameter is needed. The periodic matrices $A(z)$ and $B(z)$ can now be represented in a continuous way with the use of *sine* and *cosine* functions. The parameter-varying terms in (B.2) are defined in the following way:

$$\begin{aligned} \Delta A(z) &= \sum_{i=1}^{2}\sum_{j=1}^{2} F_i \Delta_j(z) E_{jia}, \\ \Delta B(z) &= \sum_{i=1}^{2}\sum_{j=1}^{2} F_i \Delta_j(z) E_{jib}, \end{aligned}$$

where the vectors F and E have appropriate dimensions, the scheduling variables $\Delta_1(z)$ and $\Delta_2(z)$ are found to be $sin(\omega t)$ and $cos(\omega t)$ respectively. A plot which shows what the different parameters are in the original matrices $A_{1..36}$ and $B_{1..36}$ and in the new representation $A_n + \Delta A(z)$ and $B_{2n} + \Delta B(z)$ are found in the appendix.

3 Control Design

The purpose of $\mathscr{H}_\infty$ control is to minimize the effect of disturbances on the controlled output. The control design is formulated in terms of linear matrix inequalities (LMIs). After manipulating the linear model obtained from FAST, we end up

with a state space system with parameter-varying A and B matrices. This model is more accurate than if we just took the average of all the 36 models. By using a LPV model of the system we are able to catch some of the dynamics thats is lost under the linearization. The challenge is now to incorporate these additional terms into the control design.

These robust control designs mostly deal with frequency domain aspects of the closed loop system, but it is well known that the location of the closed loop poles play a large role in the transient behavior of the controlled system. By adding pole placement to the list of constraints we can prevent large poles and we can end up with a system which can respond in a realistic way. The controller we are searching for will try to keep the generator speed at its rated value while mitigating oscillations in the drive train and in the tower.

The LMIs for the control design are solved using YALMIP (Löfberg, 2004) interfaced with Matlab and we are using the solver SeDuMi. This solver is searching for two positive definite matrices X and Y which stabilities the LTI system. If these matrices exist we can calculate the controller. The next sections presents how to obtain the LMIs for the controller design and also how to incorporate the parameter-varying part of the state space system.

3.1 System representation

Fig. B.2 shows the output-feedback control scheme, where $P(s)$ is the generalized

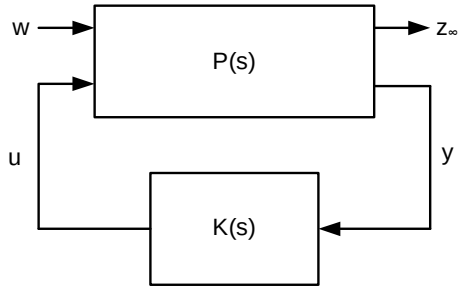

Figure B.2: output-feedback block diagram

plant and $K(s)$ is the controller. The two blocks represent the equations in (B.3)-

(B.4). $P(s)$ includes the wind turbine model and the signals of interest.

$$\begin{aligned} \dot{x} &= Ax + B_1 w + B_2 u, \\ z_\infty &= C_{1i} x + D_{1i} w + D_{2i} u, \\ y &= C_2 x + D_{21} w, \end{aligned} \tag{B.3}$$

where A, B_2 and C_2 represent the matrices from the standard state space form in (B.1). To include the parameter-varying matrices, A is substituted with $A(z)$ and B_2 with $B(z)$. The other matrices are considered with appropriate dimensions. u is the control input, w is the disturbance signal and y is the measured output. The signal z_∞ is the controlled output for $\mathscr{H}_\infty$ performances measure. For system (B.3), the dynamic output-feedback, $u(s) = K(s)y(s)$, is of the following form:

$$K(s) \begin{cases} \dot{\zeta} = A_k \zeta + B_k y, \\ u = C_k \zeta + D_k y. \end{cases} \tag{B.4}$$

The closed loop system is given in (B.5) with the states $x_{cl} = [x \ \zeta]^T$.

$$\begin{aligned} \dot{x}_{cl} &= A_{cl} x + B_{cl} w, \\ z_\infty &= C_{cl} x + D_{cl} w. \end{aligned} \tag{B.5}$$

The closed loop system is divided into two parts, one with constant state space matrices and one where the parameter-varying matrices are.

$$\begin{aligned} \left(\begin{array}{c|c} A_{cl} & B_{cl} \\ \hline C_{cl} & D_{cl} \end{array}\right) &= \left(\begin{array}{c|c} A_{cl1} & B_{cl1} \\ \hline C_{cl1} & D_{cl1} \end{array}\right) + \left(\begin{array}{c|c} A_{cl2}(z) & B_{cl2}(z) \\ \hline 0 & 0 \end{array}\right) \\ &= \left(\begin{array}{cc|c} A_n + B_{2n} D_k C_2 & B_{2n} C_k & B_1 + B_{2n} D_k D_{21} \\ B_k C_2 & A_k & B_k D_{21} \\ \hline C_{1i} + D_{2i} D_k C_2 & D_{2i} C_k & D_{1i} + D_{2i} D_k D_{21} \end{array}\right) \\ &+ \left(\begin{array}{cc|c} \Delta A(z) + \Delta B(z) D_k C_2 & \Delta B(z) C_k & \Delta B(z) D_k D_{21} \\ 0 & 0 & 0 \\ \hline 0 & 0 & 0 \end{array}\right). \end{aligned} \tag{B.6}$$

3.2 H_∞ Control

Because of the parameter-varying state space system we now get an additional term to the standard Bounded Real Lemma (BRL). This additional term is the second part of the summation in constraint (B.7). We want to make sure that the closed-loop $\mathscr{H}_\infty$ norm of the closed loop transfer function does not exceed γ. This is true if and only if there exist a symmetric matrix X such that

$$\begin{pmatrix} A_{cl1}^T X + X A_{cl1} & X B_{cl1} & C_{cl1}^T \\ * & -\gamma I & D_{cl1}^T \\ * & * & -\gamma I \end{pmatrix} + \begin{pmatrix} A_{cl2}^T(z) X + X A_{cl2}(z) & X B_{cl2}(z) & 0 \\ * & 0 & 0 \\ * & * & 0 \end{pmatrix} < 0, \tag{B.7}$$

$$X > 0. \tag{B.8}$$

3.3 Change of Variables

Obviously, the $\mathscr{H}_\infty$ constraint (B.7) is not an LMI because of the nonlinear terms which occur when we close the loop. In order to transform these nonlinear terms into proper LMIs we need to do two things. First, we need to linearize them with the use of change of variables. Second, we need to remove the parameter-varying terms. The linearization part is not as straight forward as for the state-feedback case, additional information about this can be found in (Scherer et al., 1997).
The new Lyapunov matrix is partitioned in the following form.

$$\mathscr{X} = \begin{bmatrix} Y & N \\ N^T & \# \end{bmatrix}, \qquad \mathscr{X}^{-1} = \begin{bmatrix} X & M \\ M^T & \# \end{bmatrix}, \tag{B.9}$$

where X and Y are symmetric matrices of dimension $n \times n$. It is not necessary to know the matrices noted as #.

In addition, we define the following two matrices

$$\Pi_1 = \begin{bmatrix} X & I \\ M^T & 0 \end{bmatrix}, \qquad \Pi_2 = \begin{bmatrix} I & Y \\ 0 & N^T \end{bmatrix}, \tag{B.10}$$

that, as can be inferred from the identity $\mathscr{X}\mathscr{X}^{-1} = I$, satisfies

$$\mathscr{X}\Pi_1 = \Pi_2. \tag{B.11}$$

Then, the following change of controller variables are defined

$$\begin{aligned} \hat{A} &= NA_kM^T + NB_kC_2X + YB_{2n}C_kM^T \\ &\quad + Y(A_n + B_{2n}D_kC_2)X, && \text{(B.12)} \\ \hat{B} &= NB_k + YB_{2n}D_k, && \text{(B.13)} \\ \hat{C} &= C_kM^T + D_kC_2X, && \text{(B.14)} \\ \hat{D} &= D_k. && \text{(B.15)} \end{aligned}$$

Now we are ready to convert our nonlinear matrix inequalities into LMIs. By performing congruence transformation with $diag(\Pi_1, I, I)$ on the obtained inequality (B.7), we end up with following matrix inequality:

$$\begin{aligned} \Sigma_1 &+ sym(G_1\Delta_1(z)H_1) + sym(G_2\Delta_1(z)H_1) \\ &+ sym(G_1\Delta_1(z)H_2) + sym(G_2\Delta_1(z)H_2) \\ &+ sym(G_3\Delta_2(z)H_3) + sym(G_4\Delta_2(z)H_3) \\ &+ sym(G_3\Delta_2(z)H_4) + sym(G_4\Delta_2(z)H_4) < 0, \end{aligned} \tag{B.16}$$

where the matrix Σ_1 and the vectors G_i and H_i are defined in the appendix.

Lemma 1 (Khargonekar et al., 1990)*:* Given $\Sigma = \Sigma^T$, G, Δ and H of appropriate dimensions with $\Delta^T\Delta \leq I$, then the matrix inequality

$$\Sigma + sym(G\Delta H) < 0$$

holds for all Σ if and only if there exist a scalar $\varepsilon > 0$ such that

$$\Sigma + \varepsilon GG^T + \varepsilon^{-1} H^T H < 0.$$

By using Lemma 1 we are able to remove the parameter-varying parts $\Delta_i(z)$ in the matrix inequality (B.16). We end up with a new LMI which contains the constants ε_1 and ε_2.

$$\begin{aligned} \Sigma_1 &+ 2\varepsilon_1 G_1 G_1^T + 2\varepsilon_1^{-1} H_1^T H_1 + 2\varepsilon_1 G_2 G_2^T + 2\varepsilon_1^{-1} H_2^T H_2 \\ &+ 2\varepsilon_2 G_3 G_3^T + 2\varepsilon_2^{-1} H_3^T H_3 + 2\varepsilon_2 G_2 G_4^T + 2\varepsilon_2^{-1} H_4^T H_4 < 0. \end{aligned} \tag{B.17}$$

By using the Schur complement we can convert (B.17) into the following LMIs:

$$\begin{pmatrix} \Sigma_1 & \Sigma_2 \\ * & \Sigma_3 \end{pmatrix} < 0, \tag{B.18}$$

$$\begin{pmatrix} X & I \\ I & Y \end{pmatrix} > 0, \tag{B.19}$$

where

$$\begin{aligned} \Sigma_2 &= \begin{bmatrix} \varepsilon_1 G_1 & H_1^T & \varepsilon_1 G_2 & H_2^T & \varepsilon_2 G_3 & H_3^T & \varepsilon_2 G_4 & H_4^T \end{bmatrix}, \\ \Sigma_3 &= diag\{ -\tfrac{1}{2}\varepsilon_1 I_{2\times 2}, -\tfrac{1}{2}\varepsilon_1 I_{2\times 2}, -\tfrac{1}{2}\varepsilon_1 I_{2\times 2}, -\tfrac{1}{2}\varepsilon_1 I_{2\times 2}, \\ &\quad -\tfrac{1}{2}\varepsilon_2 I_{2\times 2}, -\tfrac{1}{2}\varepsilon_2 I_{2\times 2}, -\tfrac{1}{2}\varepsilon_2 I_{2\times 2}, -\tfrac{1}{2}\varepsilon_2 I_{2\times 2} \}. \end{aligned} \tag{B.20}$$

3.4 LMI Region

An LMI region is any convex subset $\mathscr{D}$ of the complex plane that can be characterized as an LMI in z and $\bar{z}$ (Chilali and Gahinet, 1996) as follows:

$$D = \{z \in C : \bar{L} + \bar{M} z + \bar{M}^T \bar{z} < 0\}, \tag{B.21}$$

for some fixed real matrices $\bar{M}$ and $\bar{L} = \bar{L}^T$, where $\bar{z}$ is a complex number. This class of regions encompasses half planes, strips, conic sectors, disks, ellipses, and any intersection of the above. From (Chilali and Gahinet, 1996), we find that, all

eigenvalues of the matrix A is in the LMI region $\{z \in C : [\bar{l}_{ij} + \bar{m}_{ij} z + \bar{m}_{ji} \bar{z}]_{i,j} < 0\}$ if and only if there exists a symmetric matrix X such that

$$\left[\bar{l}_{ij} X + \bar{m}_{ij} A^T X + \bar{m}_{ji} X A\right]_{i,j} < 0, \qquad X > 0. \tag{B.22}$$

Also, here we need to include the change of variables and remove the parameter-varying terms, this is done in (B.23). The LMI is obtained in a manner similar to the one that was used for the $\mathscr{H}_\infty$ constraint.

$$\begin{pmatrix} \Sigma_4 & \Sigma_5 \\ * & \Sigma_3 \end{pmatrix} < 0, \tag{B.23}$$

where

$$\Sigma_5 \;=\; \begin{bmatrix} \varepsilon_1 P_1 & N_1^T & \varepsilon_1 P_2 & N_2^T & \varepsilon_2 P_3 & N_3^T & \varepsilon_2 P_4 & N_4^T \end{bmatrix},$$

and Σ_4 and the other terms in Σ_5 are defined in Appendix.

Remark 1. It is observed that the inequalities (B.18), (B.19) and (B.23) are linear in $\left(X,\, Y,\, \hat{A},\, \hat{B},\, \hat{C},\, \hat{D}\right)$ and thus the standard LMI techniques can be exploited to find the LMI solutions. It is also seen from the above results that there exists much freedom contained in the design of control law, such as the choices of appropriate ε_1 and ε_2. This design freedom can be exploited to achieve other desired closed-loop properties.

The desired region $\mathscr{D}$ is a disk (Fig. B.3), with center located along the x-axis (distance q from the origin) and radius r. This determines the region

$$\mathscr{D} = \begin{pmatrix} -r & q+z \\ q+\bar{z} & -r \end{pmatrix}. \tag{B.24}$$

From this we can find the matrices $\bar{L}$ and $\bar{M}$, which is the two matrices that determines the LMI region.

All constraints in (B.18), (B.19) and (B.23) are now subjected to the minimization of the objective function, which is the $\mathscr{H}_\infty$-norm. They need to be solved in terms of $\left(X,\, Y,\, \hat{A},\, \hat{B},\, \hat{C},\, \hat{D}\right)$.

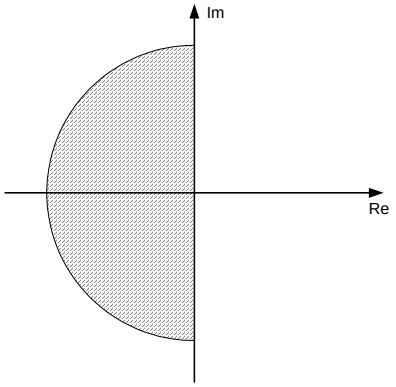

Figure B.3: LMI region $\mathscr{D}$

Once all these matrices are obtained, the controller matrices are computed in the following way. First we obtain M and N from the factorization problem

$$MN^T = I - XY. \tag{B.25}$$

Second, the controller matrices are computed from the following relationship;

$$\begin{aligned} D_k &= \hat{D}, && \text{(B.26)} \\ C_k &= \left(\hat{C} - D_k C_2 X\right)\left(M^T\right)^{-1}, && \text{(B.27)} \\ B_k &= N^{-1}\left(\hat{B} - Y B_{2n} D_k\right), && \text{(B.28)} \\ A_k &= N^{-1}\left(\hat{A} - N B_k C_2 X - Y B_{2n} C_k M^T\right. \\ &- \left. Y\left(A_n + B_{2n} D_k C_2\right) X\right)\left(M^T\right)^{-1}. && \text{(B.29)} \end{aligned}$$

4 Simulation Results

The simulations are carried out with FAST software interfaced with Matlab/Simulink. The controllers are tested on the fully nonlinear system with 22 out of 24 DOFs enabled. Yaw - and platform surge - motion are left out. The wind turbine system is subjected to extreme wind conditions. The wind profile is a 50 year extreme case with an average speed of 18 $[m/s]$ (Fig. B.4) and a turbulence intensity of 17%. Significant wave hight is 6 $[m]$ with a peak wave period of 10 $[s]$ The wind profile is obtained from the software Turbsim (Jonkman, 2009).

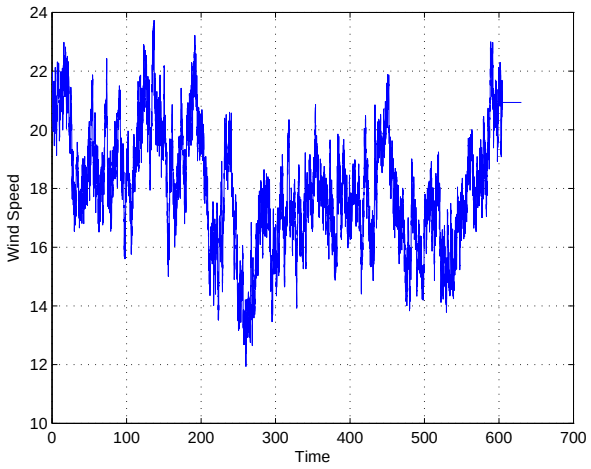

Figure B.4: Wind profile

Suitable results are found with the following $\mathscr{H}_\infty$ performance measure

$$z_\infty = x_1 + x_2 + x_6 + u. \tag{B.30}$$

The blue line in the plots is the result where the parameter-varying terms are taken into consideration in the controller design. The red line shows the result where the parameter-varying terms are left out. We also show NREL's PI gain scheduled controller (cyan colored line) as a reference plot. Our two controllers are designed and tested on exactly the same operating conditions, i.e. same performance measure, same pole placement constraint and same wind condition. From Figs. (B.5)-(B.6) we see that the blue line is operating more steady around the rated values for the rotor and generator, which are 12.1 $[RPM]$ and 1173.7 $[RPM]$, respectively. This will in turn result in a smother torque output, as seen in Fig. (B.7).

Our two controller designs show a large increment in pitching activity. If we inspect the pitching rate, we see that it is not more than $5-10$ $[deg/s]$, and hence should be withing the wind turbine's limit. The blue line in Fig. (B.9) shows that the amplitude of the oscillations are lower in the fore-aft direction than in the other two plots. From these plots we see that the results are according to the controller objectives.

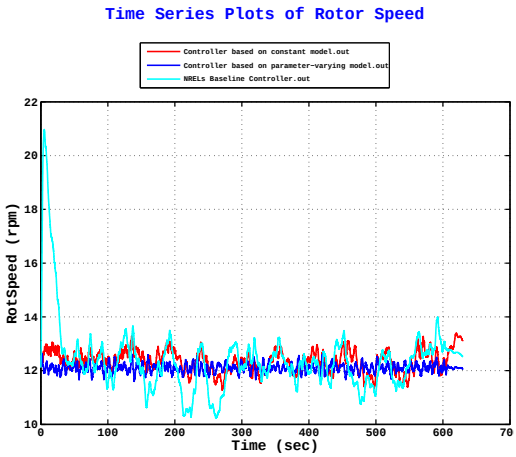

Figure B.5: Rotor speed

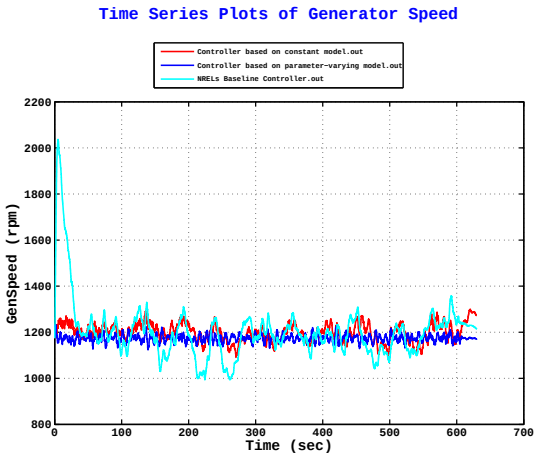

Figure B.6: Generator speed

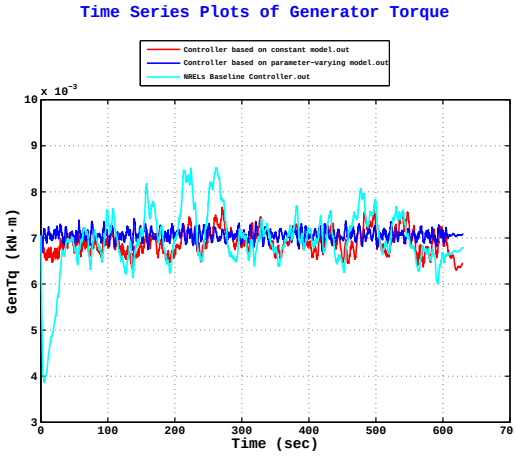

Figure B.7: Generator torque

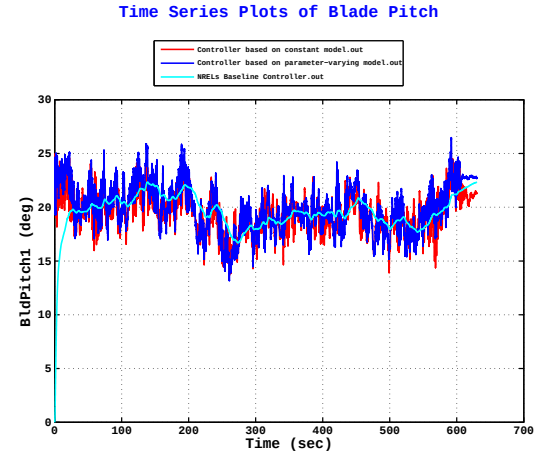

Figure B.8: Blade pitch

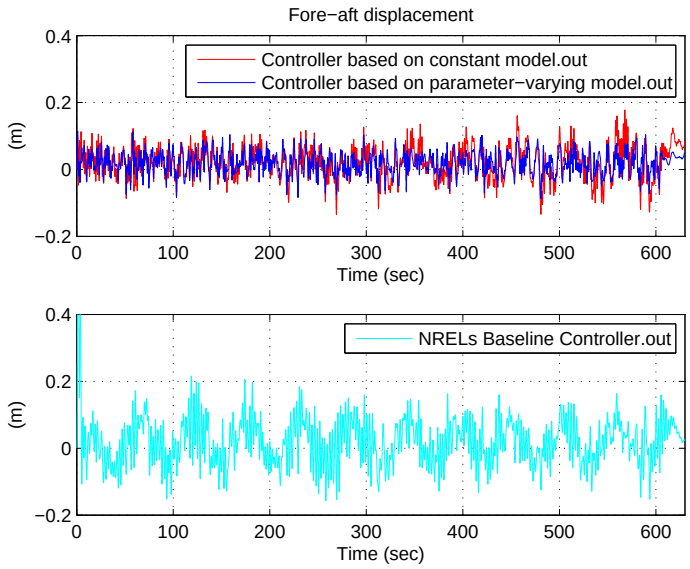

Figure B.9: Tower fore-aft

5 Conclusions

In this paper we have obtained and linearized a wind turbine model using the commercial software FAST. The output from the linearization is a family of models describing the turbine system at each 10th azimuth angle. This family of models are converted into one parameter-varying model. The new model now depends on the azimuth angle. In this way we can make the control design based on a model consisting of more information than if we had done it the conventional way, which is to use the average of the family of models. The controller is tested on the fully nonlinear system subjected to 50 year extreme wind conditions. The simulation results show a comparison between controller design done with the new method and done the conventional way. The plots show that the simulation results meet our control objectives.

Based on the results in the paper, interesting future research may be prospective as follows:

1. it is worth noting that in this paper a constant controller is designed for a parameter-varying model. A next step could be to design a parameter-varying controller, where the scheduling parameter is the azimuth angle.

2. the methods presented in (Wang et al., 2010) and (Dong et al., 2010b) can be used for a stochastic model of a wind turbine system with constrained information exchange, and a partial knowledge of the state variables.

3. fault detection and control design for wind turbine systems over a network (see for instance (Dong et al., 2010a) and (Shen et al., 2010)) can be studied in the framework of this paper.

4. though the addressed issue is the control problem, the methods proposed in the paper can be extended to filtering problem (see for instance (Shen et al., 2009)).

6 Appendix

The size of the A matrix is 6×6 and the B matrix has size 6×1. Only the last three rows are shown in Figs. (B.10) and (B.11), respectively. The first three rows contain either constant- or zeros-values. The blue line shows how the 36 linear models are distributed along the 360 azimuth angles. The red line shows our attempt to emulate these periodic matrix values with a function on the form $A_n + \Delta A(z)$ for the A-matrix and $B_{2n} + \Delta B(z)$ for the B-matrix.

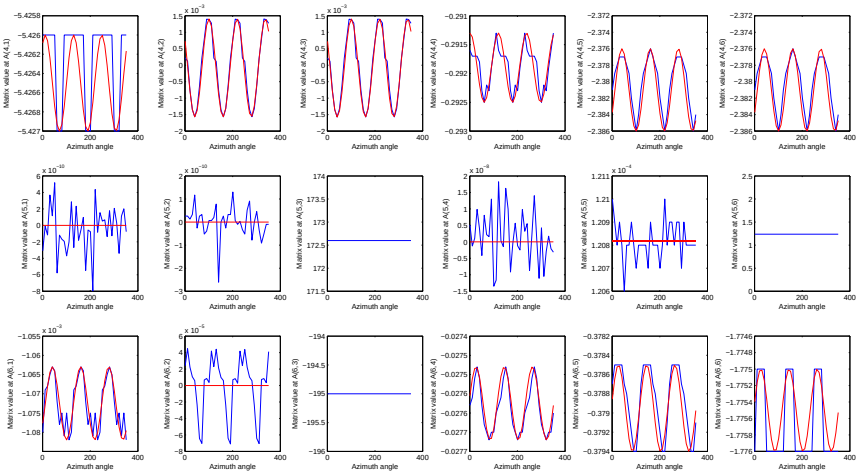

Figure B.10: Parameters in A-matrix row 4-6

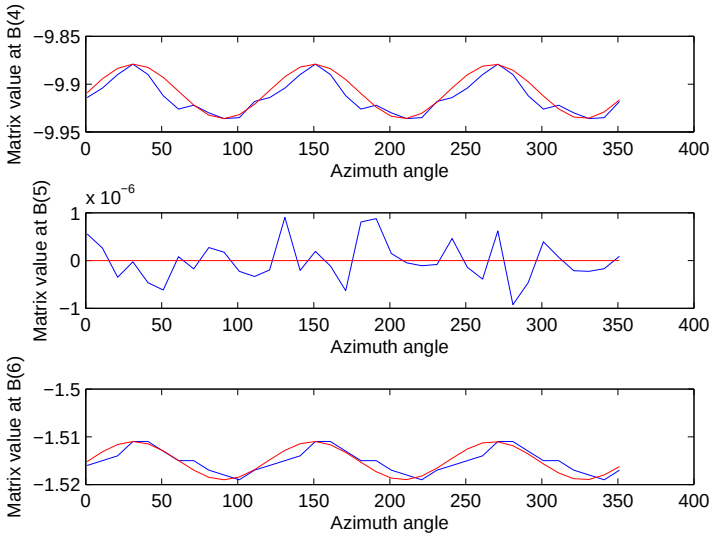

Figure B.11: Parameters in B-matrix row 4-6

$$\Sigma_1 = \begin{pmatrix} sym\left(AX + B_{2n}\hat{C}\right) & \hat{A}^T + A + B_{n2}\hat{D}C_2 & B_1 + B_{2n}\hat{D}D_{21} & XC_{1i}^T + \hat{C}^T D_{21}^T \\ * & sym\left(YA + \hat{B}C_2\right) & YB_1 + \hat{B}D_{21} & C_{1i}^T + C_2^T \hat{D}^T + D_{2i}^T \\ * & * & -\gamma I & D_{1i}^T + D_{21}^T \hat{D} D_{2i}^T \\ * & * & * & -\gamma I \end{pmatrix},$$

$$\begin{aligned} G_1 &= [F_1 \;\; 0_{1\times 8}]^T, \;\; G_2 = [0_{1\times 6} \;\; YF_1 \;\; 0_{1\times 2}]^T, \\ G_3 &= [F_2 \;\; 0_{1\times 8}]^T, \;\; G_4 = [0_{1\times 6} \;\; YF_2 \;\; 0_{1\times 2}]^T, \\ H_1 &= \left[E_{11a}X + E_{11b}\hat{C} \;\; E_{11a} + E_{11b}\hat{D}C_2 \;\; E_{11b}\hat{D}D_{21} \;\; 0\right], \\ H_2 &= \left[E_{12a}X + E_{12b}\hat{C} \;\; E_{12a} + E_{12b}\hat{D}C_2 \;\; E_{12b}\hat{D}D_{21} \;\; 0\right], \\ H_3 &= \left[E_{21a}X + E_{21b}\hat{C} \;\; E_{21a} + E_{21b}\hat{D}C_2 \;\; E_{21b}\hat{D}D_{21} \;\; 0\right], \\ H_4 &= \left[E_{22a}X + E_{22b}\hat{C} \;\; E_{22a} + E_{22b}\hat{D}C_2 \;\; E_{22b}\hat{D}D_{21} \;\; 0\right], \end{aligned}$$

$$\Sigma_4 = \left(\bar{L} \otimes \begin{pmatrix} \mathbf{X} & I \\ I & \mathbf{Y} \end{pmatrix} + \bar{M} \otimes \begin{pmatrix} A\mathbf{X} + B_{2n}\hat{\mathbf{C}} & A + B_{2n}\hat{\mathbf{D}}C_z \\ \hat{\mathbf{A}} & \mathbf{Y}A + \hat{\mathbf{B}}C_z \end{pmatrix}\right.$$

$$+\bar{M}^T \otimes \left(\begin{array}{cc} A\mathbf{X}+B_{2n}\hat{\mathbf{C}} & A+B_{2n}\hat{\mathbf{D}}C_z \\ \hat{\mathbf{A}} & \mathbf{Y}A+\hat{\mathbf{B}}C_z \end{array} \right)^T \Bigg),$$

$$\begin{aligned}
G_1 &= [F_1 \ 0_{1\times 6}]^T, \ G_2 = [0_{1\times 6} \ \mathbf{Y}F_1]^T, \ G_3 = [F_2 \ 0_{1\times 6}]^T, \\
G_4 &= [0_{1\times 6} \ \mathbf{Y}F_2]^T, \ H_{1-2} = \left[E_{11a}\mathbf{X}+E_{11b}\hat{\mathbf{C}} \ E_{11a}+E_{11b}\hat{\mathbf{D}}C_2\right], \\
H_{2-2} &= \left[E_{12a}\mathbf{X}+E_{12b}\hat{\mathbf{C}} \ E_{12a}+E_{12b}\hat{\mathbf{D}}C_2\right], \\
H_{3-2} &= \left[E_{21a}\mathbf{X}+E_{21b}\hat{\mathbf{C}} \ E_{21a}+E_{21b}\hat{\mathbf{D}}C_2\right], \\
H_{4-2} &= \left[E_{22a}\mathbf{X}+E_{22b}\hat{\mathbf{C}} \ E_{22a}+E_{22b}\hat{\mathbf{D}}C_2\right], \ N_1 = I_{2\times 2}\otimes H_{1-2}, \\
N_2 &= I_{2\times 2}\otimes H_{2-2}, \ N_3 = I_{2\times 2}\otimes H_{3-2}, \ N_4 = I_{2\times 2}\otimes H_{4-2}, \\
H_1 &= M\otimes G_{1-2}, \ H_2 = M\otimes G_{2-2}, \ H_3 = M\otimes G_{3-2}, \ H_4 = M\otimes G_{4-2}.
\end{aligned}$$

Acknowledgment

This work has been (partially) funded by Norwegian Centre for Offshore Wind Energy (NORCOWE) under grant 193821/S60 from Research Council of Norway (RCN). NORCOWE is a consortium with partners from industry and science, hosted by Christian Michelsen Research.

REFERENCES

Bakka, T. and Karimi, H. R. (2012). Mixed H_2/H_∞ control design for wind turbine system with pole placement constraints. pages 4775–4780. Proceedings of the 31*st* Chinese Control Conference.

Bakka, T., Karimi, H. R., and Duffie, N. A. (2012). Gain scheduling for output H_∞ control of offshore wind turbine. pages 496–501. Proceedings of the 22^{nd} International Offshore and Polar Engineering Conference.

Bianchi, F., Battista, H., and Mantz, R. (2007). *Wind Turbine Control Systems: Principles, Modelling and Gain Scheduling Design*. Springer.

Bottasso, C. L. and Croce, A. (2009). Cp-lambda user manual. Technical report, Dipartimento di Ingnegneria Aerospaziale, Politecnico di Milano.

Chilali, M. and Gahinet, P. (1996). H_∞ design with pole placement constraints: An LMI approach. *IEEE Transactions on Automatic Control*, 41(3):358–367.

Dong, H., Wang, Z., and Gao, H. (2010a). Robust H_∞ filtering for a class of nonlinear networked systems with multiple stochastic communication delays and packet dropouts. *IEEE Transactions on Signal Processing*, 58(4):1957–1966.

Dong, H., Wang, Z., Ho, D. W. C., and Gao, H. (2010b). Robust H_∞ fuzzy output-feedback control with multiple probabilistic delays and multiple missing measurements. *IEEE Transactions on Fuzzy Systems*, 18(4):712–725.

Eide, R. and Karimi, H. R. (2011). Control design methodologies for vibration mitigation on wind turbine systems. In *Vibration Analysis and Control - New Trends and Developments*. InTech, Chichester, UK.

Jonkman, B. (2009). Turbsim users guide: Version1.50. Technical report, National Renewable Energy Laboratory.

Jonkman, J. and Buhl, M. L. J. (2005). FAST users guide. Technical report NREL/EL-500-38230, National Renewable Energy Laboratory.

Jonkman, J., Butterfield, S., Musial, W., and Scott, G. (2009). Definition of a 5-MW reference wind turbine for offshore system development. Technical report NREL/TP-500-38060, National Renewable Energy Laboratory.

Karimi, H. R. (2011). Wavelet-based optimal control of a wind turbine system: A computational approach. *Journal of Advanced Mechanical Design, Systems, and Manufacturing*, 5(3):171–186.

Karimi, H. R. and Bakka, T. (2011). Stochastic analysis and h_∞ control of wind turbine systems with wireless sensor networks. pages 1086–1095. Proceedings of the 24^{th} International Congress on Condition Monitoring and Diagnostic Engineering Management.

Khargonekar, P. P., Petersen, I. R., and Zhou, K. (1990). Robust stabilization of uncertain linear systems: Quadratic stabilizability and control theory. *IEEE Transactions on Automatic Control*, 35(3):356–361.

Kusiak, A., Li, W., and Song, Z. (2010). Dynamic control of wind turbines. *Renewable Energy*, 35(2):456463.

Kusiak, A. and Zhang, Z. (2012). Control of wind turbine power and vibration with a data-driven approach. *Renewable Energy*, 43:7382.

Larsen, T. J. and Hansen, A. M. (2007). How 2 HAWC2, The user's manual. Technical report, Risø.

Löfberg, J. (2004). YALMIP: A toolbox for modeling and optimization in MATLAB. pages 284–289. In Proceedings of IEEE International Symposium on Computer Aided Control Systems Design.

Melício, R., Mendes, V. M. F., and Catalão, J. P. S. (2011). Comparative study of power converter topologies and control strategies for the harmonic performance of variable-speed wind turbine generator systems. *Energy*, 36(1):520–529.

Mullane, A., Lightbody, G., and Ya, R. (2001). Adaptive control of variable speed wind turbines. *Rev. Energ. Ren.: Power Engineering*, pages 101–110.

Rocha, R., Filho, L. S. M., and Bortolus, M. V. (2005). Optimal multivariable control for wind energy conversion system A comparison between H_2 and H_∞ controllers. pages 7906–7911. Proceedings of the 44th IEEE Conference on Decision and Control, and the European Control Conference.

Scherer, C., Gahinet, P., and Chilali, M. (1997). Multi objective output feedback control via LMI optimization. *IEEE Transactions on Automatic Control*, 42(7):896–911.

Shen, B., Wang, Z., Shu, H., and Wei, G. (2009). H_∞ filtering for nonlinear discrete-time stochastic systems with randomly varying sensor delays. *Automatica*, 45(11):1032–1037.

Shen, B., Wang, Z., Shu, H., and Wei, G. (2010). Robust H_∞ finite-horizon filtering with randomly occurred nonlinearities and quantization effects. *Automatica*, 46(11):1743–1751.

Song, Y. D. and Dhinakaran, B. (2000). Variable speed control of wind turbines using nonlinear and adaptive algorithms. *Journal of Wind Engineering and Industrial Aerodynamics*, 85:293–308.

Steinbuch, M. and Bosgra, O. H. (1988). Optimal output feedback of a wind energy conversion system. pages 313–319. Proceedings of IFAC Power Systems Modelling and Control Applications.

Valenciaga, F. and Puleston, P. F. (2000). An adaptive feedback linearization strategy for variable speed wind energy conversion systems. *International Journal of Energy Research*, 24(2):151–161.

Wang, Z., Ho, D. W. C., Dong, H., and Gao, H. (2010). Robust H_∞ finite-horizon control for a class of stochastic nonlinear time-varying systems subject to sensor and actuator saturations. *IEEE Transactions on Automatic Control*, 55(7):1716–1722.

Paper C

H_∞ Static Output-Feedback Control Design with Constrained Information for Offshore Wind Turbine System

T. Bakka and H. R. Karimi

This paper has been published as:

T. Bakka and H. R. Karimi, "H_∞ Static Output Feedback Control Design with Constrained Information for Offshore Wind Turbine System", *Journal of The Franklin Institute*, doi:10.1016/j.jfranklin.2013.05.028, 2013.

H_∞ Static Output-Feedback Control Design with Constrained Information for Offshore Wind Turbine System

T. Bakka and H. R. Karimi
Department of Engineering
Faculty of Engineering and Science, University of Agder
Jon Lilletunsvei 9, 4879 Grimstad, Norway.

***Abstract* —** This paper deals with H_∞ static output-feedback control design with constrained information for offshore wind turbines. Constrained information indicates that a special zero-nonzero structure is imposed on the static output-feedback gain matrix. A practical use of such an approach is to design a decentralized controller for a wind turbine. This will also benefit the controller in such a way that it is more tolerant to sensor failure. Furthermore, the model under consideration is obtained by using the wind turbine simulation software FAST. Sufficient conditions to design an H_∞ controller are given in terms of Linear Matrix Inequalities (LMIs). Simulation results are given to illustrate the effectiveness of the proposed methodology for different cases of the control gain structures.

Keywords — Wind turbine, H_∞ control, constrained information.

1 Introduction

In these green times, renewable power sources are a popular topic all over the world. The growth in the wind power industry has been tremendous over the last decade and it is nowadays one of the most promising sources for renewable energy. Since the early 1990s wind power industry has enjoyed a renewed interest, and the total installed capacity is increasing heavily every year. According to The World Wind Energy Association's (WWEA) 2012 half-year report, the top world leading countries are China, USA, Germany, Spain and India. Together they represent 74% of the total global capacity. Fig. C.1 illustrates the total installed capacity world wide

since 2001, the figure shows an increase of about 21% each year. In order to sustain this growth in the wind industry sector, advanced control is one area where this can be achieved. Although the majority of the world wide installed wind parks are situated onshore, there is an interest to install new offshore wind parks. The wind velocities are both higher and more stable in offshore environments. Offshore turbines are often either fixed to the soil or they stand on monopoles or other structures. These structures are installed in shallow waters, typical depths up to 60$[m]$. For many countries it would be beneficial to also be able to install wind turbines in deeper waters, in depths up to 1000 [m]. Hywind is one example for a floating wind turbine solution. This is a turbine which is currently in operation and is located right off the Norwegian west coast. It is a model of Hywind this paper is dealing with.

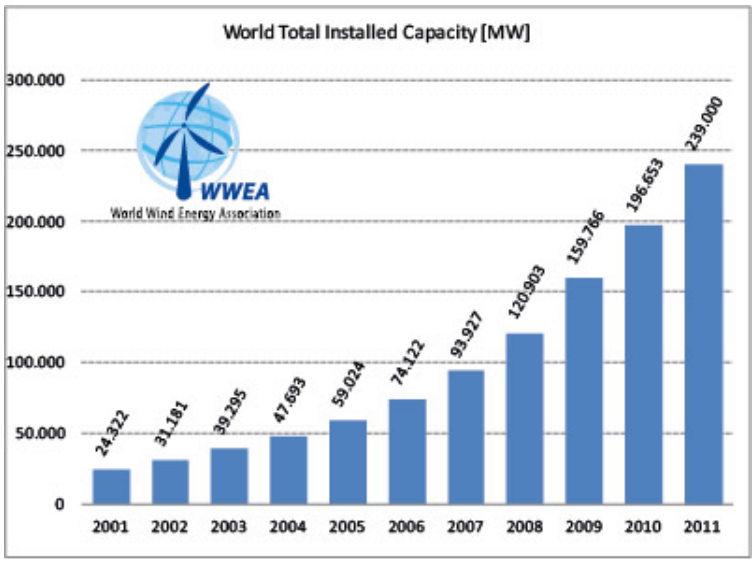

Figure C.1: Total installed wind power capacity from 2001-2011 in $[MW]$

Wind turbines are complex mechanisms. In general, they consist of four major components: rotor, transmission, generator and a support structure. In addition, there is a control system causing the turbine to behave in a suitable manner. Over the years, there have been presented many ways to model the wind turbine, for instance, single mass models (Abdin and Xu, 2000), multiple mass models (Muyeen et al., 2007) and complex flexible multi-body models. The latter seems to have gained a lot of interest in recent years, much because these methods are incorporated into special wind turbine simulation software, such as HAWC2 (Larsen and Hansen, 2007), Cp-

Lambda (Bottasso and Croce, 2009) and FAST (Jonkman and Buhl, 2005).
The region of operation for a typical wind turbine is often divided into four regions, shown in Fig. C.2. In region I ($v < v_{cut-in}$) the wind speed is lower than the cut-in wind speed and no power can be produced. In region II ($v_{cut-in} < v < v_{rated}$) the blade pitch is usually kept constant while the generator torque is the controlling variable. In region III ($v_{rated} < v < v_{cut-out}$) the main concern is to keep the rated power and generator speed by pitching the blades. In region IV ($v > v_{cut-out}$) the wind speed is too high, and the turbine is shut down. This paper is focused on the above rated wind speed scenario, i.e. region III.

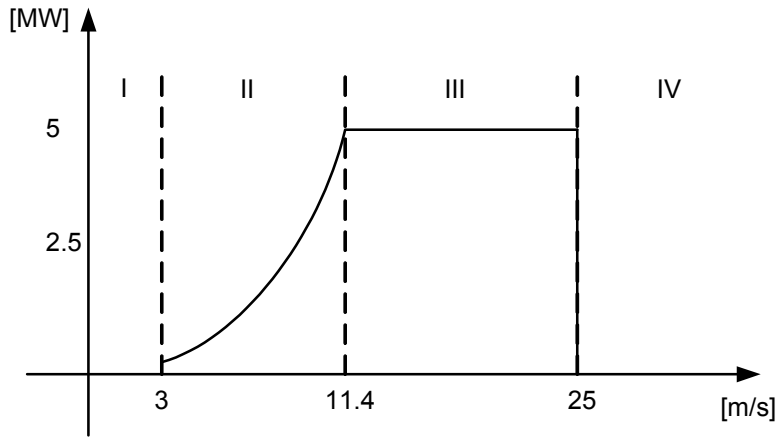

Figure C.2: Region of operation

It is tempting to just put a well designed onshore controller and install it on an offshore turbine. In principle one can do this, but there is no guarantee that the closed-loop system will be stable. The major difference between the onshore and the offshore turbine is the natural frequencies. The natural frequencies will decrease significantly once the turbine is mounted on a floating foundation. First, lets say the turbine is located onshore. Then the lowest tower frequency is typically $0.5[Hz]$, which is the tower fore-aft bending mode. Once this turbine is put offshore, some additional vibration modes appear, see Fig. C.3. These are much more low frequent, and the lowest frequencies are in the area $0.01 - 0.04[Hz]$. When the turbine is designed the designers already know the wind and wave frequencies in the area, and design the turbine structure accordingly. This is to make sure that the surrounding environment will not excite any of the structural vibration modes. For non-floating

turbines, the soil also plays a major role in relation to the structural natural frequencies, as discussed in (AlHamaydeh and Hussain, 2011). A controller for an onshore turbine, typically has a frequency of $0.1[Hz]$, i.e. lower than the tower fore-aft bending mode. If this controller was implemented on the offshore turbine, then the controller would be faster than the tower vibration modes. This can cause a stability issue once the wind speed is above rated. One can quite easily visualize why this becomes a problem. It is known that, in the above rated wind speed conditions the controlling variable is the blade pitch angle. When the wind speed increases, the blades will pitch out of the wind in order not to gain higher generator speed. This means that the aerodynamic forces acting on the tower will decrease and it will start to move forward. It is during this motion the stability issue occurs and it is directly related to the pitching frequency of the blades. Let's consider two scenarios: 1) the onshore controller is being used, 2) the offshore controller is being used. In the first scenario, the blades are being pitched out of the wind at a higher frequency than the tower is moving forward. The consequence is that the tower will lose most of its aerodynamic damping. The result is that the tower and eventually the generator will start to oscillate and eventually become unstable. In the second scenario the blades are being pitched out of the wind with a lower frequency than the tower is moving forward. Therefore, the tower will not loose as much of the aerodynamic damping, and the overall system will maintain its stability.
In today's industry, PI or PID controllers are commonly used. These are designed by keeping in mind these critical frequencies. Pole placement is one way of getting the closed-loop system poles at the right locations. The control design proposed in this paper does not directly include these stability constraints, but they are indirectly included since the proposed controller design is model-based and guarantees stability. This problem will be demonstrated in the simulation results.

The wind turbine is a highly nonlinear system. The nonlinearity is caused by the conversion of wind to electrical power. According to (Eggleston and Stoddard, 1987) the extracted electrical power from the wind can be formulated as

$$P_a = \frac{1}{2}\rho\pi R^2 v^3 C_p(\lambda,\beta). \tag{C.1}$$

The dimensionless tip-speed-ratio (TSR) λ is defined as

$$\lambda = \frac{\omega_r R}{v}, \tag{C.2}$$

where ω_r is the rotational speed of the rotor, R is the rotor radius and v is the wind speed acting on the blades. From (C.1) the expressions for the aerodynamic torque and thrust force are found as follows:

$$T_a = \frac{1}{2}\rho\pi R^3 v^2 \frac{C_p(\lambda,\beta)}{\lambda}, \tag{C.3}$$

$$F_t = \frac{1}{2}\rho\pi R^2 v^2 C_T(\lambda,\beta). \tag{C.4}$$

where T_a is the aerodynamic torque, F_t is the thrust force, ρ is the air density and β is the blade pitch angle. C_p is known as the power coefficient and depends on how the turbine is designed. It is an expression describing the relationship between power available in the wind and how much it is possible to extract. It is not possible to extract all the wind. If this were to happen, then the wind would have to completely stop after hitting the blades. The theoretical upper limit for the power extraction is known as the Betz limit. Albert Betz showed that only 59.3% of the theoretical power can be extracted, no matter how well designed the turbine is. In reality, after all the losses and friction are accounted for, only about $40-50\%$ is actually extracted. C_T has a similar explanation, but dealing with thrust force. Both expressions depend on the TSR λ and the blade pitch angle β.

A variety of control techniques are often solved by formulating the problem in terms of Linear Matrix Inequalities (LMIs) (Boyd et al., 1994). Formulating the problem in such a way gives an opportunity to impose a special structure on the LMI variables. This comes in very handy when it comes to constrained information systems. This means that it is possible to design a controller which can handle the fact that not all the information in the feedback loop is used. There can be several reasons for this, i.e. some of the information is simply not needed, some of the sensors are especially prone to failure, switching between controllers and they do not need the same information, etc. State-feedback is widely used in control applications, but in practice full state measurement is usually not possible. A more practical approach

is output-feedback. However, the output gain matrix is not computed as easily as in the state-feedback case, where a simple change of variables converts a non-convex problem into a convex problem. In the output-feedback case, the gain matrix is not directly isolated from the other LMI variables. In (Zečević and Šiljak, 2004, 2008, 2010) they proposed an explicit solution to calculate the gain matrix. In (Rubió-Massegú et al., 2012), an even simpler solution is found. With the solution found in (Rubió-Massegú et al., 2012), it is possible to impose zero-nonzero constraints on the LMI variables. Other solutions to make the system more tolerant to failures have been suggested in (Sloth et al., 2011) and (Kamal et al., 2012). Faults in the grid can also cause the turbine to behave in a non-satisfactory manner, this is discussed and dealt with in (Zhang et al., 2011).

Nowadays, modern wind turbines are getting bigger and bigger and are often located in harsh environments. This leads to larger loads on critical parts and the possibility of sensor failure is always present. This paper tries to alleviate these two issues. A traditional controller might force the turbine to shut down completely, if a sensor in the feedback loop should fail. With the controller designed in this paper, the turbine is able to stay in operation, although the failed sensor should of course be fixed as soon as possible. This is not managed without consequences, as will be discussed later in the paper.
First, an H_∞ controller is designed to minimize the effect of disturbance on the controlled output, practically this means it is possible to dampen unwanted oscillations on critical parts due to turbulent wind. Second, the controller is designed *a priori* to reduce effects of sensor failures that might occur.

This paper is organized as follows. Section II describes the model under consideration and how the wind turbine model and blade pitch actuators are interconnected. Section III goes into the control design and how it is possible to calculate the constrained gain matrix. Simulation results for both the linear model and the nonlinear model are presented in Section VI. Finally, concluding remarks and suggestions to future work are discussed in Section V.

Notation. Throughout this paper, the notations $\Re^n$ and $\Re^{n\times m}$ denote, respectively, the n dimensional Euclidean space and the set of all $n \times m$ real matrices. Superscript "$^\mathsf{T}$" denotes matrix transposition and I and 0 are the identity matrix and the zero

matrix with compatible dimensions, respectively. The symbol $\otimes$ denotes Kronecker product. The notation $P > 0$ means that P is real symmetric and positive definite and the symbol $*$ denotes the transpose elements in the symmetric positions. $diag\{\cdots\}$ represents a block diagonal matrix and the operator $sym(A)$ represents $A + A^T$. All LMI variables are written with boldface font.

2 Model Description

The model under consideration is obtained from FAST (Fatigue, Aerodynamics, Structures, and Turbulence) (Jonkman and Buhl, 2005), which is a fully nonlinear wind turbine simulation software developed at the National Renewable Energy Laboratory (NREL) in Denver, USA. The code models the wind turbine as a combination of both rigid and flexible bodies. These bodies are then connected with several degrees of freedoms (DOFs). The code provides with a nonlinear model with up to 24 DOFs. The turbine model is floating and is rated for 5 [MW], the main specifications are summarized in Table C.1. More detailed information about the specifications can be found in (Jonkman et al., 2009). Fig. C.3 shows the floating wind turbine. The platform DOFs are also indicated on the figure, they include; translational heave, sway and surge motion and rotational yaw, pitch and roll motion. Heave movement is defined along the z-axis, sway is along the y-axis, and surge is along the x-axis. Yaw motion is defined about z-axis, pitch is about the y-axis and roll is about the x-axis. This gives six DOFs.

Four more DOFs are related to the tower, two for longitudinal direction and two for lateral direction. Yaw motion of the nacelle provides one DOF. Variable generator- and rotor speeds gives another two DOFs, this also includes drive train flexibility. Nine DOFs for the blades, that is; three for blade flapwise tip motion for the first mode, three for tip displacement for each blade for the second flapwise mode and another three for the blade edgewise tip displacement for the first edgewise mode. The last two DOFs are for rotor- and tail furl. In total this adds up to 24 DOFs.

In order to utilize linear control techniques, a linear model is needed. The linear model is also obtained form FAST. A model with a low number of DOFs is preferred for the controller design, otherwise the model is simply too complicated in

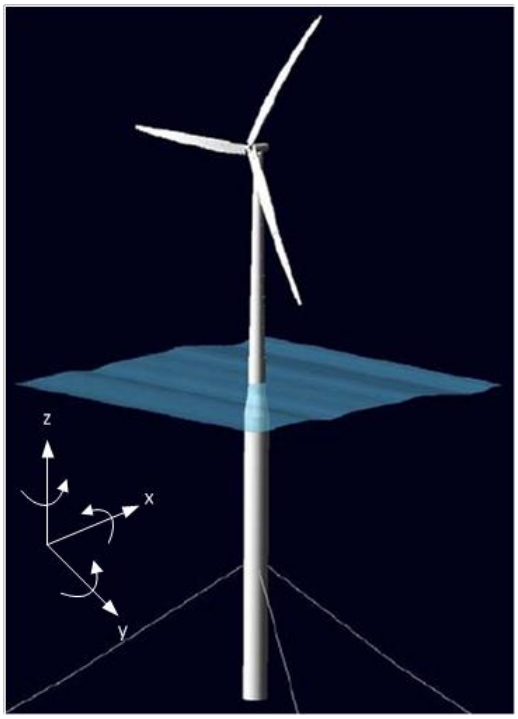

Figure C.3: Floating wind turbine (Jonkman, 2010)

Rated power	5 $[MW]$
Rated wind speed	11.6 $[m/s]$
Rated rotor speed	12.1 $[RPM]$
Rotor radius	63 $[m]$
Hub hight	90 $[m]$

Table C.1: Basic facts of NREL‘s OC3 turbine

order to get a feasible solution. Three DOFs are selected for the linear model, they are; platform pitch (1 DOF) and drive train (2 DOFs). The drive train includes the rotor and generator inertia, which are connected with springs, dampers and a gearing. FAST is not equipped with any blade pitch actuators, these are therefore added to the model after the linearization. A blade pitch actuator is the mechanism that physically rotates the turbine blade. The linear model obtained from FAST without any pitch actuators is in the following standard state-space form.

$$\begin{aligned} \dot{x} &= Ax + Bu, \\ y &= Cx, \end{aligned} \tag{C.5}$$

where x is the state vector with dimensions $\Re^{n\times 1}$, u is the control signal with dimensions $\Re^{p\times 1}$, y is the model outputs with dimensions $\Re^{m\times 1}$ and A, B and C are the state-space matrices with dimensions $\Re^{n\times n}$, $\Re^{n\times p}$ and $\Re^{m\times n}$, respectively. y contains measurements for platform pitch angle, rotor speed and generator speed. The specific dimensions for system (C.5) are; $n = 6$, $p = 3$ and $m = 3$.

This paper deals with individual pitch control, therefore three blade pitch actuators are added to the linear model. The three second order actuators are considered to be equal to each other, their properties are specified in the appendix. The DOFs for the updated model are; blade I actuator, blade II actuator, blade III actuator, platform pitch, drive train and generator. This gives a total of six DOFs with twelve states, i.e. one position- and velocity- state for each degree of freedom. Then, an augmented system can be derived and represented in the following state-space formulation

$$\begin{aligned} \dot{X} &= A_t X + B_1 \omega + B_t u, \\ z &= C_z X + D_z u, \\ y &= C_t X, \end{aligned} \tag{C.6}$$

where X is an augmented state vector which contains all the aforementioned twelve states and ω and z are disturbance and controlled output, respectively. The updated dimensions for system (C.6) are; $n = 12$, $p = 3$ and $m = 3$. The state-space matrices

A_t, B_t and C_t are defined as follows:

$$\begin{aligned} A_t &= \begin{bmatrix} I_3 \otimes A_a & 0 \\ B \otimes C_a & A \end{bmatrix}, B_t = \begin{bmatrix} I_3 \otimes B_a \\ 0 \end{bmatrix}, \\ C_t &= \begin{bmatrix} 0 & C \end{bmatrix}, \end{aligned} \tag{C.7}$$

where A_a, B_a and C_a are the state-space matrices for the pitch actuator, the matrix values can be found in the appendix. The rest of the state-space matrices B_1, C_z and D_z are defined in Section IV.
In this paper, a static output-feedback controller $u = Ky$ is to be determined under constrained information, i.e. a zero-nonzero structure on the control gain matrix by utilizing LMIs such that the following requirements are met:

1. The following closed-loop system is asymptotically stable;

$$\left(\begin{array}{c|c} A_{cl} & B_{cl} \\ \hline C_{cl} & 0 \end{array}\right) = \left(\begin{array}{c|c} A_t + B_t K C_t & B_1 \\ \hline C_z + D_z K C_t & 0 \end{array}\right). \tag{C.8}$$

2. Under zero initial condition, the closed-loop system satisfies $\|z(t)\|_2 < \gamma \|\omega(t)\|_2$ for any non-zero $\omega(t) \in L_2[0,\infty]$ where γ is a positive scalar.

3 Controller Design

H_∞ control is chosen because of its ability to minimize any energy-bounded disturbance on the controlled output. Also, since the linear model is of low order and the nonlinear model is of high order, this so-called advanced control design technique can catch a part of the unmodeled dynamics. The main issue in this section is to design a controller which is able to handle constrained information, i.e. only a part of the available information will be used to calculate the control signal. In this case, that is to design a decentralized controller. What is meant with decentralized control, is that none of the calculated control signals should directly interfere with each other. The considered system consists of three inputs and three outputs, this indicates that the gain matrix is square and of dimension $\Re^{3\times 3}$. By imposing a diagonal

structure on the gain matrix, this is possible. The solution found in (Rubió-Massegú et al., 2012), makes it possible to impose zero-nonzero constraints on the LMI variables. The control problem is formulated in terms of LMIs, and are solved using YALMIP (Löfberg, 2004) interfaced with Matlab.

The H_∞ performance constraints for a state-feedback system formulated in terms of LMIs are as follows:

$$\begin{pmatrix} sym\,(A_t\mathbf{X}+B_t\mathbf{Y})+\gamma^{-2}B_1B_1^T & * \\ C_z\mathbf{X}+D_z\mathbf{Y} & -I \end{pmatrix} < 0, \qquad \mathbf{X} > 0. \tag{C.9}$$

Remark 1. In a manner similar to (Bakka et al., 2012), it is possible to present a new H_∞ performance criterion for the robust stability analysis of the system (C.6) with norm-bounded time-varying parameter uncertainties in the state-space matrices.

Remark 2. It is worth noting that the number of variables to be determined in the LMIs (C.9) are: $n\times(1+n)/2+p\times n+1$. It is also observed that the LMIs (C.9) is linear in the set of matrices $\mathbf{X}$ and $\mathbf{Y}$, and the scalar γ^{-2}.

For the state-feedback case, the gain matrix is calculated as $\tilde{K}=\mathbf{Y}\mathbf{X}^{-1}$. In the output-feedback case, the state gain matrix factors as the product $\tilde{K}=KC_t$, where C_t is given from the state-space system. Now, when the output gain matrix is required, a solution to (C.9) needs to be found such that the product $\mathbf{Y}\mathbf{X}^{-1}$ factors as

$$\mathbf{Y}\mathbf{X}^{-1}=KC_t. \tag{C.10}$$

To solve this, (Rubió-Massegú et al., 2012) suggests the following change of variables

$$\mathbf{X} = Q\mathbf{X}_QQ^T+R\mathbf{X}_RR^T, \tag{C.11}$$

$$\mathbf{Y} = \mathbf{Y}_RR^T, \tag{C.12}$$

where $\mathbf{X}_Q$ and $\mathbf{X}_R$ are symmetric matrices with dimensions $\Re^{(n-m)\times(n-m)}$ and $\Re^{m\times m}$, respectively, and $\mathbf{Y}_R$ has dimension $\Re^{p\times m}$. The matrix Q is the nullspace of C_t and

R can be calculated as follows:

$$R = C_t^T \left(C_t C_t^T\right)^{-1} + QL, \tag{C.13}$$

where L is an arbitrary matrix with dimensions $\Re^{(n-m)\times m}$.
In order to obtain a diagonal structure on the gain matrix K, simply force a diagonal structure on $\mathbf{X}_R$ and $\mathbf{Y}_R$, while $\mathbf{X}_Q$ is a full matrix.

$$\mathbf{X}_R = diag\left\{\mathbf{X}_{R1}, \mathbf{X}_{R2}, \mathbf{X}_{R3}\right\}, \tag{C.14}$$

$$\mathbf{Y}_R = diag\left\{\mathbf{Y}_{R1}, \mathbf{Y}_{R2}, \mathbf{Y}_{R3}\right\}. \tag{C.15}$$

Remark 3. In the output-feedback constrained case, the number of variables to be determined in the corresponding LMIs are: $(n-m)\times\left((n-m)+1\right)/2+m+(p\times m)/3+1$.
In order to solve the LMIs (C.9), first define $\nu = \gamma^{-2}$. Then maximize ν and solve the LMIs in terms of $\mathbf{X}_Q, \mathbf{X}_R, \mathbf{Y}_R$. Once $\mathbf{X}$ and $\mathbf{Y}$ from (C.11)-(C.12) are calculated it is possible to find the gain matrix $K = \mathbf{Y}_R\mathbf{X}_R^{-1}$, satisfying $\mathbf{Y}\mathbf{X}^{-1} = KC_t$. Additional information and proofs about this can be found in the aforementioned references.

4 Simulation Results

In this section the proposed control design methodology is applied to the wind turbine system. The simulation is divided into two parts, one dealing with the linear model and one dealing with the nonlinear model. First, both the full information gain and the constrained gain are tested with the linear model. Second, the constrained gain controller is tested with the nonlinear model. The figures contain plots for simulations done with the constrained controller and with the baseline controller. The baseline is intended as a reference plot and is included in the FAST package. But first of all, suitable matrix values for B_1, C_z and D_z needs to be found.
The effect of disturbance on the linear model is assumed to affect the platform pitch angle and the rotor- and generator speed. In this analysis the disturbance vector is chosen to be:

$$B_1 = \begin{bmatrix} 0_{1\times 9} & 0.1 & 1 & 1 \end{bmatrix}^T. \tag{C.16}$$

This means that the platform pitch speed will not be as influenced by the disturbance as the rotor- and generator speed. The performance measure matrices are considered as

$$C_z = \begin{bmatrix} 97C_{t1} - C_{t2} \\ C_{t3} \\ (.) \end{bmatrix}, \tag{C.17}$$

$$D_z = diag\{100, 80, 10\}, \tag{C.18}$$

where $(.) = [10 \;\; 0 \;\; 10 \;\; 0 \;\; 10 \;\; 0 \;\; 0_{1\times 6}]$ and C_{ti} represent the i-th row of C_t. The first row of C_z handles drive train oscillations. Rotor speed times the gearing ratio minus the generator speed should be kept zero, i.e. minimizing oscillations. In row 2 the platform pitch movement is penalized and row 3 handles the blade pitch motion. Suitable results were found with a diagonal structure on the matrix D_z.

Figs. C.4 and C.5 show the outputs (first column) and the blade pitch angles (second column) for the closed-loop linear system. Simulation is carried out with initial values for platform pitch angle, generator speed and rotor speed. In Fig. C.4 no faults occur in the system and both controllers achieve an acceptable performance. In Fig. C.5 a sensor failure is imposed on the system. For the full structure of the control gain K, values for all three blades are calculated and the output values are not too different from the results in Fig. C.4. For the diagonal structure of the control gain K, only values for blades 1 and 2 are calculated, the value for blade 3 is depending on a working sensor nr. 3. In the case of a failure in sensor nr. 3, the two systems do not behave too different. It is worth mentioning that scenarios where sensor nr. 1 and nr. 2 fails have also been investigated. Only one sensor fails at the time. Now, the behavior of the two systems become very different. Results from these scenarios show that the system with the diagonal gain is stable regardless of which of the sensors that fails. In contrast to tests done with the full gain, where the system becomes unstable if sensor nr. 1 or nr. 2 fails, but as the figure shows, stays stable when sensor nr. 3 fails.

The full and the diagonal controllers are given in (C.19) and (C.20), respectively, and the γ-values for the two cases are compared in Table C.2.

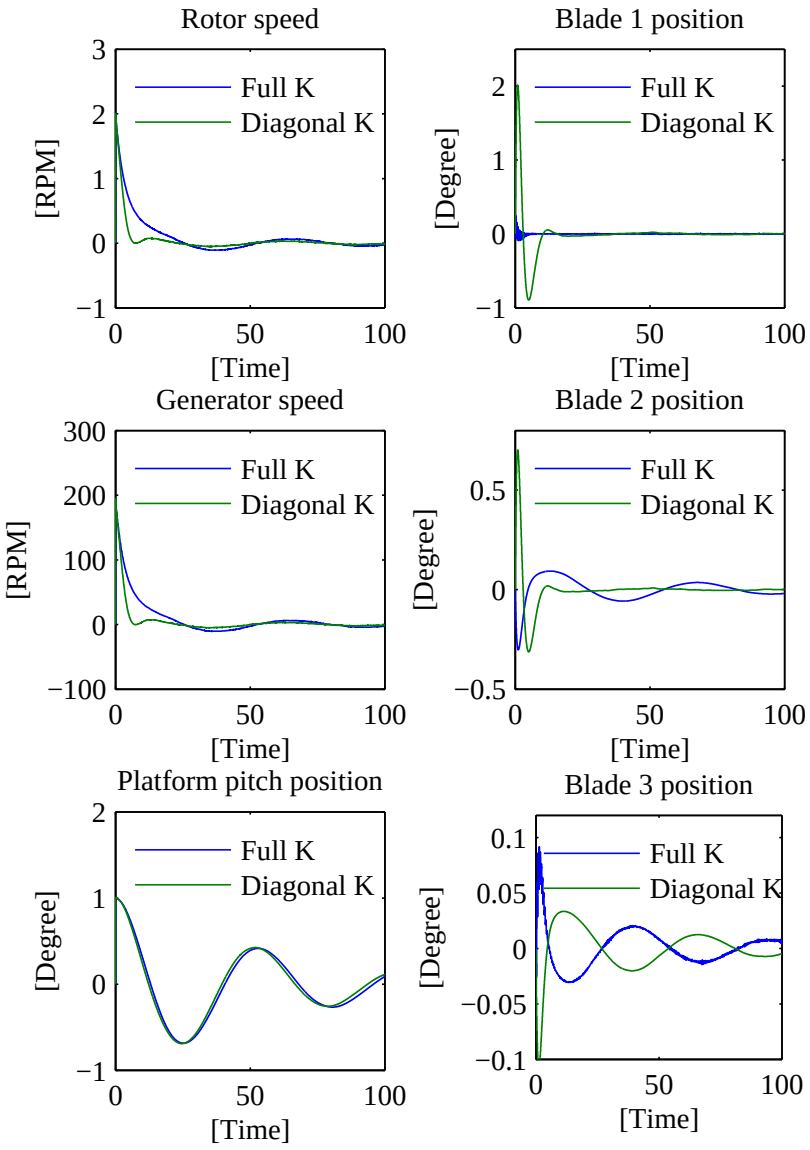

Figure C.4: System outputs and blade pitch angle, no faults

γ-value for full gain	γ-value diagonal gain
208	6331

Table C.2: γ-values

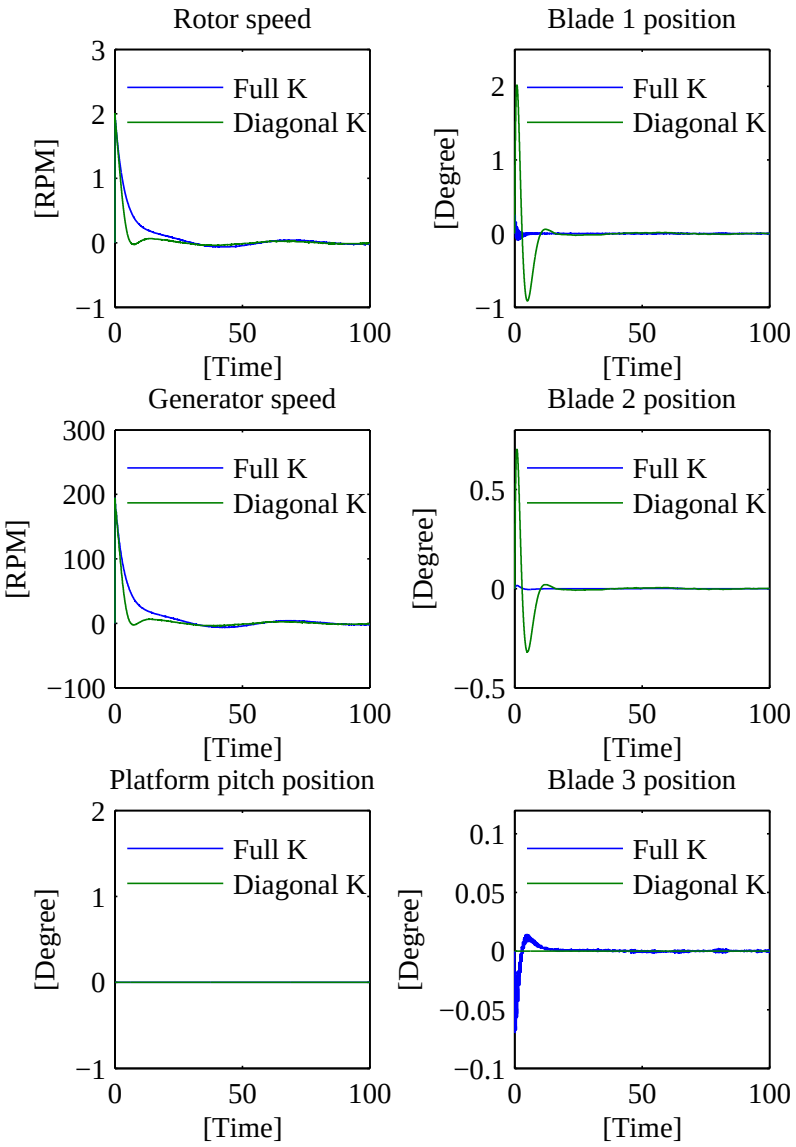

Figure C.5: System outputs and blade pitch angle, sensor 3 has failed

$$K_{full} = \begin{bmatrix} -0.9676 & 0.01 & 0 \\ 0.0037 & 0 & -0.0125 \\ 0.1988 & -0.0021 & 0.0043 \end{bmatrix}, \quad \text{(C.19)}$$

$$K_{diagonal} = diag\{0.0470, 0.0003, -0.0042\}. \quad \text{(C.20)}$$

Simulation of the nonlinear model is carried out in Matlab/Simulink interfaced with FAST. 27 DOFs are now available, counting the 24 DOFs from FAST and the 3 DOFs extra from the pitch actuators. The input to the model is turbulent wind, and the wind profile is obtained from the software Turbsim (Jonkman, 2009), which also is a software developed at the NREL. The profile is a 1-year extreme case with an average speed of 18 $[m/s]$ and a turbulence intensity of 6%, see Fig. C.6. Significant wave height is 6 $[m]$ with a peak wave period of 10 $[s]$. The time-series are of 600 $[s]$, but the first 200 $[s]$ are taken out due to transient behavior. The gain matrix in the feedback loop is now constrained to have diagonal structure. A fault is introduced to the system after 200 $[s]$. This fault causes sensor nr. 3 to stop working, i.e. blade nr. 3 is not moving. This fault only happens to simulations with the constrained controller, and not for the baseline simulation. It may be noted that the γ-value is considerably higher when the diagonal structure constraint is imposed. This makes sense because the number of LMI variables have now decreased and there are a lower number of variables available when it comes to finding the lowest γ-value, as indicated by **Remark 2** and **Remark 3.** Simulation done with the baseline controller is also included in the figures as a reference plot. This baseline controller comes with the FAST package and is a gain-scheduled PI-controller. The controller proposed in this paper is individual pitch in contrast to the baseline which is a collective pitch controller.

In order to evaluate the drive train oscillations, the standard deviation of the speed difference between rotor - and generator - speed is calculated. The values are normalized in such a way that the value for the baseline controller is used as reference and given value 1, see Tab. C.3. This means, in terms of standard deviation, the

Baseline	Constrained gain
1	0.93

Table C.3: Normalized values for standard deviation of drive train oscillations

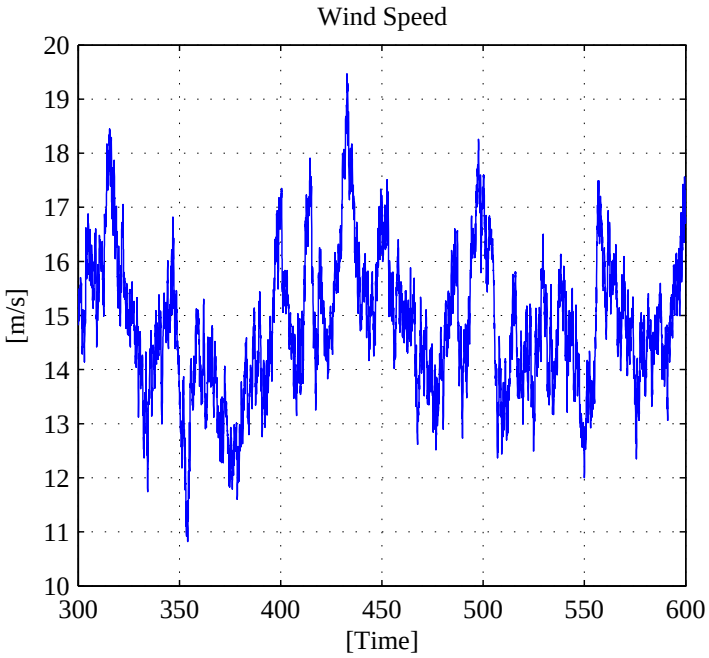

Figure C.6: Wind profile

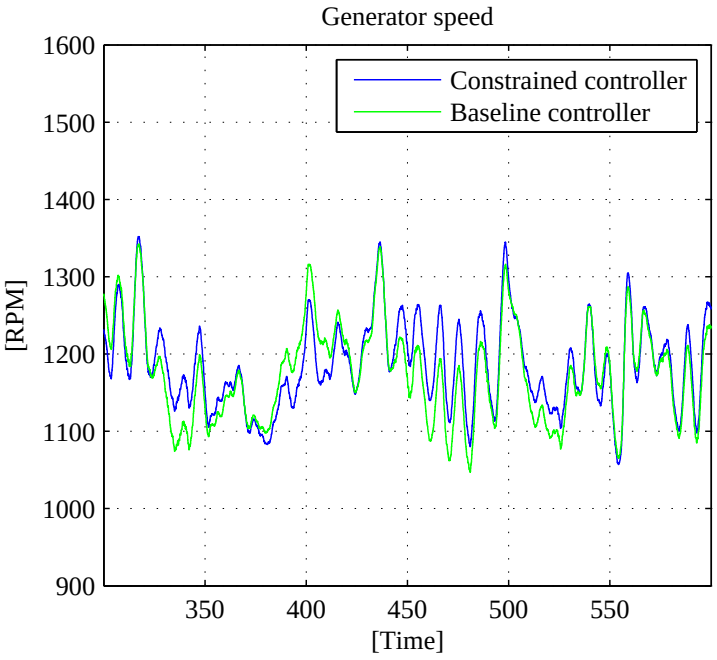

Figure C.7: Generator speed

constrained gain is 7% better than the baseline.

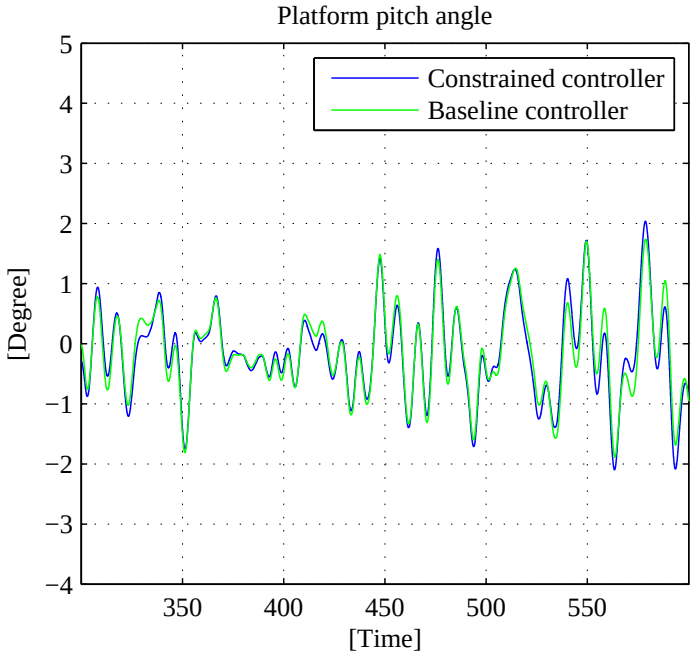

Figure C.8: Platform pitch angle

By using an individual pitch controller, it is possible to have a controller which handles events such as sensor failure in a good way. That is; if one of the sensors in the feedback loop fails, only one of the blades will directly experience this failure. This can be achieved with a decentralized individual pitch controller. It is seen from Figs. C.7-C.11 that the controller behaves in a satisfactory manner and the overall system is stable, even if blade 3 is not moving. The behavior of the system is not as steady as in the references (Bakka and Karimi, 2012a,b; Bakka et al., 2012), but the main advantage with the approach proposed in this paper is that the system is much more robust when it comes to sensor failures.

From Fig. C.11 it is seen that the thrust force has some peaks below zero, this means the tower is moving forward. That is, the tower experiences negative aerodynamic damping. This issue was discussed in the introduction of this paper. As the plots show, and Table C.4 imply, enough aerodynamic damping is acting on the tower. Hence, the overall system remains stable.

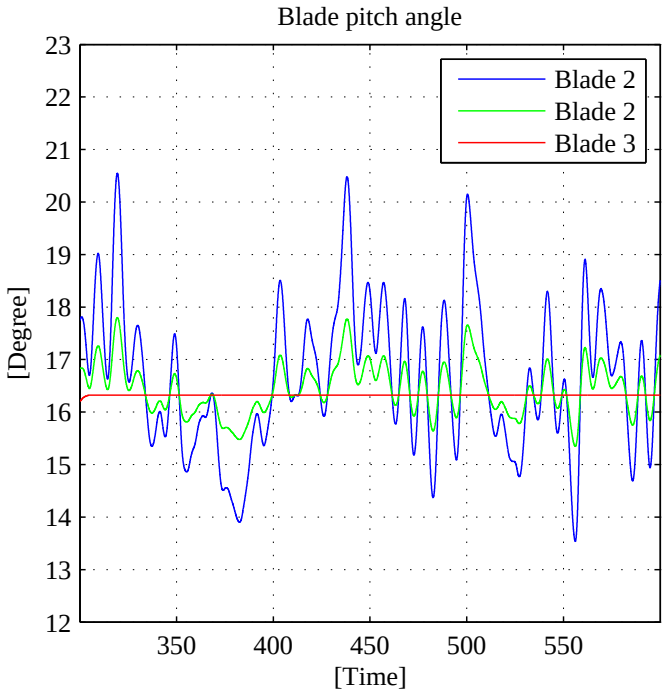

Figure C.9: Blade pitch angle

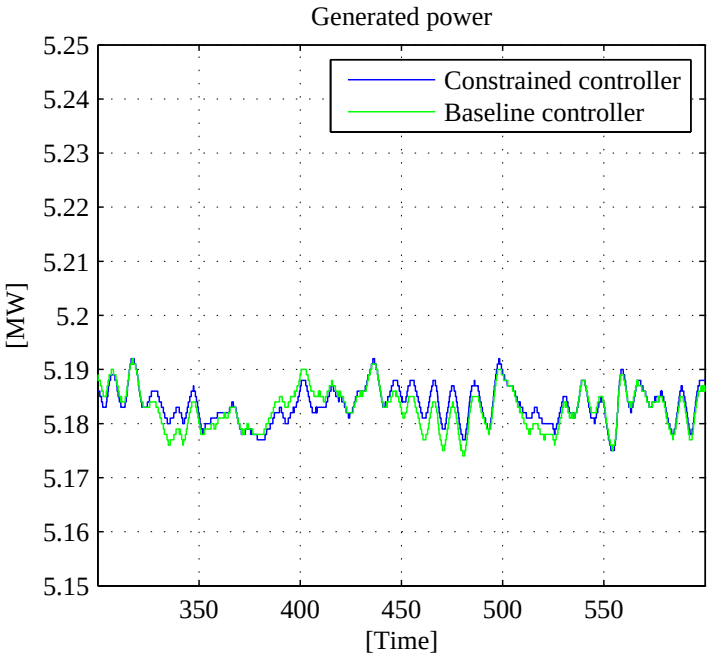

Figure C.10: Generated power

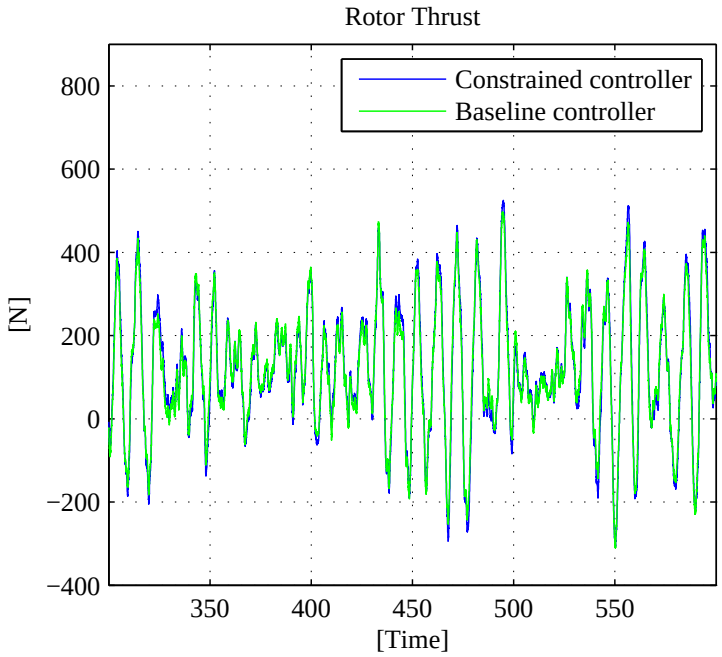

Figure C.11: Rotor thrust force

Fig. C.12 shows the normalized standard deviations from selected time-series. By allowing the turbine to stay in operation even if one of the sensors fail, is not without consequence. The force acting on the structure is now much more unsymmetrical than if all three blades were pitching. This will introduce additional fluctuations in the yaw moment, as seen from the histogram. Although, the mean value is almost 40% lower than the baseline value, see Fig. C.13.

A table describing the most critical natural frequencies are shown in Table C.4. These are found by calculating the Fast Fourier Transform (FFT) from the closed-loop time-series. From the discussion about critical frequencies in the introduction, it is seen from the table that the natural frequencies are where they should be.

Platform surge	0.015 $[Hz]$
Platform pitch	0.049 $[Hz]$
Platform heave	0.1 $[Hz]$
Blade pitch	0.03 $[Hz]$

Table C.4: Critical natural frequencies

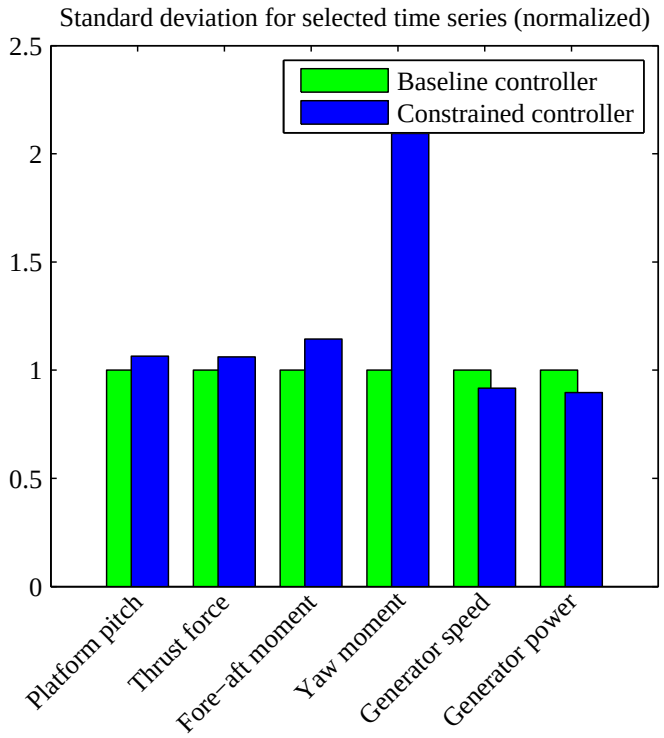

Figure C.12: Normalized standard deviations for selected time-series

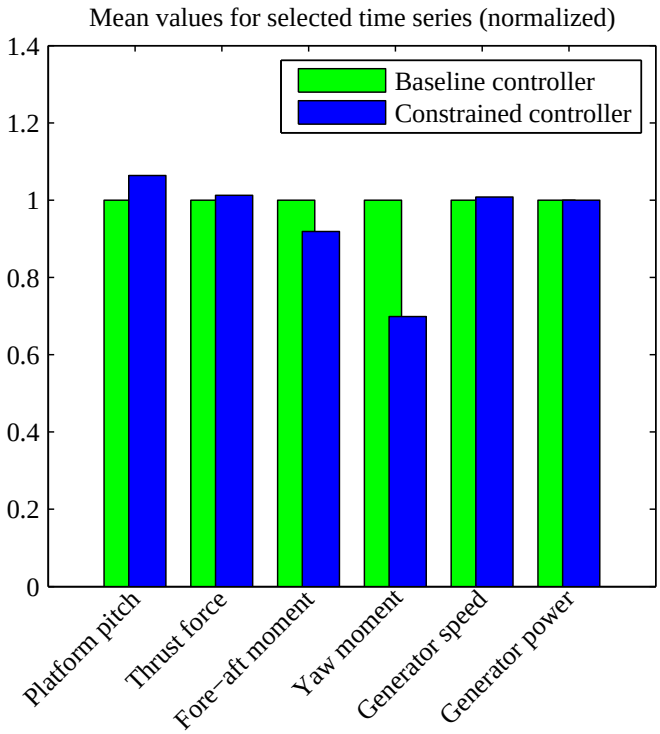

Figure C.13: Normalized mean values for selected time-series

5 Conclusions

This paper proposes an individual pitch static output-feedback controller for a offshore floating wind turbine system. A constrained control gain matrix is designed, this means that a special zero-nonzero structure is imposed on the output-feedback gain matrix. The usefulness of the approach proposed in this paper comes into play if failures occur. In the considered system there are three inputs and three outputs. If one sensor fails, only one blade pitch actuator will be influenced. The model under consideration is obtained from the software FAST. The model is fully nonlinear and in addition to the added pitch actuators the model consists of 27 DOFs. A linear model is obtained in order to perform the controller design, and simulations are carried out to verify the design. Simulation results performed both on the linear model and on the fully nonlinear system are presented in order to show the effectiveness of the controller design methodology.
Future work will investigate fault detection and linear parameter-varying (LPV) control design for a range of operating conditions.

6 Appendix

A dynamic model is constructed for each of the three linear pitch actuators:

$$\dot{x}_a = \underbrace{\begin{bmatrix} -2\omega_n\zeta & -\omega_n^2 \\ 1 & 0 \end{bmatrix}}_{A_a} x_a + \underbrace{\begin{bmatrix} 1 \\ 0 \end{bmatrix}}_{B_a} u_1, \tag{C.21}$$

$$y = \underbrace{\begin{bmatrix} 0 & \omega_n^2 \end{bmatrix}}_{C_a} x_a, \tag{C.22}$$

where the natural frequency is $\omega_n = 0.88$ and the damping ratio is $\zeta = 0.9$.

Acknowledgment

This work has been (partially) funded by Norwegian Centre for Offshore Wind Energy (NORCOWE) under grant 193821/S60 from Research Council of Norway

(RCN). NORCOWE is a consortium with partners from industry and science, hosted by Christian Michelsen Research.

REFERENCES

Abdin, E. S. and Xu, W. (2000). Control design and dynamic performance analysis of a wind turbine induction generator unit. *IEEE Transactions on Energy Conversion*, 15(1):91–96.

AlHamaydeh, M. and Hussain, S. (2011). Optimized frequency-based foundation design for wind turbine towers utilizing soil-structure interaction. *Journal of The Franklin Institute*, 348(7):1470–1487.

Bakka, T. and Karimi, H. R. (2012a). Multi-objective control design with pole placement constraints for wind turbine systems. In *Advances on Analysis and Control of Vibrations - Theory and Applications*. InTech, Chichester, UK.

Bakka, T. and Karimi, H. R. (2012b). Robust H_∞ dynamic output feedback control synthesis with pole placement constraints for offshore wind turbine systems. *Mathematical Problems in Engineering*, 2012(Article ID 616507):18 pages.

Bakka, T., Karimi, H. R., and Duffie, N. A. (2012). Gain scheduling for output H_∞ control of offshore wind turbine. pages 496–501. Proceedings of the 22^{nd} International Offshore and Polar Engineering Conference.

Bottasso, C. L. and Croce, A. (2009). Cp-lambda user manual. Technical report, Dipartimento di Ingnegneria Aerospaziale, Politecnico di Milano.

Boyd, S., Ghaoui, L., Feron, E., and Balakrishnan, V. (1994). *Linear Matrix Inequalities in Systems and Control Theory*. SIAM Studies in Applied Mathematics.

Eggleston, D. M. and Stoddard, F. S. (1987). *Wind Turbine Engineering Design*. Van Nostrand Reinhold Co.

Jonkman, B. (2009). Turbsim users guide: Version1.50. Technical report, National Renewable Energy Laboratory.

Jonkman, J. (2010). Definition of the floating system for phase iv of oc3. Technical report nrel/tp-500-47535, National Renewable Energy Laboratory.

Jonkman, J. and Buhl, M. L. J. (2005). FAST users guide. Technical report NREL/EL-500-38230, National Renewable Energy Laboratory.

Jonkman, J., Butterfield, S., Musial, W., and Scott, G. (2009). Definition of a 5-MW reference wind turbine for offshore system development. Technical report NREL/TP-500-38060, National Renewable Energy Laboratory.

Kamal, E., Aitouche, A., Ghorbani, R., and Bayrat, M. (2012). Robust fyzzy fault-tolerant control of wind energy conversion systems subjected to sensor faults. *IEEE Transactions of Sustainable Energy*, 3(2):231–241.

Larsen, T. J. and Hansen, A. M. (2007). How 2 HAWC2, The user's manual. Technical report, Risø.

Löfberg, J. (2004). YALMIP: A toolbox for modeling and optimization in MATLAB. pages 284–289. In Proceedings of IEEE International Symposium on Computer Aided Control Systems Design.

Muyeen, S. M., Ali, M. H., Takahashi, R., Murata, T., Tamura, J., Tomaki, Y., Sakahara, A., and Sasano, E. (2007). Comparative study on transient stability analysis of wind turbine generator system using different drive train models. *IET Renewable Power Generation*, 1(2):131–141.

Rubió-Massegú, J., Rossell, J. M., Karimi, H. R., and Palacios-Quiñonero, F. (2012). Static output-feedback control under information structure constraints. *Automatica*, 49(1):313–316.

Sloth, C., Esbensen, T., and Stoustrup, J. (2011). Robust and fault-tolerant linear parameter-varying control of wind turbines. *Mechatronics*, 21(4):645–659.

Zečević, A. I. and Šiljak, D. D. (2004). Design of robust static output feedback for large-scale systems. *IEEE Trans. on Automatic Control*, 49(11):2040–2044.

Zečević, A. I. and Šiljak, D. D. (2008). Control design with arbitrary information structure constraints. *Automatica*, 44(10):2642–2647.

Zečević, A. I. and Šiljak, D. D. (2010). *Control of complex systems: Structural constraints and uncertainty*. Springer.

Zhang, F., Leithead, W. E., and Anaya-Lara, O. (2011). Wind turbine control design to enhance the fault ride-through capability. *IET Conference on Renewable Power Generation*, pages 1–6.

Paper D

Linear Parameter-Varying Modeling and Control of an Offshore Wind Turbine with Constrained Information

T. Bakka, H. R. Karimi and S. Christiansen

This paper has been submitted to:

T. Bakka, H. R. Karimi and S. Christiansen, ”Linear Parameter-Varying Modeling and Control of an Offshore Wind Turbine with Constrained Information”, *Submitted to IET Control Theory & Applications*, 2013.

Linear Parameter-Varying Modeling and Control of an Offshore Wind Turbine with Constrained Information

T. Bakka[1], H. R. Karimi[1] and S. Christiansen[2]
[1]Department of Engineering
Faculty of Engineering and Science, University of Agder
Jon Lilletunsvei 9, 4879 Grimstad, Norway.
[2]Department of Electronic Systems, Aalborg University
Fredrik Bajers Vej 7, 9220 Aalborg , Denmark.

***Abstract* —** This paper deals with linear parameter-varying (LPV) modeling and output-feedback H_∞ control design for an offshore wind turbine. The controller is designed with consideration that not all the information in the feedback loop will be used. This constraint is incorporated into the design procedure. Constrained information means that a special zero-nonzero pattern is forced upon the gain matrix. The constrained controller is obtained based on parameter-dependent Lyapunov functions and formulated in terms of linear matrix inequalities (LMIs). Since the functions are dependent on the wind speed and accurate wind speed measurements are rarely available in practice, an Extended Kalman filter (EKF) is used to estimate the wind speed. The controller is designed in such a way that it should maintain its stability and performance even if one of the sensors in the feedback loop should malfunction. The control objectives are to mitigate oscillations in the structure and drivetrain, to smoothen power/torque output in addition to keep the closed-loop system stable. This should be achieved by means of individual blade pitch. A traditional procedure for designing a controller for such a system is to choose an operating point and assume it works in a suitable way under the influence of turbulent wind. In this paper, the wind turbine model is obtained from the software FAST. To design the controller, the model is linearized about several operating points. The degrees of freedom in the linearized model are chosen according to the controller objectives. The linear models are valid within the span of operating points. Finally, the controller is tested on the fully nonlinear system under the

influence of turbulent wind and a scenario where one of the sensors in the feedback loop is malfunctioning. The closed-loop response of the presented controller is compared to the closed-loop response of the baseline controller included in the FAST package along with a controller designed based on a single linearized model.

Keywords — LPV modeling, constrained information, H_∞ control, wind turbine.

1 Introduction

In recent years there has been an increasing interest in wind energy. According to The World Wind Energy Association the worldwide wind energy reached a capacity of 254,000 MW in June 2012. Although the majority of the installed capacity is on land, many offshore parks have been built in recent years. Most of these parks have turbines which are either fixed to the soil or they stand on monopoles or other structures. Some of the major offshore wind farms in Europe are located in the United Kingdom (UK) and Denmark (DK), to name a few; Greater Gabbard (UK), Whalney (UK), Sheringham Shoal (UK), Horns Rev (DK) and Rødsand (DK). The turbines in these farms are installed in shallow waters, typical depths ranging from 10-30 [m]. For many countries such as Spain, United States, Japan, Korea and Norway it would be beneficial to also be able to install wind turbines in deeper waters, in depths up to several hundred meters. The existing offshore fixed-bottom wind turbines are not suited for such deep water. Hywind (Skaare et al., 2007) is one example of a floating wind turbine solution. This turbine was installed back in 2009 and is still in operation. It is located in the north sea, right off the Norwegian west coast. To be able to control these turbines in a suitable way is important, in order to keep them stable and in operation, simultaneously, for as long as possible. The region of operation for a typical wind turbine is often divided into four regions, see Fig. D.1. In region I ($v < v_{cut-in}$) the wind speed is lower than the cut-in wind speed and no power can be produced. In region II ($v_{cut-in} < v < v_{rated}$) the blade pitch is usually kept constant while the generator torque is the controlling variable. In this region the main objective is to maximize the power output. In region III ($v_{rated} < v < v_{cut-out}$) the main concern is to keep the rated power and speed simul-

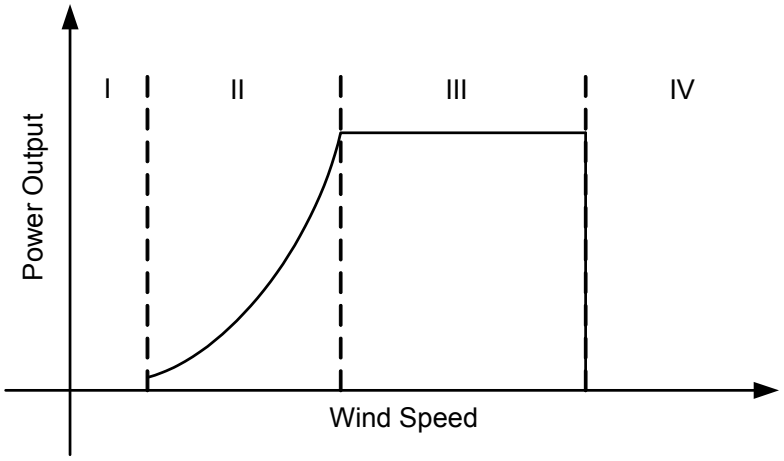

Figure D.1: Region of operation for a typical wind turbine

taneously. This is achieved by means of pitching the blades into or out of the wind, depending on the wind situation. In region IV $(v > v_{cut-out})$ the wind speed is too high, and the turbine is shut down. This paper is focused on the above rated wind speed scenario, i.e. region III.

Advanced control techniques are often solved by formulating the problem in terms of Linear Matrix Inequalities (LMIs) (Boyd et al., 1994). By formulating the problem in such a way, gives an opportunity to impose a special zero-nonzero structure on the LMI variables. This comes in very handy when dealing with constrained information systems. Linear parameter-varying (LPV) systems can also be handled within the LMI framework. Recently, linear controllers have been extensively used for power regulation through the control of blade pitch angle in wind turbine systems. However, the performance of these linear controllers is limited by the highly nonlinear characteristics of the wind turbine. Advanced control is one research area where such improvement can be achieved. On the other hand, over the last three decades, considerable attention has been paid to robustness analysis and control of linear systems affected by structured real parameters, so-called LPV systems. An LPV system can be viewed as a nonlinear system that is linearized along a trajectory determined by the parameter vector. Hence, the parameter vector of an LPV system corresponds to the operating points of the nonlinear system. In the LPV framework, it is assumed that the parameter vector is measurable or non-measurable. In the latter case the parameter vector can be estimated. In many industrial applica-

tions, like flight control and process control, the operating point can indeed be determined from measurement, making the LPV approach viable. Interesting works where LPV control is used in relation to wind turbines can be found in references such as (Bianchi et al., 2007) and (Østergaard et al., 2009). A nice collection of LPV related papers can be found in (Mohammadpour and Scherer, 2012). Previous related works from the authors which are dealing with wind turbine control can be found in (Bakka and Karimi, 2012) and (Bakka et al., 2012).

State-feedback is widely used in control applications, but in practice full state measurements are rarely possible. A more practical approach is output-feedback. However, the output gain matrix is not computed as easy as in the state-feedback case, where a simple change of variables converts a non-convex problem into a convex problem. In the output-feedback case, the gain matrix is not directly isolated from the other LMI variables. In (Zečević and Šiljak, 2004), (Zečević and Šiljak, 2008) and (Zečević and Šiljak, 2010) the authors propose an explicit solution for the gain matrix and in (Rubió-Massegú et al., 2012) the authors develop a more effective and efficient method for computational feasibility issues of static output-feedback controller gains. With the method found in (Rubió-Massegú et al., 2012), it is possible to impose zero-nonzero constraints on the LMI variables. Other methods to make the system more tolerant to failures have been investigated in (Sloth et al., 2011) and (Kamal et al., 2012).

This paper is dealing with an offshore floating turbine, now the control design becomes even more important. The wrong control design could easily force the turbine to be shut down. Nowadays, modern wind turbines are getting bigger and bigger and are often located in harsh environments, such as offshore conditions. This leads to larger loads and there is always the possibility of sensor failure. Since immediate maintenance for these turbines are not possible, a way to keep them in operation according to prescribed performance measures would be beneficial. This paper tries to include four concrete issues in the controller design. 1) Limit oscillations in drivetrain and platform. 2) Keep generator speed at its rated value. 3) Limit influence on the control loop in case of sensor failure. 4) The controller is designed within the LPV framework. In this relation an individual pitch with constrained gain control scheme is suggested. The ability to impose special structure on the gain matrix

come in handy if for example; there are some sensors in the feedback loop which are especially prone to failure. In this way one can isolate the faulty measurement to only impact one of the pitch actuators, instead of all three. A diagonal structure for the gain matrix will be used, in this way, none of the pitch actuator signals will directly interfere with each other. In conventional control, in the worst case, the turbine might have to shut down because a sensor is malfunctioning. With the control proposed in this paper, the turbine can continue operating properly in the event of a failure. Even though, the failure should be fixed as soon as possible. The main contribution of this paper is to design an LPV controller under a constrained gain matrix for a floating wind turbine system.

This paper is organized as follows. In Section 2, an LPV model of the wind turbine system is proposed. The controller design is discussed in detail in Section 3, where it will be shown how it is possible to obtain a diagonal structure for the gain matrix. In Section 4 the simulation results are presented. Conclusions and suggestions for future work are described in Section 5.

Notation. Throughout this paper, the notations $\Re^n$ and $\Re^{n\times m}$ denote, respectively, the n dimensional Euclidean space and the set of all $n\times m$ real matrices. Superscript T denotes matrix transposition and I and 0 are the identity matrix and the zero matrix with compatible dimensions, respectively. The symbol $\otimes$ denotes Kronecker product of two matrices. The notation $P>0$ means that P is real symmetric and positive definite and the symbol $*$ denotes the transpose elements in the symmetric positions, $diag\{...\}$ represents a block diagonal matrix and the operator $sym(A)$ represents $A+A^T$. All LMI variables are written with boldface.

2 Model Description

The model used in this paper is obtained from the software FAST (Fatigue, aerodynamic, structural and turbulence) (Jonkman, 2010), which is a fully nonlinear wind turbine simulation software. The OC3-Hywind model is a 5 [MW] offshore floating turbine (Jonkman et al., 2009), its main specifications are listed in Tab. D.1. This turbine model is an up scaled version of Statoil's 2.3 [MW] Hywind Demo turbine.

Rated power	5 $[MW]$
Rated wind speed	11.6 $[m/s]$
Rated rotor speed	12.1 $[RPM]$
Rotor radius	63 $[m]$
Hub hight	90 $[m]$

Table D.1: Main specifications of NREL's OC3 turbine

The nonlinear model obtained from FAST, is linearized around several operating conditions. All conditions are above rated wind speed, this indicates that the controller objectives are the same for each point. The objectives should be achieved by means of individual pitching of the blades. The nonlinear model consists of 24 degrees of freedom (DOF). This is all the available DOFs in FAST, if one desires, it is easy to switch the different DOFs on and off. This is convenient if just a simple model is necessary, and this is what is needed for the linearized model. The DOFs for the linear model are selected while keeping the controller objectives in mind, these include; platform pitch, generator and rotor dynamics. Pitch actuators will be added later in this section. This will add three additional DOFs to the linear model. In total there are 9 DOFs with 18 states, two for each DOF (position and velocity). With this linear model, most of the dynamics which are relevant for the controller objectives should be reflected. There are three measured signals in the feedback loop; generator speed, rotor speed and platform pitch angle. By using these three signals in the feedback loop, the three blade pitch angles can be calculated. A set of nine linearization points, ranging from 14 [m/s] to 22 [m/s], are obtained. The linearized models obtained from FAST are on the following standard state-space form

$$\begin{aligned} \dot{x} &= A_i x + B_i u, \qquad i = 1,...,9 \\ y &= Cx, \end{aligned} \tag{D.1}$$

where the state-space matrices A_i, B_i and C are of dimensions $R^{n\times n}$, $R^{n\times m}$ and $R^{q\times n}$, respectively, where n, m and q are 6, 3 and 3, respectively. From system (D.1) it is seen that A_i and B_i vary, depending on the operating point, i.e. wind speed. While the C matrix is constant since it only handles the measurements. The system can

now be formulated on a generalized form in (D.2).

$$\begin{aligned} \dot{x} &= A_i x + B_i u + B_w \omega, \qquad i = 1, ..., 9 \\ z &= C_z x + D_z u, \\ y &= Cx, \end{aligned} \tag{D.2}$$

where the additional term B_w describes how the disturbance enters the system, C_z and D_z handle the performance measures, i.e. the controller objectives.

So far, one state-space system for each operating point is obtained. In order to utilize the suggested control technique a continuous model of the set of state-space systems is needed. Least mean square method is used to construct this continuous affine model. The two parameter-dependent matrices are defined in the following affine way

$$A(\sigma) = A_a + \sigma A_b, \tag{D.3}$$

$$B(\sigma) = B_a + \sigma B_b, \tag{D.4}$$

where the scalar parameter σ satisfies $\underline{\sigma} \leq \sigma(t) \leq \overline{\sigma}$ and $\underline{\rho} \leq \dot{\sigma}(t) \leq \overline{\rho}$, that is $\sigma \in [\underline{\sigma} \ \ \overline{\sigma}]$ and $\rho \in \left[\underline{\rho} \ \ \overline{\rho}\right]$.
From (D.3)-(D.4) it is seen that the state-space system is now parameter-dependent on σ, which is the wind speed. The wind speed will later in the paper be estimated for this purpose.
As FAST does not include any pitch actuators, these are added to the parameter-dependent state-space system. One pitch actuator system is considered for each blade. As seen in the combined system (D.5), all the parameter dependency is limited to the A matrix.

$$\begin{aligned} \dot{x}_{aug} &= A_{aug}(\sigma) x_{aug} + B_{aug} u + B_{aug,w} \omega, \\ y &= C_{aug} x_{aug}, \end{aligned} \tag{D.5}$$

where the new augmented state $x_{aug} = \left[x_p^T \ x^T\right]^T$ has the following corresponding

state-space matrices:

$$A_{aug}(\sigma) = \underbrace{\begin{bmatrix} I_3 \otimes A_p & 0 \\ B_a \otimes C_p & A_a \end{bmatrix}}_{A_{aug,a}} + \sigma \underbrace{\begin{bmatrix} 0 & 0 \\ B_b \otimes C_p & A_b \end{bmatrix}}_{A_{aug,b}}, \tag{D.6}$$

$$B_{aug} = \begin{bmatrix} I_3 \otimes B_p \\ 0 \end{bmatrix}, \tag{D.7}$$

$$C_{aug} = \begin{bmatrix} 0 & C \end{bmatrix}, \tag{D.8}$$

where A_p, B_p and C_p, are the blade pitch actuator state-space matrices (See appendix for matrix values), $B_{aug,w}$ is defined in Section IV, $A_{aug,a}$ and $A_{aug,b}$ are the new augmented matrices of (D.3)-(D.4).

3 Control Synthesis

This section mainly deals with the controller design process and briefly discusses the extended Kalman filter. The main objective is to design an output-feedback LPV controller which is able to handle structure constraints on the output-feedback gain matrix. The LPV controller depends on the wind speed parameter, which is estimated by the extended Kalman filter. Fig. D.2 shows a block diagram, this block diagram describes the basics of the closed-loop system. In the first feedback loop, three values (y_1) are used to estimate the effective wind speed (σ). In the second feedback loop, three sensor values (y_2) are used to calculate the three blade pitch angles (β). These output values correspond to (D.5). As discussed in Section II, this means the feedback gain is a 3 by 3 matrix. This section considers calculation of an output-feedback gain matrix with a diagonal structure. In this way not all the available information will be used to calculate each of the blade pitch angles and none of the three control signals will directly interfere with each other. That is, should a failure happen to for instance sensor one, then this will not directly influence control signal two or three.

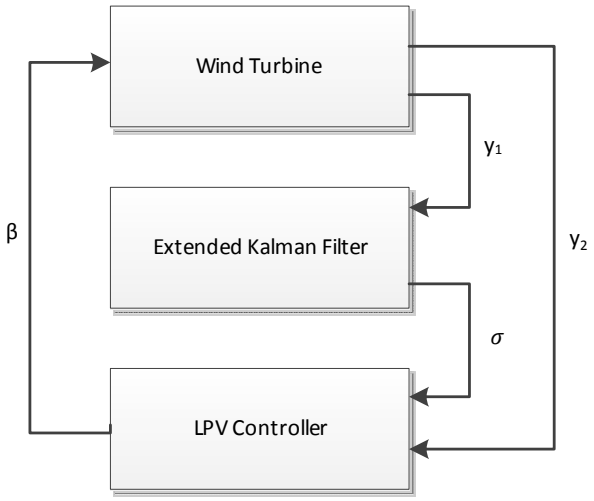

Figure D.2: Block diagram of closed-loop system

3.1 Extented Kalman Filter

It is possible to estimate the effective wind speed based on measurements of rotor speed, blade pitch angle and generator torque. The effective wind speed represents the average wind field over the rotor disc, i.e what is experienced by the blades. An extended Kalman filter is used based on a simple model of the drivetrain and a turbulence model, the output from the extended Kalman filter is the effective wind speed. For the actual development of the filter readers are referred to (Knudsen et al., 2011).
The drivetrain and wind model is modeled as first-order systems with no losses.

$$J_{eq}\dot{\Omega}_{DT} = T_a - T_g, \tag{D.9}$$

$$\dot{v}_t = -\frac{\pi v_m}{2L} + n_1, \tag{D.10}$$

$$\dot{v}_m = n_2, \tag{D.11}$$

$$\sigma = v = v_m + v_t, \tag{D.12}$$

where $J_{eq} = J_r + n_g^2 J_g$, $T_g = T_e n_g$, v_t is turbulence, v_m is the mean wind speed and L is the turbulence length scale parameter. The wind model is driven by Gaussian white noise, entering the model by n_1 and n_2. This model is nonlinear due to the nonlinear relationship between wind speed and aerodynamic torque. In order to

estimate the states, the time update uses information about the model dynamics and the model uncertainties.

$$\hat{x}_k^- = A_{ekf}\hat{x}_{k-1} + B_{ekf}u_{k-1}, \tag{D.13}$$

$$P_k^- = A_{ekf}P_{k-1}A_{ekf}^T + Q, \tag{D.14}$$

where matrices $\left(A_{ekf}, B_{ekf}, C_{ekf}\right)$ are state-space matrices of a linearized version of (D.9)-(D.10), Q is incremental process noise covariance and P_k is the state estimate error covariance. The measurement update uses information about the model outputs and measurement noise.

$$K_k = P_k^- C_{ekf}^T \left(C_{ekf}P_k^- C_{ekf}^T + R\right), \tag{D.15}$$

$$\hat{x}_k = \hat{x}_k^- + K_k\left(z_k - C_{ekf}\hat{x}_k^-\right), \tag{D.16}$$

$$P_k = \left(I - K_k C_{ekf}\right)P_k^-, \tag{D.17}$$

where R is measurement noise covariance, K_k is the Kalman gain and z_k is the measurements.

3.2 Controller Design

For obtaining the results of H_∞ controller synthesis, the wind speed parameter in (D.5) needs to be estimated according to subsection 3.1. As described in (Boyd et al., 1994), the H_∞ constraint for a linear time-invariant (LTI) system with state-feedback is formulated as follows:

$$\begin{pmatrix} sym\left(A_{aug}X + B_{aug}Y\right) + \gamma^{-2}B_{aug,w}B_{aug,w}^T & \left(C_Z X + D_Z Y\right)^T \\ * & -I \end{pmatrix} < 0, \tag{D.18}$$

$$X > 0. \tag{D.19}$$

In the state-feedback case the gain matrix is calculated from $K = YX^{-1}$. In the output-feedback case, the gain matrix factors as the product $\tilde{K} = KC_{aug}$, where C_{aug} is given from (D.8). In order to get the output-feedback gain, a solution to (D.18)-

(D.19) needs to be found such that the product YX^{-1} factors as

$$KC_{aug} = YX^{-1}. \tag{D.20}$$

In a recent work by (Rubió-Massegú et al., 2012), a procedure which handles this problem in a very systematic way is developed. Another benefit with this approach is that it is possible to impose structural constraints on the gain matrix. It is introduced to use the following change of variables

$$\begin{aligned} X &= QX_QQ^T + RX_RR^T, && \text{(D.21)} \\ Y &= Y_RR^T, && \text{(D.22)} \end{aligned}$$

where $X_Q(\sigma)$ and $X_R(\sigma)$ are $R^{(n-q)\times(n-q)}$ and $R^{(q\times q)}$ symmetric matrices, respectively, and $Y_R(\sigma)$ is a $R^{(m\times q)}$ matrix. The Q matrix is the nullspace of C, and R can be calculated from the following expression

$$R = C_{aug}^T\left(C_{aug}C_{aug}^T\right)^{-1} + QL, \tag{D.23}$$

where L is an arbitrary matrix with dimensions $R^{(n-q)\times q}$. One of the main contributions in this paper is to force the Lyapunov matrices to be parameter-dependent. The Lyapunov matrices (D.24) are now portioned in the same affine way as the matrices $A(\sigma)$ and $B(\sigma)$ in (D.3)-(D.4).

$$\begin{aligned} X_Q(\sigma) &= X_{Q0} + \sigma X_{Q1}, \\ X_R(\sigma) &= X_{R0} + \sigma X_{R1}, \\ Y_R(\sigma) &= Y_{R0} + \sigma Y_{R1}. && \text{(D.24)} \end{aligned}$$

By changing $\nu = \gamma^{-2}$ in the LMIs (D.18)-(D.19), the problem becomes convex and by maximizing ν it is possible to find the Lyapunov matrices in (D.24). In order to obtain the diagonal structure for the output-feedback gain the LMI variables $X_R(\sigma)$ and $Y_R(\sigma)$ also have to have a diagonal structure. Choosing the Lyapunov matrices as described, the output-feedback gain can be calculated from $K(\sigma) = Y_R(\sigma)X_R^{-1}(\sigma)$. The interested reader can read the proofs in (Rubió-Massegú et al.,

2012). In order to guarantee the controller stability and performance within the bounds of the scheduling parameter, some additional LMIs are required. The system is depending on one parameter and as indicated earlier this parameter has an upper and a lower bound, both on the parameter itself and on the derivative. One LMI is needed to check each vertex, i.e. this gives an addition of 2^i LMIs, where i is the number of vertices. As a consequence of the parameter dependency, at the upper left position in the H_∞ constraint (D.18), the expression is quadratic in σ. By imposing the definiteness of the terms involving σ^2, that is

$$sym\left(A_{aug,b}QX_{Q1}Q^T\right) + sym\left(A_{aug,b}RX_{R1}R^T\right) \geq 0 \tag{D.25}$$

the quadratic function of σ is convex.

The total set of LMIs needed to solve the LPV constrained static output-feedback problem are as follows:

$$\begin{pmatrix} sym\left(A_{aug}\left(\sigma_i\right)X\left(\sigma_i\right)\right) + sym\left(B_{aug}\left(\sigma_i\right)Y\left(\sigma_i\right)\right) + \nu B_{aug,w}B_{aug,w}^T \pm \rho_p \frac{\partial X}{\partial \sigma} & \\ * & \left(C_ZX\left(\sigma_i\right) + D_ZY\left(\sigma_i\right)\right)^T \\ & -I \end{pmatrix} < 0,\ i = p = 1,2 \tag{D.26}$$

$$sym\left(A_{aug,b}QX_{Q1}Q^T\right) + sym\left(A_{aug,b}RX_{R1}R^T\right) \geq 0, \tag{D.27}$$

$$\begin{pmatrix} X_{Q0} & 0 \\ 0 & X_{Q1} \end{pmatrix} > 0, \tag{D.28}$$

$$\begin{pmatrix} X_{R0} & 0 \\ 0 & X_{R1} \end{pmatrix} > 0, \tag{D.29}$$

where i is the number of vertices. The derivative term of the Lyapunov function is found to be

$$\frac{\partial X}{\partial \sigma} = QX_{Q1}Q^T + RX_{R1}R^T. \tag{D.30}$$

From the optimization the matrices $X_{Q0}, X_{Q1}, X_{R0}, X_{R1}, Y_{R0}$ and Y_{R1} are obtained. At each time step during the simulation, a new value for $A_{aug}(\sigma), X_R(\sigma)$ and $Y_R(\sigma)$ are calculated. The controller gain matrix $K(\sigma)$ is calculated from the expression

$K(\sigma) = Y_R(\sigma)X_R^{-1}(\sigma)$. In this way the output-feedback controller will change depending on σ.

4 Simulation Results

In this section the different simulation results will be discussed and presented. The controllers are tested on the fully nonlinear system, where all the available DOFs are enabled. The input to the system is a turbulent wind profile with an average wind speed of 18 [m/s] with a turbulence intensity of 6 % with corresponding waves. The wind profile is obtained from Turbsim (Jonkman, 2009), and is emulating a one year extreme wind speed condition. In the simulation example the plots concerning the two controllers designed in this paper experiences a fault after 500 [s]. This is not the case for the baseline controller, where no fault occurs. The gain scheduled PI controller is not designed to handle such an event. The fault causes sensor three to stop working, i.e. blade three has stopped moving, see Fig. D.6. The system is made in such a way that the actuator which controls blade number three keeps its last value prior the fault. In this way, the value does not drop to zero. Time series of 1000 [s] are obtained, but the first 400 [s] are removed due to transient behavior. Each of the figures show simulations done with three different controllers. The blue curve shows simulations done with the constant constrained gain controller. The red curve is for the LPV constrained gain controller and the green curve is FASTs baseline controller. The baseline controller is intended as a reference plot and comes with the FAST package.

As mentioned in Section 2, the controller objectives are to mitigate oscillations on critical parts of the system, to damp any movement which potentially can make the system unstable, such as platform pitch movement, and keep the overall system stable. These objectives are given as the performance measure z, as in (D.2) with the following matrices:

$$B_{aug,w} = [1_{12\times 1}], \tag{D.31}$$

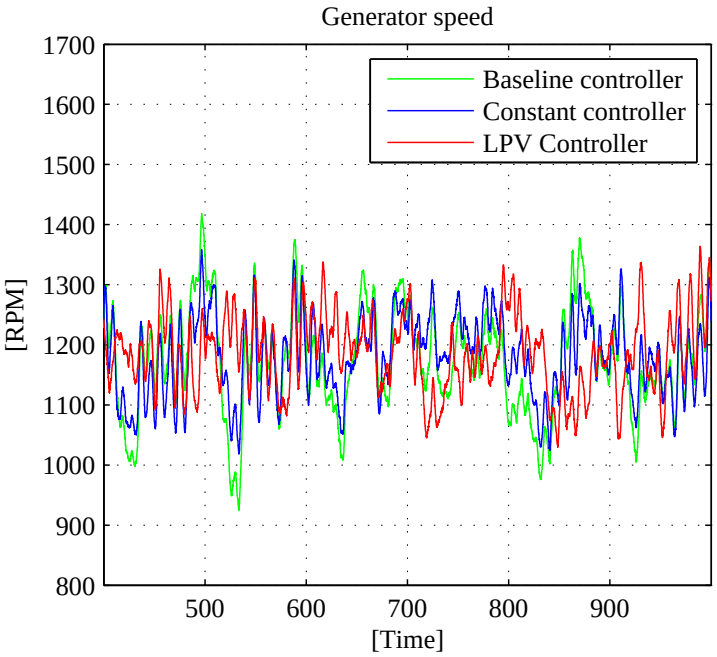

Figure D.3: Time series of generator speed

$$C_Z = \begin{bmatrix} C_1 - C_2/n_g \\ C_3 \\ 10\,0\,10\,0\,10\,0\,0_{1\times 6} \end{bmatrix}, \tag{D.32}$$

$$D_Z = diag\{10^3,\ 10^3,\ 10^3\}, \tag{D.33}$$

B_w is the disturbance matrix, and indicates which states that are disturbed. By giving this matrix only ones, the idea is to simulate a situation which is tougher than reality. The first row of C_Z handles the drivetrain oscillation, by subtracting the generator speed (C_2) divided by the gearing ratio n_g from the rotor speed (C_1). The second and third row handle platform pitch - and blade pitch movement, respectively. Suitable results were found with a diagonal structure for the D_Z matrix. The same performance measures are used for both the blue and the red curve. The outcome from the LMI calculations are listed in the appendix, that is, the Lyapunov matrices used online to calculate the LPV constrained controller and the constant constrained controller. In order to check the drivetrain oscillations, the standard deviation for the speed difference between rotor speed and generator speed is calcu-

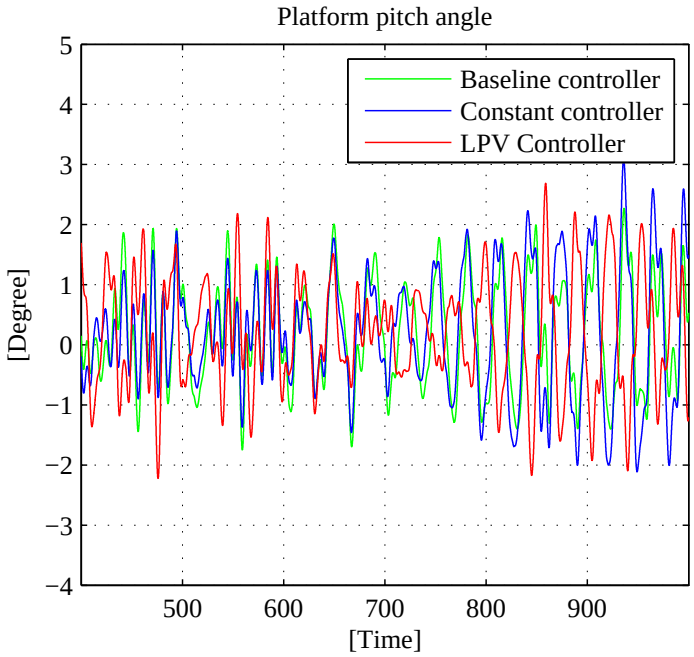

Figure D.4: Time series of platform pitch angle

lated. The values are normalized. That is, the reference value is the baseline result, which is given value 1. For the remaining two controllers, a value below 1 indicates better and vice versa. Multiply by 100 to get the percentage.

Baseline	Constant controller	LPV controller
1	0.98	0.96

Table D.2: Normalized values for drivetrain oscillations

From the Table D.2 it is seen that the two controllers designed in this paper does damp the drivetrain oscillations slightly better than the baseline controller.
A time series plot of the generator speed with different controllers is presented in Fig. D.3. It is seen that the constant constrained gain controller (blue) is slightly better than FASTs gain scheduled PI controller (green). But the controller that gives the better responds is the LPV constrained gain controller (red). Several observations indicate this. Firstly, it is operating more closely to the rated condition for the

generator. Secondly, the power output does not fluctuate as much as the two others (Fig. D.5). See also the mean and standard deviation plots in Figs. D.7-D.8. With these performance measures and with the fault present in the system, is was not possible to dampen the platform pitch movement (Fig. D.4) more than indicated in these plots.

After 700 [s] the platform is starting to gain a bit more amplitude in the pitch direction, but it does not become unstable. Control simulations of 2000 [s] are done to check this. The major consequence for introducing a failure to the closed-loop system is the nonsymmetrical loading on the tower. This is especially prominent in the yaw direction, where the standard deviations are considerably larger than the values for the baseline controller (no fault occurs with baseline), while the mean values are lower. See the histogram in Figs. D.7-D.8. The blade pitch movement for the LPV controller is shown in Fig. D.6. It is seen that the three blades are more or less following each other until the fault occurs. At time equals 500 [s] the third blade pitch actuator stops moving. This is emulating a sensor failure. As the plot shows, only one pitch actuator is influenced by the fault.

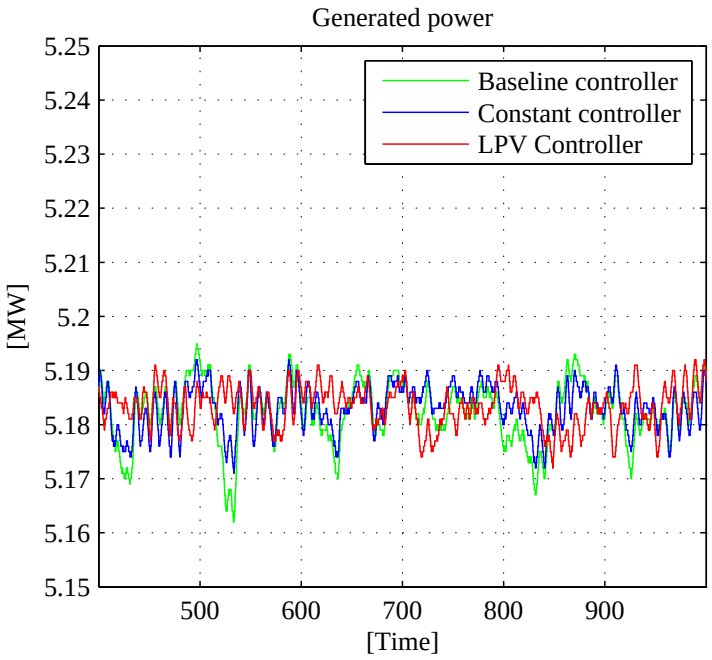

Figure D.5: Time series of generated power

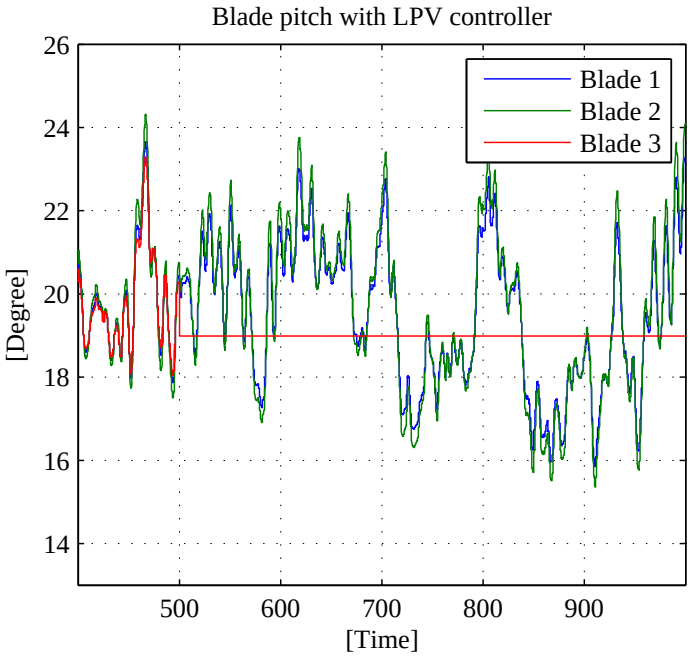

Figure D.6: Time series of blade pitch angles

From the histogram in Fig. D.7, it is seen that the LPV controller has a lower standard deviation for generator speed and for generator power. The large yaw moment value is because of the fault which is introduced in the system. The constant controller also causes the system to experience a large standard deviation in the yaw moment, due to the fault. But it has a better performance for the generator speed. The corresponding mean values can be seen in Fig. D.8.

5 Conclusion and Future Work

The purpose of this paper was to design an output-feedback linear parameter-varying (LPV) controller for an offshore wind turbine with constrained information. The scheduling parameter for the LPV controller is the effective wind speed. Based on available measurement an extended Kalman filter is used to estimate the effective wind speed. The wind turbine model is obtained from the software FAST and all simulations are done in Matlab/Simulink. A wind turbine is a highly nonlinear

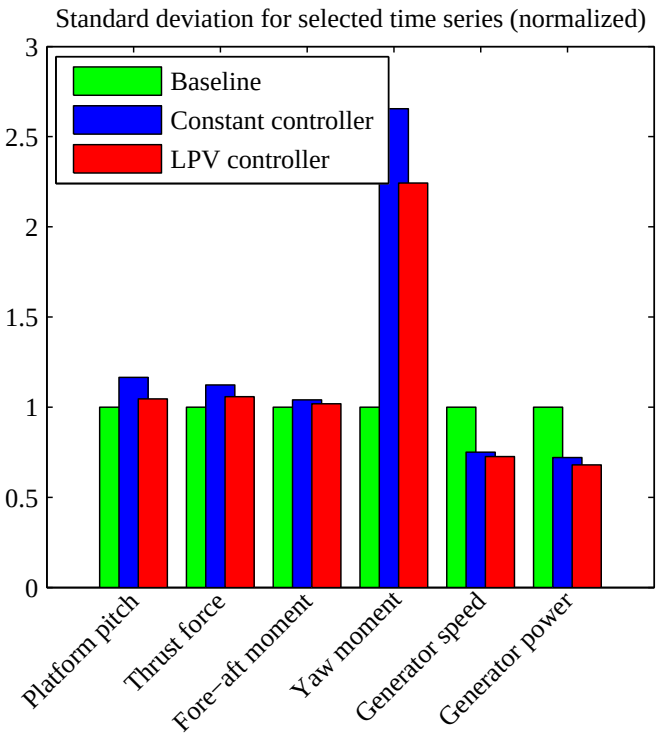

Figure D.7: Normalized standard deviations for selected time series

mechanism, and in order to use the controller design techniques proposed in this paper, a linearized model is needed. To linearize the model at only one operating point is a bit optimistic, therefore an LPV control approach is suggested. LPV control is a step in between linear control and nonlinear control. The design is done on the basis of linear techniques and when it is implemented, the benefits from nonlinear control are utilized. That is, it will perform and maintain stability in the whole operation region. With this method, LPV controller with constrained gain is constructed. Constrained gain means a special zero-nonzero pattern can be imposed on the gain matrix. In this paper, a controller gain with a diagonal structure is designed. From the simulation results it is seen that closed-loop system do behave according to the controller objectives and it maintains stability when a fault occurs to one of the sensors in the feedback loop.

Regarding the constrained gain matrix, this paper has focused on a diagonal struc-

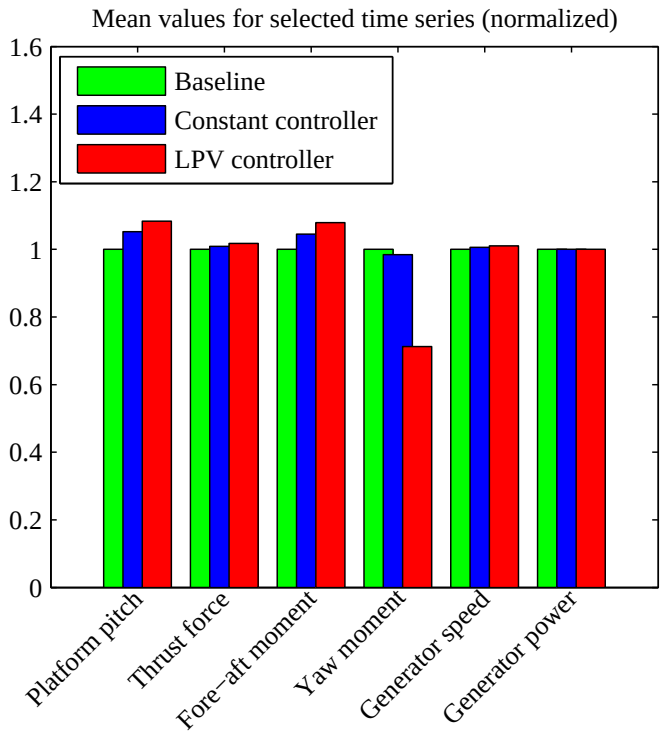

Figure D.8: Normalized mean values for selected time series

ture. It is completely up to the designer to choose the zero-nonzero pattern for the gain matrix. In other cases different patterns than diagonal may be appropriate.

Acknowledgment

This work has been (partially) funded by Norwegian Centre for Offshore Wind Energy (NORCOWE) under grant 193821/S60 from Research Council of Norway (RCN). NORCOWE is a consortium with partners from industry and science, hosted by Christian Michelsen Research.

6 Appendix

Blade pitch actuator model:

$$\begin{aligned} \dot{x}_p &= A_p x_p + B_p u, \\ y &= C_p x_p, \end{aligned}$$

where

$$A_p = \begin{bmatrix} -2\omega_n\zeta & -\omega_n^2 \\ 1 & 0 \end{bmatrix}, B_p = \begin{bmatrix} 1 \\ 0 \end{bmatrix}, C_p = \begin{bmatrix} 0 & \omega_n^2 \end{bmatrix}.$$

The natural frequency is $\omega_n = 0.88$ and the damping ratio is $\zeta = 0.9$. There is a total of three of these pitch actuators models in the turbine model, one for each blade.

Constant constrained gain: $K_{constant} = diag\{0.0315,\ 0.0008,\ 0.00017\}$

Lyapunov matrices used online to calculate the LPV constrained gain:

$$\begin{aligned} Y_{r0} &= diag\{0.0006,\ -0.3788,\ 0.0005\} \times 10^{-3}, \\ Y_{r1} &= diag\{0.0008,\ 1.2192,\ -0.0002\} \times 10^{-2}, \\ X_{r0} &= diag\{1.9527 \times 10^{-4},\ 13.9305,\ 0.0012\}, \\ X_{r!} &= diag\{7.7424 \times 10^{-8},\ 0.0231,\ 1.5532 \times 10^{-6}\}. \end{aligned}$$

REFERENCES

Bakka, T. and Karimi, H. R. (2012). Robust H_∞ dynamic output feedback control synthesis with pole placement constraints for offshore wind turbine systems. *Mathematical Problems in Engineering*, 2012(Article ID 616507):18 pages.

Bakka, T., Karimi, H. R., and Duffie, N. A. (2012). Gain scheduling for output H_∞ control of offshore wind turbine. pages 496–501. Proceedings of the 22^{nd} International Offshore and Polar Engineering Conference.

Bianchi, F., Battista, H., and Mantz, R. (2007). *Wind Turbine Control Systems: Principles, Modelling and Gain Scheduling Design*. Springer.

Boyd, S., Ghaoui, L., Feron, E., and Balakrishnan, V. (1994). *Linear Matrix Inequalities in Systems and Control Theory*. SIAM Studies in Applied Mathematics.

Jonkman, B. (2009). Turbsim users guide: Version1.50. Technical report, National Renewable Energy Laboratory.

Jonkman, J. (2010). NTWC design codes. Technical report, National Renewable Energy Center.

Jonkman, J., Butterfield, S., Musial, W., and Scott, G. (2009). Definition of a 5-MW reference wind turbine for offshore system development. Technical report NREL/TP-500-38060, National Renewable Energy Laboratory.

Kamal, E., Aitouche, A., Ghorbani, R., and Bayrat, M. (2012). Robust fyzzy fault-tolerant control of wind energy conversion systems subjected to sensor faults. *IEEE Transactions of Sustainable Energy*, 3(2):231–241.

Knudsen, T., Bak, T., and Soltani, M. (2011). Prediction models for wind speed at turbine locations in a wind farm. *Wind Energy*, 14(7):877–894.

Mohammadpour, J. and Scherer, C. (2012). *Control of Linear Parameter Varying Systems with Application*. Springer.

Østergaard, K., Stoustrup, J., and Brath, P. (2009). Linear parameter varying control of wind turbines covering both partial load and full load conditions. *International Journal of Robust Nonlinear Control*, 19(1):92–116.

Rubió-Massegú, J., Rossell, J. M., Karimi, H. R., and Palacios-Quiñonero, F. (2012). Static output-feedback control under information structure constraints. *Automatica*, 49(1):313–316.

Skaare, B., Hanson, T. D., Nielsen, F. G., Yttervik, R., Hansen, A. M., Thomsen, K., and Hansen, T. J. (2007). Integrated dynamic analysis of floating offshore wind turbines. Technical report, Risø.

Sloth, C., Esbensen, T., and Stoustrup, J. (2011). Robust and fault-tolerant linear parameter-varying control of wind turbines. *Mechatronics*, 21(4):645–659.

Zečević, A. I. and Šiljak, D. D. (2004). Design of robust static output feedback for large-scale systems. *IEEE Trans. on Automatic Control*, 49(11):2040–2044.

Zečević, A. I. and Šiljak, D. D. (2008). Control design with arbitrary information structure constraints. *Automatica*, 44(10):2642–2647.

Zečević, A. I. and Šiljak, D. D. (2010). *Control of complex systems: Structural constraints and uncertainty*. Springer.